Volume 94 • Number 1 • February 2023
Established in 1923 • ISSN 1945-0702

The Chemist

Journal of the American Institute of Chemists

In this Issue

Image courtesy of Pixabay

Official journal of
The American Institute of Chemists, Inc.
http://www.theaic.org/pub_thechemist_journals/

The Chemist

Established in 1923, The Chemist is the official publication of The American Institute of Chemists, Inc. (AIC). The Chemist was published quarterly in magazine format up until 2006. The Chemist is currently being set up and formatted as an online journal.

Editors
Alexander G. Zestos, *American University, USA*
Nayiri M. Kaissarian

Editorial Assistant Deborah Cate
Manuta Chemical Consulting

Art & Web Direction
Roy Hagen
Roy Hagen Web Design, USA

Editorial Review Board

John E. E. Baglin.....*IBM Almaden Research Center, USA*
Rodney Bennett.....*JRF America, USA*
Xiongwei Cai.....*Biogen Idec, USA*
Donna Chamely-Wiik.....*Florida Atlantic University, USA*
Jerry Ray Dias.....*University of Missouri-Kansas City, USA*
J. Stephen Duerr.....*Chemlabconsulting, LLC, USA*
Lawrence Duffy.....*University of Alaska Fairbanks, USA*
Nwadiuto Esiobu.....*Florida Atlantic University, USA*
Peter D. Fade.....*Wayne State University, USA*
Abraham George.....*Mar Ivanios College, India*
David Gossman.....*Gossman Consulting, Inc., USA*
Margaret Hall.....*University of Southern Mississippi, USA*
K. R. Haridas.....*Kannur University, India*
John Hill.....*La Trobe University, Australia*
Avishek Karmakar .....*Drexel University, USA*
Edward J. Kikta, Jr.....*FMC Corporation, USA*
David Devraj Kumar.....*Florida Atlantic University, USA*
Gopendra Kumar.....*University of Botswana, Botswana*
James Kumi-Diaka.....*Florida Atlantic University, USA*
Gary R. List.....*US Department of Agriculture, USA*
Bushan Mandava.....*Mandava Associate, LLC*
David M. Manuta.....*Manuta Chemical Consulting, Inc., USA*
Dayal T. Meshri.....*Advance Research Chemicals, Inc., USA*
E. Gerald Meyer.....*University of Wyoming, USA*
Robert F. Moran.....*Wentworth Institute of Technology, USA*
Wayne A. Morris.....*Morris-Kopec Forensics, Inc., USA*
Ronald Persin.....*Lnk2Lrn, USA*
Gary F. Porter.....*Bergan Community College, USA*
Manit Rappon.....*Lakehead University, Canada*
James A. Roe.....*Loyola Marymount University, USA*
David W. Riley.....*Extrusion Engineers, USA*
PradeepShrestha.....*Chemical Biology Lab, NIH*
James S. Smith.....*Trillium, Inc., USA*
Joy E. Stewart.....*Broward College, USA*
Saligrama Subbarao.....*Lincoln University, USA*
P. V. Thomas.....*Mar Ivanios College, India*
Ramkumar Varadharajan.....*Patna University, India*
Ranjit K. Verma.....*Patna University, India*
Rock J. Vitale.....*Environmental Standards, Inc., USA*
Xu Wang ..... *Research Scientist, Facebook (META, USA*
Kurt Winkelmann.....*Florida Tech, USA*
Wenhui Zeng .....*Florida Tech, USA*

The American Institute of Chemists, Inc. does not necessarily endorse any of the facts or opinions expressed in the articles, book reviews, or advertisements appearing in The Chemist.
Subscription: $35 per year to members, $100 per year to non-members. Single copy: $50.
The Chemist (ISSN-0009-3025) is published online by The American Institute of Chemists, Inc.

© The AIC 2023. All rights reserved.

Volume 94 | Issue 1 | 2023

The Chemist

Journal of the American Institute of Chemists

The Chemist (Established in 1923)
Copyright 2023. The American Institute of Chemists, Inc.

© The AIC 2023. All rights reserved.

Editorial

Alexander G. Zestos, Ph. D
American University

Nayiri M. Kaissarian, Ph.D

For the 2023 issue of The Chemist published by the American Institute of Chemists, we present a well-rounded variety of articles written by authors from all over the world. Following the theme of chemistry for an ever-changing world, we have articles from all diverse areas of chemistry from authors all over the world.

To begin, we first honor contributions from American Institute of Chemists Pioneer Awardees. We first honor Prof. Chi-Huey Wong from Scripps University in San Diego. Dr. Wong is a world-renowned expert in the fields of bioorganic and synthetic chemistry. His lab's current interests are centered on the development of discovery tools for understanding the role of biological glycosylation in cancer progression, bacterial and viral infection, neurodegenerative disorder and immune response.

In his review article "Recent Advances in Carbohydrate Chemistry and Application," Dr. Wong writes about cutting advances in carbohydrate chemistry. In this review, Prof. Wong highlights recent advances in carbohydrate chemistry and glycobiology. This work has created a better understanding of carbohydrates and the associated biological glycosylation. Prof. Wong describes new advances in carbohydrate synthesis and its application to the understanding of glycosylation in protein folding, cancer progression, influenza and SARS-CoV-2 infection and the development of carbohydrate-based medicines. Particular emphasis is also placed on cancer-cell specific glycans and further showing the importance of glycosylation from a wide variety of applications.

Moreover, our other Chemical Pioneer Award winner is Prof. Alison Butler from the Department of Chemistry at the University of California, Santa Barbara. Dr. Butler is a prolific scholar in the field of bioinorganic chemistry, metallobiochemistry and chemical biology, specifically with an emphasis on elucidating roles of metal ions in catalytic activities of metalloenzymes, and discovering molecules and processes by which microbes acquire the transition metals needed to grow. In her article "Marine Microbial Siderophores: Reactivity and Structural Diversity," Siderophores are discussed in detail, which are ligands with a high affinity for ferric ion and which facilitate transport of Fe(III) into and within bacteria that are isolated from open ocean isolates. This includes suites of amphiphilic siderophores that vary in the nature of the fatty acid appendages, photoreactive Fe(III)-siderophore complexes as a result of coordination to α- hydroxy carboxylic acid groups, and a new series of tris catechol siderophores.

In addition to the articles from the Chemical Pioneer Award winners, we have received several other contributions to the issue. In "Surface Chemistry and Biomolecule Density Impact Adsorbed Cellulase Activity," Vasicek et. al depict how functional group and biomolecule density on silica-coated iron oxide nanoparticles relate to the activity of adsorbed cellulases. The adsorption percent was related to greater functional group density, while the specific activity was inversely proportional to functional group density. The work has vast implications on the use of cellulosic ethanol production by immobilizing cellulases to ensure an abundance of cellulase is immobilized in an active conformation. Rheima et. al contributed "Eco-friendly Method of Synthesis CeO2 Nanoparticles by Watercress Plant Extract for Removal of Cibacron Red Dye from Aqueous Solutions." In this

© The AIC 2023. All rights reserved.

study, the authors discuss the environmentally friendly synthesis of CeO2 nanoparticles using plant extract from watercress and calcination. They found that the observed adsorption properties are efficacious for removing dye from aqueous solutions.

In “Estimation of Nonlinear Regression Parameters Precision” Prasanth Sambaraju discusses the calculation of the parameter precision values in nonlinear regression using Microsoft Excel. Example calculations are performed on nonlinear datasets from NIST Statistical reference datasets, where the parameters are initially estimated by using Solver and then by using Finite differences method parameter precision values are calculated. Dr. Tah’s group performed another estimation study in their contribution “Estimation of Serum Tumor Markers and Some Biochemical Parameters of Breast Cancer Patients.” In this study, they determined the levels of certain tumor markers (CA15.3, CEA) and some biochemical parameters (calcium, vitamin D3, alkaline phosphatase, uric acid, creatinine, and urea) in breast cancer women with different stages. They found a significant increase in CEA and CA15.3 values in women with breast cancer as compared to the control group, which should have vast implications in both breast cancer diagnostics and potential treatments.

AL-Salman and colleagues contributed “Formulation and Sustained-Release of Verapamil Hydrochloride Tablets,” where they discussed the synthesis of Verapamil hydrochloride effervescent tablets through direct compression. The tablets were thoroughly characterized by in vitro testing such as stability, floating (buoyancy), water uptake, differential scanning calorimetry, Fourier-transfer infrared spectroscopy (FT-IR) and other related techniques, which gave important information on their properties.

Our issue concludes with a conversation by Emma Sagarese and poem submitted from Meyer R. Rosen FAIC, FRSC, CPC, CChE. This last contribution truly shows the versatility and presence of chemistry in all fields of knowledge and the intersection between science and art.

We hope that you enjoy this issue and consider submitting a manuscript for consideration and publication to The Chemist in the near future.

Best regards,

Alexander G. Zestos, Ph.D Nayiri M. Kaissarian, Ph.D

© The AIC 2023. All rights reserved.

The Chemist
Journal of the American Institute of Chemists

Recent Advances in Carbohydrate Chemistry and Application

Chi-Huey Wong

Department of Chemistry, The Scripps Research Institute
La Jolla, California 92037, USA

Abstract: Recent advances in carbohydrate chemistry and glycobiology have led to a better understanding of carbohydrates and the associated biological glycosylation in biology. This report describes new advances in carbohydrate synthesis and its application to the understanding of glycosylation in protein folding, cancer progression, influenza and SARS-CoV-2 infection and the development of carbohydrate-based medicines.

Key Words: glycan array, programmable synthesis, vaccine, cancer, SARS-CoV-2

1. Introduction

Carbohydrates are one of the four major classes of biomolecules that make up cells. They are often linked to lipids as glycolipids or to proteins as glycoproteins through glycosylation. These glycoconjugates are often expressed on cell surface and are involved in almost everything, including protein folding, viral infection, spread of cancer cells, differentiation of stem cells, egg-sperm interaction, and many other biological recognition events. Despite their importance, the roles of carbohydrates and the associated glycosylation reactions in biology and disease progression have not been well understood, mainly due to the lack of tools and methods and the availability of homogeneous substances for the study of this class of molecules. So, over the years, we have been actively involved in the development of new methods for the study of carbohydrates and the associated glycosylation reactions [1]. These include the development of programmable one-pot chemical synthesis and chemoenzymatic synthesis of oligosaccharides and glycoproteins, design of glycosylation probes for identification of cancer-specific glycans on cell surface, and development of glycan microarrays for the high throughput analysis of protein-sugar interaction. These methods have led to a better understanding of glycosylation in biology and the

© The AIC 2023. All rights reserved.

development of new medicines, such as carbohydrate-based vaccines against cancer and viral infection, homogeneous anti-bodies with well-defined Fc glycan to improve effector functions and inhibitors of carbohydrate enzymes associated with disease progression (Figure 1).

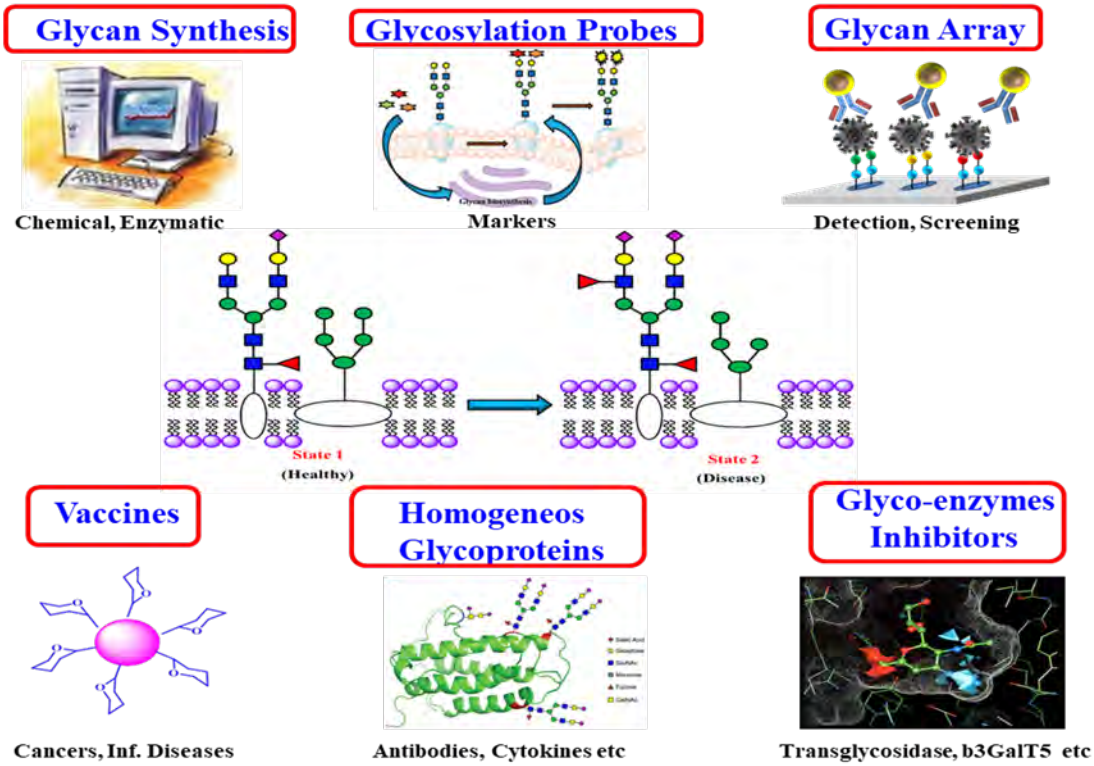

Figure 1. Development of new tools and methods for the study of cell-surface glycans: chemo-enzymatic and programmable one-pot synthesis of oligosaccharides, design of glycosylation probes to monitor biological glycosylation, and glycan microarray to study protein-glycan interaction. These methods have been used for development of vaccines against cancer and microbial infection, homogeneous antibodies to improve effector functions and glyco-enzyme inhibitors.

2. Programmable One-Pot and Chemo-enzymatic Synthesis of Oligosaccharides

In 1999, my laboratory developed the first programmable one-pot synthesis of oligosaccharides using a library of about 50 building blocks with defined relative reactivity value (RRV) for sequential glycosylation reaction [2]. Since then, we have expanded the library to more than 50,000 building blocks with predicted RRV using machine learning [3], and also included the reactivity of hydroxyl acceptors in the presence of protecting groups [4]. We have also updated the software to

© The AIC 2023. All rights reserved.

guide the selection of building blocks for one-pot reaction. To use the program, one can simply enter the glycan sequence of interest to the computer, and it will show the building blocks to be added sequentially to a reaction mixture, starting from the most reactive to the least reactive one. After all the building blocks are added, the product with protecting groups is formed quickly, usually in minutes, and after global deprotection and purification, the oligosaccharide is obtained. This rapid programmable synthesis method has been used for the synthesis of various glycans including heparin pentasaccharides (Figure 2, [5]),

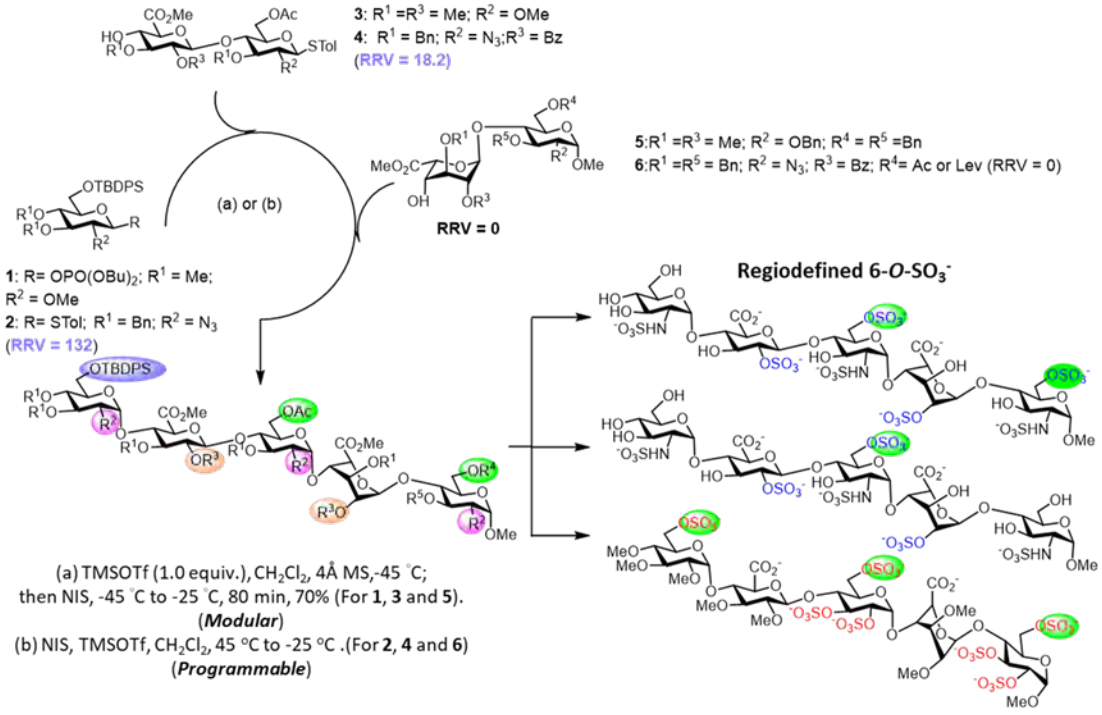

Figure 2. Programmable and Modular Synthesis of Heparin Pentasaccharides

and it is expected that this method and the automated solid-phase synthesis [6], as well as the enzymatic method, will be used to further expand the structural diversity of glycans [1].

The development of programmable one-pot method was inspired by the way an oligosaccharide is made by enzymes in our body. As shown in the enzymatic synthesis of cancer-specific Globo-H and SSEA4 (Figure 3, [7]), the first enzyme product becomes the substrate of the second enzyme, and its product becomes the substrate of the third enzyme. So, the final product can be obtained in a one-pot manner with all the enzymes mixed together, including the sugar nucleotide regeneration system that was designed to reduce the cost and eliminate the problem of feed-back inhibition caused by the released nucleoside phosphate in the glycosylation reaction.

© The AIC 2023. All rights reserved.

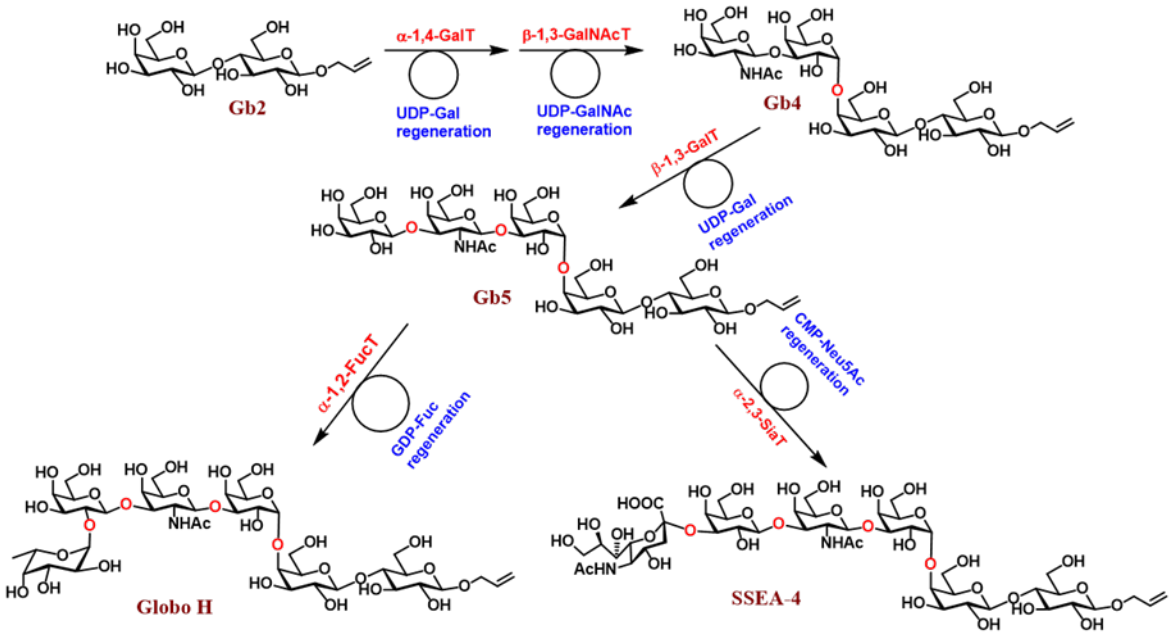

Figure 3. Chemo-enzymatic Synthesis of the Globo-series Glycans of SSEA3, SSEA4 and Globo-H

3. Glycan Microarray

With various glycans available, we can use them to create glycan arrays for the study of protein-glycan interaction [8].

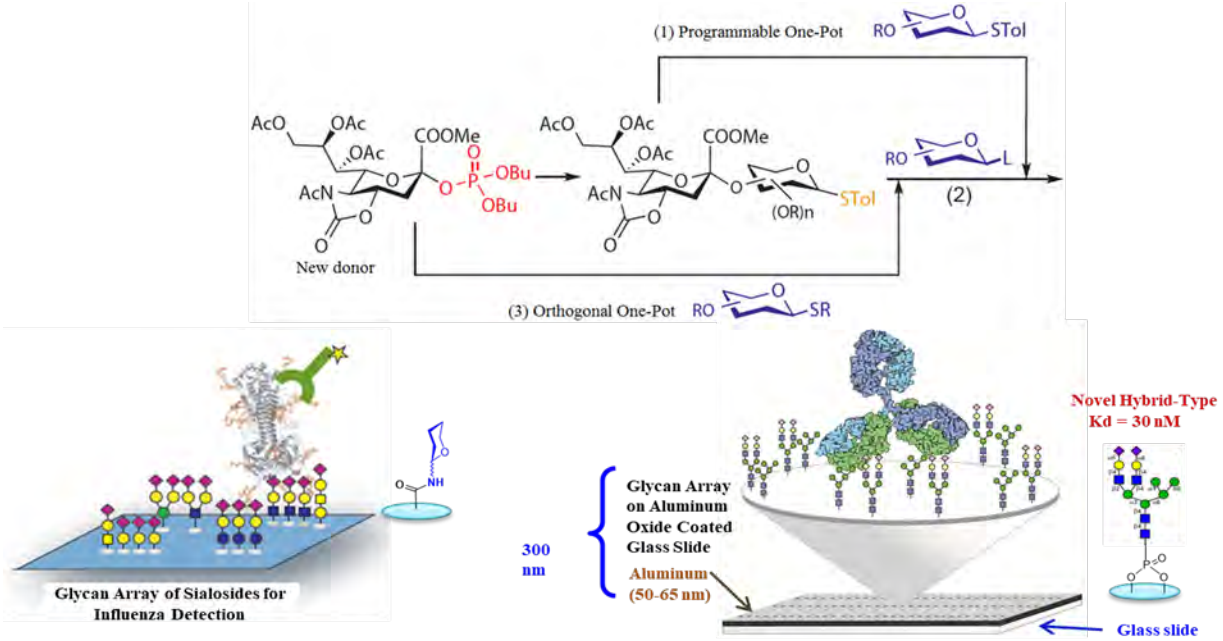

Figure 4. Synthesis of Sialosides and N-glycans for the Preparation of Glycan Array

© The AIC 2023. All rights reserved.

Figure 4 shows the profiling of influenza hemagglutinins interacting with an array of sialosides on a glass slide. We know human influenza virus recognizes alpha-2,6-linked sialosides and avian virus recognizes 2,3-linked sialosides on the surface of epithelial cells in our upper and lower airway tracks. Using the glycan array, we can further understand the nature and structure of the internal glycans recognized by different hemagglutinin subtypes and define their binding specificity. We also developed the more homogeneous aluminum oxide-coated glycan array to profile some of the broadly neutralizing antibodies isolated from HIV positive patients who did not develop into AIDS [9]. These antibodies are known to target some unusual N-glycans on gp120 and neutralize over 70% of the more than 2000 HIV variants known to date. As an example, the unusual hybrid-type glycan as shown in Figure 4 was identified as a nanomolar ligand for the antibody PG9 [10] and work is in progress to use this unusual glycan as epitope for vaccine design, hopefully to elicit PG9-like antibody against HIV.

4. Impact of Glycosylation on Protein Folding

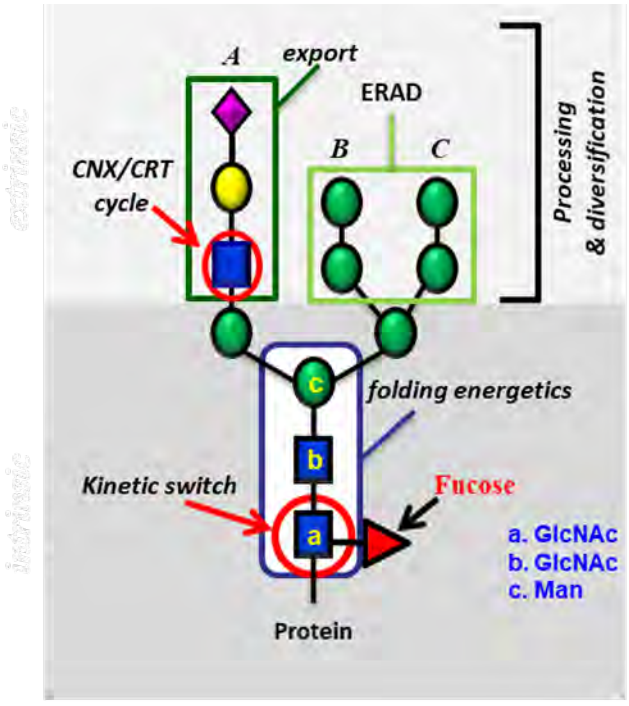

Figure 5. Impact of glycosylation on protein folding and stability using a model protein (hCD2ad) without proline and disulfide bond to interfere. The core trisaccharide is essential for protein folding and stability. GlcNAc (a) speeds up the folding by 0.8 kcal/mol and stabilizes the folded structure by 2 kcal/mol. Additional stabilization (1.1 kcal/mol) is from Man-GlcNAc (c-b). The rest of glycans are involved in function.

© The AIC 2023. All rights reserved.

To understand how glycosylation affects protein folding, we first studied the O-glycosylation where N-acetylglucosamine is attached to the Ser or Thr residue. We then studied the N-glycosylation and used hCD2ad as a model (Figure 5) because it does not have the proline residue or disulfide bond to interfere with folding. We found that the first sugar attached to the Asn residue, i.e., GlcNAc, is the most important, as it speeds up the protein folding by 0.8 kcal/mol and stabilized the folded structure by 2 kcal/mol, and another one kcal is from the second and the third sugars together. These three sugars constitute the core trisaccharide which is highly conserved from yeast to human, and the rest of sugars are not associated with folding but may involve in different recognition events [11,12].

To further understand the origin of the 2 kcal contributed by the GlcNAc residue to stabilize the protein, we performed an NMR study using another model without proline or disulfide. It showed that the GlcNAc residue has a hydrophobic interaction with the nearby Phe group that accounts for about one kcal/mol, and this interaction changes the orientation of Phe to trigger the following hydrophobic interactions in the beta sheet region, very much like a domino effect that accounts for another one kcal/mol.

5. Low-Sugar Universal Vaccines Against Influenza and SARS-CoV-2

This finding has led to the development of universal vaccines against influenza and SARS-CoV-2 through glyco-engineering. Both human viruses are RNA viruses that are easy to mutate. In addition, the virus surface immunogen, either hemagglutinin or spike (S) protein, is highly glycosylated to shield the conserved epitopes from immune response. Our proposition is to remove the shielded glycans on S protein to better expose the conserved epitopes and use the low-sugar S protein as vaccine.

The SARS-Cov-2 spike protein is a trimer and each monomer contains about 1300 amino acids, 22 N-glycosites and 2 O-glycosites. There are more than 10 million S protein sequences reported by GISAID today though most of them have insignificant mutation rate. Currently, more than 85% of confirmed cases are infected by omicron BA.2 subvariant (March 20, 2022) while 3 months ago, the delta variant accounted for more than 98% of the confirmed cases. Although current vaccines have proven highly effective against severe infection, breakthrough infection occurs relatively often, suggesting the need for a broadly protective vaccine.

We carried out the sequence alignment of more than 6 million S proteins from GISAID and identified 12 highly conserved epitopes, 7 in the receptor binding domain (RBD) and 5 in the stem domain (HR2); and 10 of these 12 epitopes are shielded by glycans.

© The AIC 2023. All rights reserved.

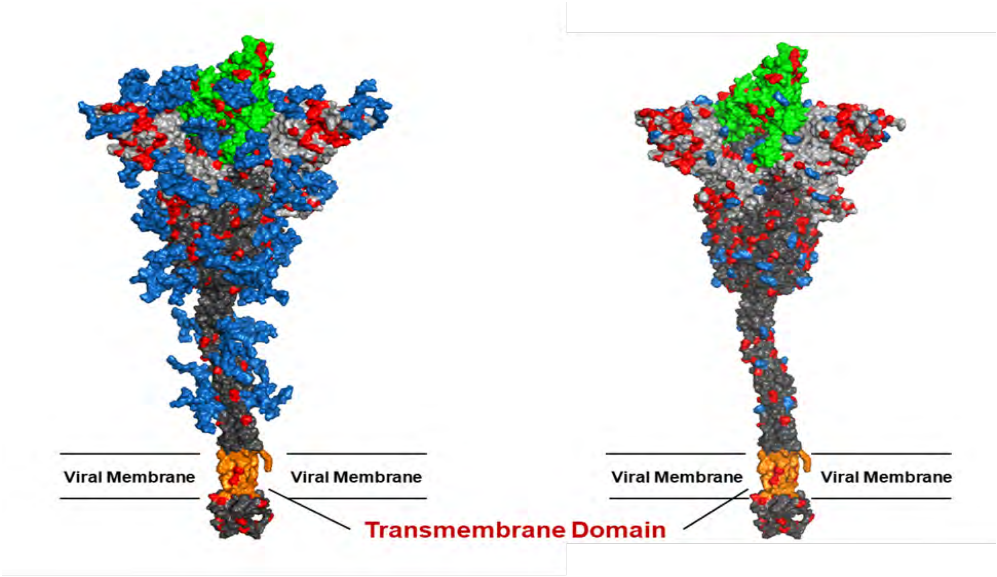

Figure 6. (Left) Fully Glycosylated Spike Protein; (Right) Mono-GlcNAc Decorated (or Low-Sugar) Spike Protein. Green RBD; gray S1; dark gray S2; blue glycans; red mutation sites (mutation rate >0.05%).

We found that when the N-glycans of the wild-type spike protein are trimmed down to a mono-GlcNAc decorated glycoform (Figure 6), it induced enhanced and broadly protective antibody, CD4 and CD8 T-cell responses against all variants of concern, including alpha, beta, gamma, delta and omicron variants (Figure 7).

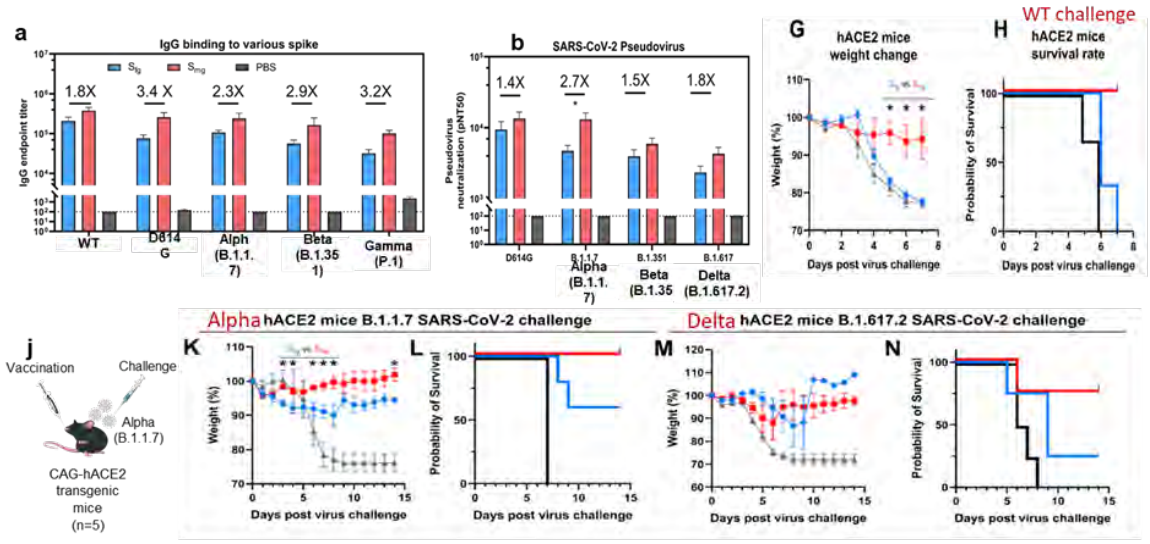

Figure 7. Mono-GlcNAc decorated (or low-sugar) spike vaccine exhibited enhanced binding, neutralization breadth and potency against SARS-CoV-2 and variants.

© The AIC 2023. All rights reserved.

We also found that vaccination in mice with the mRNA of S protein with deletion of specific glycosites, especially the N-glycosites in S2, induced more broadly protective antibody and CD8 T-cell responses against the variants of concern compared to the unmodified mRNA vaccine.

Overall, compared to the fully glycosylated S protein, the mono-GlcNAc decorated (or low-sugar) S protein vaccine generated stronger antibody and CD8 T-cell responses to S protein and stronger protective activity against variants of concern as shown in the neutralization and challenge study [13].

Using the single B cell technology, we isolated the splenocytes of mice immunized with the low-sugar S vaccine and used the fully glycosylated S protein to sort B cells for analysis, and we have identified several broadly neutral-izing antibodies, and one of these anti-bodies recognized a conserved region in RBD (417-482) with picomolar affinity and neutralizing activity. This antibody could not be generated from vaccination of the fully glycosylated S protein, probably due to the shielding of N-glycans, especially at N-165. The broadly neutralizing antibody identified from immunization of mono-GlcNAc decorated S further demonstrated that removal of shielded glycans from S protein is an effective strategy for development of a broadly protective vaccine against SARS-CoV-2 and variants.

The development of low-sugar S protein as a broadly protective vaccine is based on the strategy used in our previous development of universal vaccines against influenza virus. Like S protein, the cell surface hemagglutinin (HA) of influenza is also a trimer and each monomer contains 6 N-glycosites. We also found that the regions covered by glycans are highly conserved. We then treated the H5N1 HA protein with endoglycosidase H to make low-sugar HA (Figure 8).

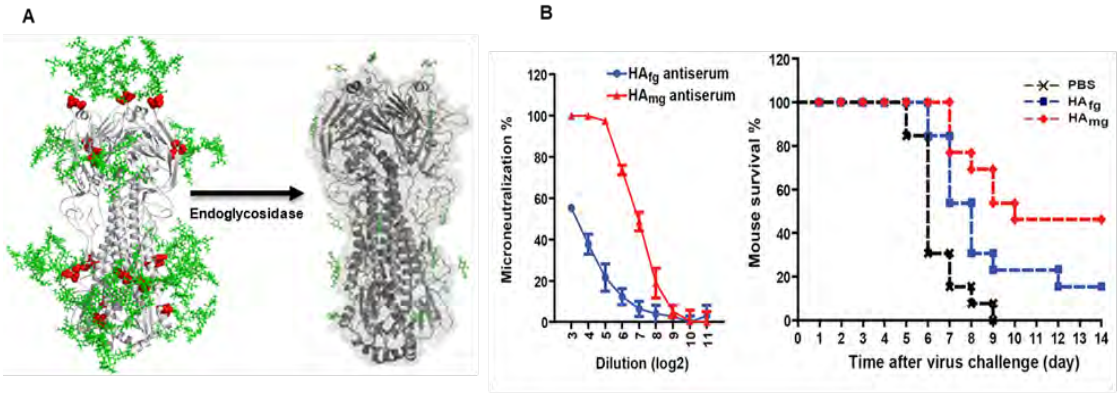

Figure 8. Development of broadly protective influenza vaccine using trimeric hemagglutinin with all 18 N-glycans trimmed down to the mono-GlcNAc state as immunogen. Such a low-sugar vaccine induced more antibodies, and CD4 (as well as CD8) T-cell responses to the conserved stem of hemagglutinin showed improved neutralization in the cell-based assay and better protection in the challenge study.

© The AIC 2023. All rights reserved.

Compared to the fully glycosylated HA, immunization of the low-sugar HA in mice generated stronger antibody and T-cell responses against H5N1 and subtypes with cross reaction against H1N1, as shown in the microneutral-ization and challenge study. Most recently, we have constructed a chimeric HA vaccine with a consensus H5 sequence as head and a consensus H1 as stem and trim the glycans of the chimeric HA to the low-sugar state. Immunization of this chimeric HA vac-cine generated a strong immune response against various H1 and H5 subtypes, and neutralized H3, H7 and H9 subtypes [14]. This chimeric HA vaccine is also highly protective against various H1N1 and H5N1 subtypes in the challenge study.

To further improve the efficacy of antibody against influenza virus, we modified the glycan of antibody FI6 which is active against most type A influenza viruses. It is known that the glycosylation of antibody at Asn-297 will affect its binding to Fc receptors on immune cells and subsequently the effector functions such as antibody-dependent cellular cytotoxicity (ADCC), antibody-dependent cellular phargo-cytosis (ADCP), complement dependent cytotoxicity (CDC) and vaccinal effect. We first trim the antibody glycan to GlcNAc followed by enzymatic trans-glycosylation to prepare a series of homo-geneous antibodies with well-defined glycan in Fc and measure their interaction with FcγIIIA receptor *in vitro* with biacore assay. This interaction is a measure of ADCC and through analysis of various homogeneous glycoforms, we found that the 2,6-siayl complex-type biantennary glycan (SCT) is the best glycan for FcγIIIA binding and is also the best for ADCC as shown in the cell-based and challenge study in mice (Figure 9).

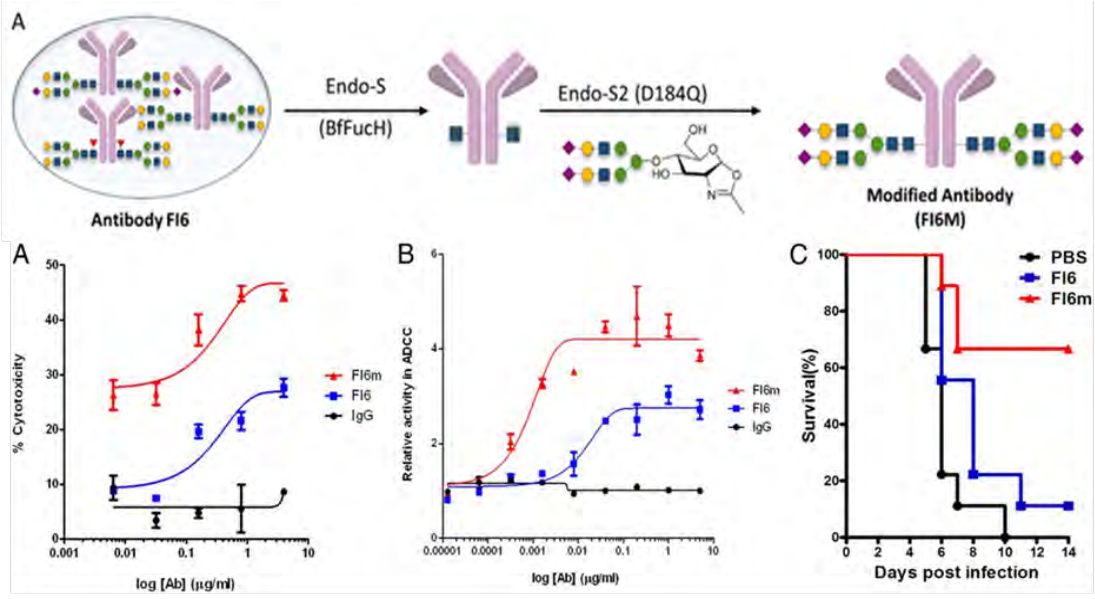

Figure 9. Optimization of broadly neutralizing anti-Influenza antibody Fl6 through glycoengineering of the Fc glycan to SCT to improve the cytotoxicity, ADCC and survival rate.

© The AIC 2023. All rights reserved.

So, any therapeutic antibody can be optimized through glycoengineering as shown here. Recently, we solved the structure of the Fc moiety containing the SCT glycan, showing that the glycan is more attached to the protein to make a better interaction with the receptor FcγIIIA (Figure 10).

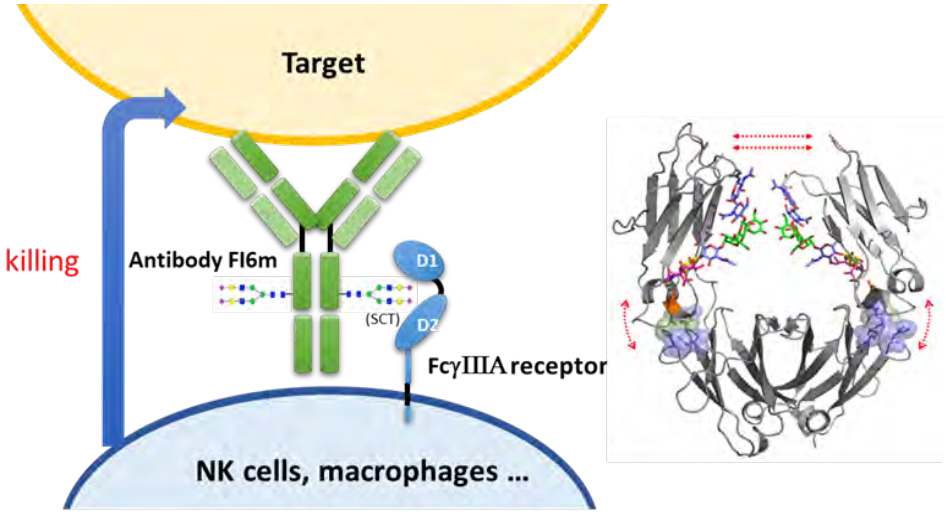

Figure 10. (Left) Homogeneous antibody with well-defined Fc-glycan (2,6-sialyl biantennary glycan) optimized for antibody dependent cellular cytotoxicity; (Right) X-ray structure of Fc-SCT showed that SCT is more attached to the antibody backbone to facilitate FcγIIIA-receptor binding.

6. Broadly Effective Carbohydrate Vaccine and Antibody against Cancer

Identifying a non-self protein antigen for cancer vaccine development is a real challenge; because cancer cells are derived from normal cells, it is difficult to find such unique proteins, if they exist. So, we decided to go after unique glycans on the cancer cell surface. The reason is that glycans are smaller in size compared to proteins and they are assembled by multiple enzymes. If the assembly lines go wrong, the glycan structure will change, and we may have a better chance to find cancer-specific glycan structures that are not present in normal cells. Since cancer cells are usually highly fucosylated and sialylated, we used the alkyne-containing glycosylation probes to monitor the fucosylation and sialylation process in normal and cancer cells (Figure 11, [15]).

© The AIC 2023. All rights reserved.

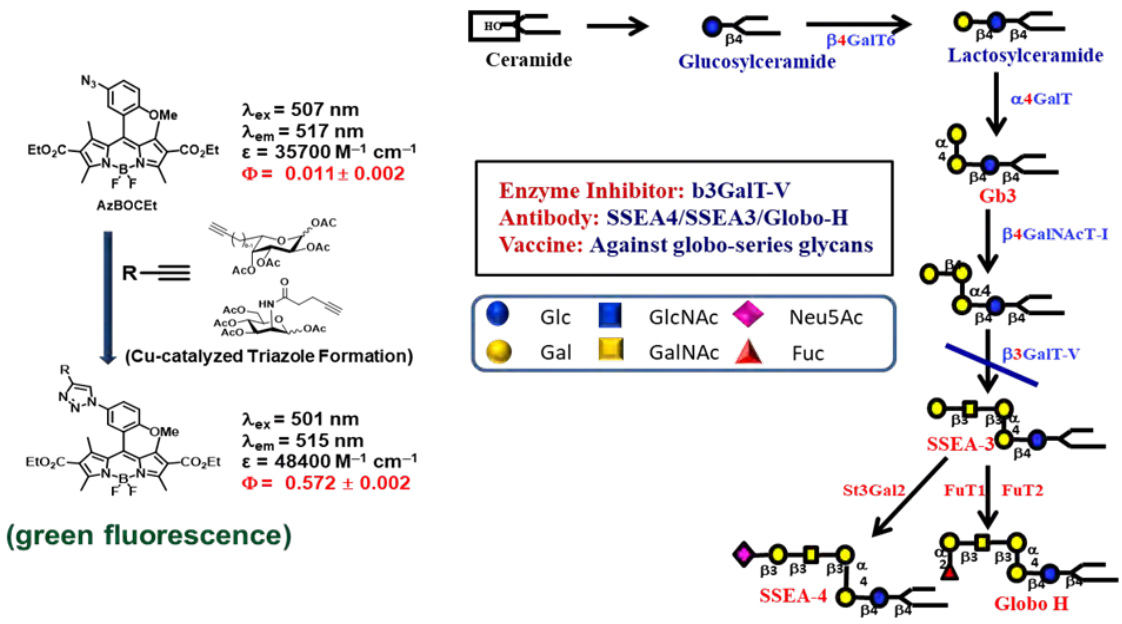

Figure 11. Identification of cancer cell-specific glycans using glycosylation probes of fucose and sialic acid containing an alkyne group. After incorporation of the probes into glycoconjugates, the cells are fixed and reacted with azido-BODIPY to form a green fluorescent triazole for LC-MS analysis to confirm that the globo-series glycans are cancer specific.

We first feed the cells with a probe to let the sugar probe incorporate into glycoproteins or glycolipids. We then fix the cell and mixed the fixed cell with BODIPY-azide for click reaction to form the fluorescent triazole adduct, that is then separated by gel and the glycan structure is determined by LC/MS analysis.

Using these probes, the globo-series glycolipids are often identified from different kinds of cancer cells, and they are absent in normal cells. These glycolipids include SSEA3, Globo-H and SSEA4, which are originally expressed on embryonic stem cells but disappear after differentiation. For some reason, they show up again in cancer cells. So far, we found that at least 15 types of cancer have expressed globo-series glycolipids, and the key enzyme that drives the expression of these glycolipids is a galactosyltransferase called B3GalT5, which catalyzes the galactosylation of Gb4 to SSEA3 and is then converted to SSEA4 and Globo-H. Using the pull-down experiment, we found that CAV1 and FAK interact with SSEA4 and Globo-H, respectively, and then AKT and RIP interact with CAV1 and FAK to form a complex. Knockdown of B3GALT5 in breast cancer cell stopped the synthesis of globo-series glycolipids and caused dissociation of the protein complex; RIP then interacts with FADD and activates caspase leading to cell apoptosis. However, the knockdown has no effect on normal cells. We also found that SSEA4 is increasingly expressed in tyrosine kinase inhibitor (TKI)-resistant non-small cell lung cancer (NSCLC) with T790M mutation; without T790M mutation, there is no significant change in the SSEA4 level. This study suggests that the TKI-resistant non-small lung cancer

© The AIC 2023. All rights reserved.

cells with T790M mutation have high expression of SSEA4 which may be a good target for therapeutic development.

Previous study showed that SSEA4 is a good target for antibody therapy against pancreatic cancer that has high expression of SSEA4 [16]. The chimeric SSEA4 antibody chMC813-70 was engineered to have the SCT glycan or the more stable 3FSCT derivative in the Fc region to enhance ADCC (Figure 12).

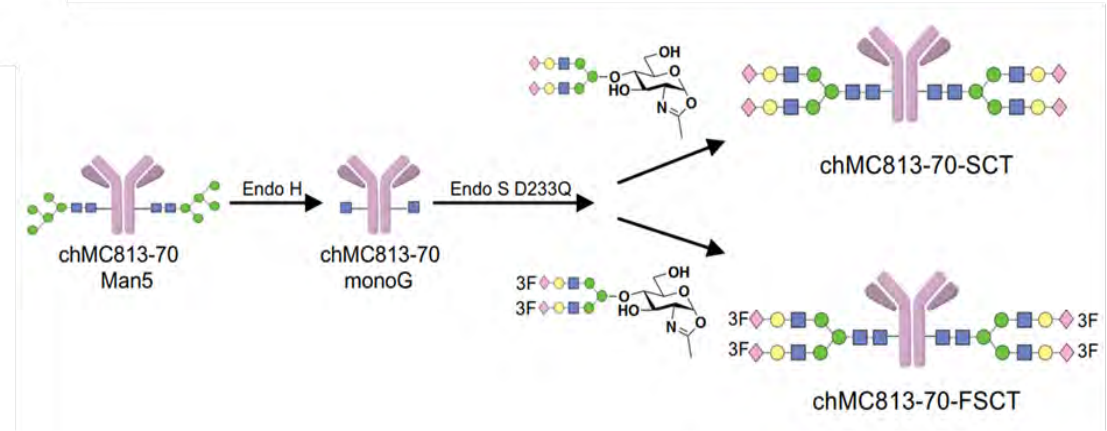

Figure 12. Homogeneous Anti-SSEA-4 Antibodies with Maximal ADCC Activity Through Fc Glycoengineering

As shown in the cell-based assay, the homogeneous antibody is more effective than the unmodified antibody against the three pancreatic cancer cell lines expressing different levels of SSEA4, and it is more effective against HPAC cells with higher expression of SSEA4. The homogeneous antibody can also be used to isolate a subpopulation of NK cells enriched with FcγIIIA receptor for ADCC. The isolated NK cells indeed showed 6-fold more effective than the unseparated NK cells in killing the target cells.

This work demonstrated that the Fc glycan of an antibody can be engineered to optimize its interaction with a specific Fc receptor to improve the corresponding specific effector function, and the homogeneous antibody can also be used to isolate a specific population of immune cells enriched with specific Fc receptor for cell-based therapy.

Globo-H was also used to develop cancer vaccines through conjugation to KLH or DT, and adjuvanted with QS21 or C34. The Globo-H/KLH/QS21 vaccine was developed by the Danishefsky group and synthesized by our method and now is in phase 3 global trial for the treatment of Globo-H positive triple negative breast (TNB) cancer patients. The Globo-H/DT/C34 vaccine developed by us with C34 adjuvant designed to increase IgG response is in phase 2 trial for the treatment of different cancers with Globo-H expression. It is interesting that both vaccines can induce immune responses to target not only Globo-H, but also the other two globo-series glycans, namely SSEA3 and SSEA4 [17].

To understand why the GH-DT vaccine induces immune response against the three globo-series glycans, we mixed dendritic cells with the vaccine and investigated how the vaccine is processed

© The AIC 2023. All rights reserved.

and presented using antibody staining and LC-MS analysis. We found that Globo-H is first processed by fucosidase 1 in early endosome to generate SSEA3, which is the common epitope of these three globo-series glycans. We also found that the antigen presentation is mainly through MHCII to produce anti-Globo-H antibody and anti-SSEA3 antibody that cross-reacted with SSEA4. When SSEA4-DT was used as a vaccine, the glycan was very slowly processed, and the antibody generated is mainly specific for SSEA4, while in the case of SSEA3-DT, it was quickly processed to the less immunogenic glycans Gb4, Gb3 and Gb2 to induce a weak and non-specific antibody response.

7. Conclusion

In summary, glycosylation is an important biological modification for normal and disease processes. Understanding the role of glycans and the associated glycolsylation reaction in biology will facilitate the development of better strategies for treatment or prevention of diseases associated with carbohydrate recognition. Over the years, advances in carbohydrate chemistry and glycobiology have made important contributions to help reach this goal.

8. Acknowledgment

Many thanks to the coworkers in the past to participate in this research, to the core facilities at Academia Sinica and Scripps Research for help to carry out the analytical and animal experiments. This work was supported by Academia Sinica, NIH and NSF

.

9. References

1. Krasnova L, Wong CH. *J. Am. Chem. Soc.*, 2019, 141, 9, 3735–3754.

2. Zhang Z, Ollmann IR, Ye XS, Wischnat R, Baasov T, Wong C. *J. Am. Chem. Soc.*, 1999, 121, 734-53.

3. Cheng CW, Zhou Y, Pan WH, Dey S, Wu CY, Hsu WL, Wong CH. *Nat. Commun.*, 2018, 9, 5202.

4. Chang CW, Lin MH, Chan CK, Su KY, Wu CH, Lo WC, Lam S, Cheng YT, Liao PH, Wong CH, Wang CC. *Angew. Chem. Int. Ed.*, 2021, 60, 12413-12423.

5. Dey S, Lo HJ, Wong CH. *J. Am. Chem. Soc.*, 2019, 141, 26, 10309–10314.

6. Pardo-Vargas A, Delbianco M, Seeberger PH. *Curr. Opin. Chem. Biol*., 2018, 46, 48–55.

7. Tsai TI, Lee HY, Chang SH, Wang CH, Tu YC, Lin YC, Hwang DR, Wu CY, Wong

© The AIC 2023. All rights reserved.

CH. *J. Am. Chem. Soc.*, 2013, 135, 14831-14839.

8. Liao HY, Hsu CH, Wang SC, Liang CH, Yen HY, Su CY, Jan JT, Ren CT, Cheng TJ, Wu CY, Wong CH. *J. Am. Chem. Soc.*, 2010, 132, 14849-14856.

9. Shivatare SS, Chang SH, Tsai TI, Tseng SY, Lin YS, Cheng YY, Ren CT, Pawar S, Tsai CS, Shi HW, Zeng YF, Liang CH, Kwong PD, Burton DR, Wu CY, Wong CH. *Nat. Chem.*, 2016, 8, 338-346.

10. Shivatare VS, Shivatare SS, Lee CC, Liang CH, Liao KS, Cheng YY, Saidachary G, Wu CY, Lin NH, Kwong PD, Burton D, Wu CY, Wong CH. *J. Am. Chem. Soc.*, 2018, 140, 5202-5210.

11. Hanson SR, Culyba EK, Hsu TL, Wong CH, Kelly JW, Powers ET. *Proc. Nat. Acad. Sci. U.S.A.*, 2009, 106, 3131-3136.

12. Culyba EK, Price JL, Hanson SR, Dhar A, Wong CH, Gruebele M, Powers ET, Kelly JW. *Science*, 2011, 331, 571-575.

13. Huang HY, Liao HY, Chen X, Cheng CW, Wang SW, Shahed-Al-Mahmud M, Chen TH, Lo JM, Liu YM, Ma HH, Chang, YH, Tsai CY, Huang PY, Chang SY, Chao TL, Kao HC, Tsai YM, Chen YH, Chen CY, Lee KC, Wu CY, Jan JT, Lin KI, Cheng TJR, Ma C, Wong CH *Sci. Transl. Med.*, 2022, 14, *eabm0899.*

14. Chen JR, Yu YH, Tseng YC, Chiang WL, Chiang MF, Ko YA, Chiu YK, Ma SH, Wu CY, Jan JT, Lin KI, Ma C, Wong CH. *Proc. Nat. Acad. Sci. U.S.A.*, 2014, 111, 2476-2481.

15. Shie JJ, Liu YC, Lee YM, Lim C, Fang JM, Wong CH. *J. Am. Chem. Soc.*, 2014, 136, 9953-9961.

16. Lin CW, Wang YJ, Lai TY, Hsu TL, Han SY, Wu HC, Shen CN, Dang V, Chen MW, Chen LB, Wong CH. *Proc. Nat. Acad. Sci. U.S.A.*, 2021, 118, e2114774118.

17. Samuel J. Danishefsky SJ, Shue YK, Chang MN, Wong CH. *Acc. Chem. Res.*, 2015, 48, 3, 643–652.

© The AIC 2023. All rights reserved.

The Chemist
Journal of the American Institute of Chemists

Marine Microbial Siderophores: Reactivity and Structural Diversity

Alison Butler

Department of Chemistry and Biochemistry, University of California
Santa Barbara, CA 93106-9510

Abstract: Most bacteria require iron to grow, yet soluble forms of iron are largely not available to microbes due to a combination of low solubility of ferric ion in the environment and sequestration in proteins and enzymes in living organisms. Microbes therefore compete for iron in various ways, including by production of siderophores, which are ligands with a high affinity for ferric ion and which facilitate transport of Fe(III) into and within bacteria. This review summarizes our work on the classes of siderophores isolated from open ocean isolates, including suites of amphiphilic siderophores that vary in the nature of the fatty acid appendages, photoreactive Fe(III)-siderophore complexes as a result of coordination to α-hydroxy carboxylic acid groups, and a new series of tris catechol siderophores.

Key Words: Siderophores

1. Introduction

The majority of bacteria require iron to grow [1,2], yet readily accessible forms of iron are not generally available to microbes because of the low solubility of ferric ion in the environment or because cellular iron is sequestered in proteins and enzymes within host organisms. In contrast to the abundance of iron in the Earth's crust – being the fourth most abundant element and the most abundant transition metal – the iron concentration in surface ocean waters is vanishingly small – at only 0.01-2 nM across open ocean regimes [3-7]. At the initial point of our investigations, we reasoned that oceanic microbes must either have evolved a special means to sequester iron, despite its low abundance in surface sea water, or that marine microbes make use of metal ions other than iron for key metabolic processes.

Many bacteria when stressed for iron produce siderophores – low molecular weight natural products that bind Fe(III) with high affinity. Siderophores can solubilize colloidal iron oxides or in some cases remove Fe(III) bound in proteins, and by so doing facilitate microbial uptake of the Fe(III)-siderophore complex. Siderophores are distinguished by

© The AIC 2023. All rights reserved.

the key functional groups that coordinate Fe(III), including catechols, hydroxamic acids, and α-hydroxycarboxylic acids, among other groups (Figure 1).

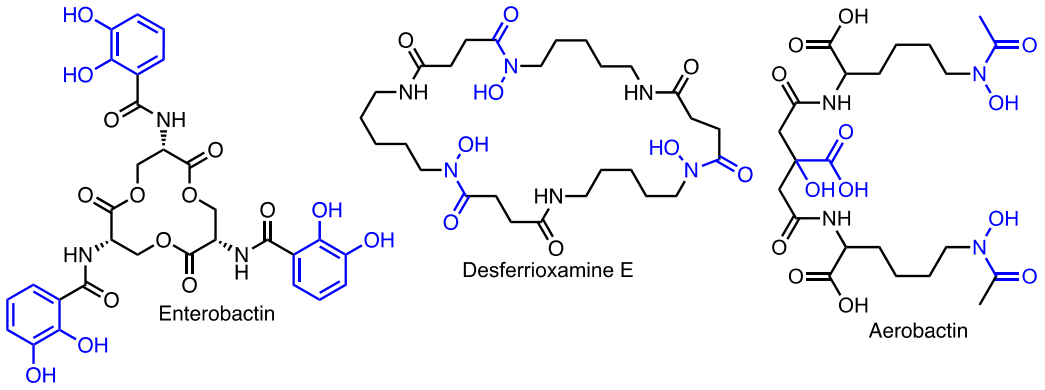

Figure 1. Structures of the siderophores enterobactin, with catechol shown in blue, desferrioxamine E with E-isomer of hydroxamic acid shown in blue, and aerobactin with the central α-hydroxycarboxylic acid shown in blue along with the Z isomers of hydroxamic acid shown in blue. The hydroximate will reside in the Z isomer on metal complexation.

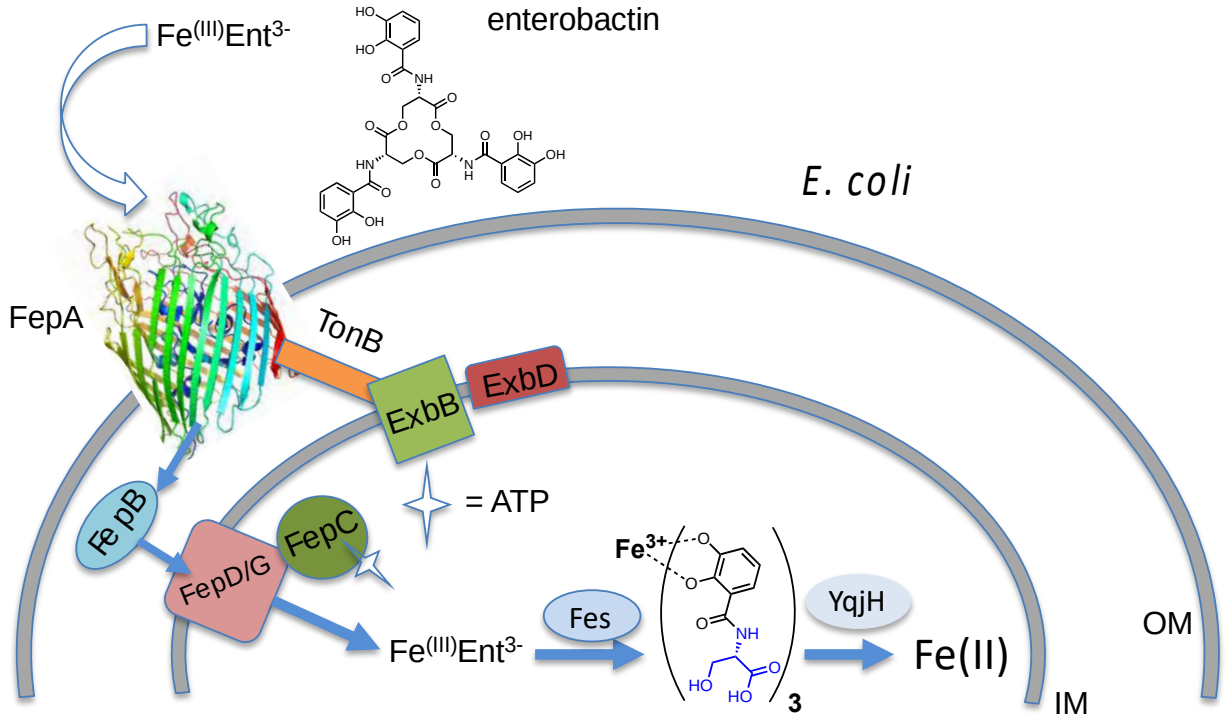

Figure 2. Uptake of $Fe^{III}Ent^{3-}$ via the OMR FepA in *E. coli*. After crossing the OM, $Fe^{III}Ent^{3-}$ is passed to the periplasmic binding protein, FepB, which delivers $Fe^{III}Ent^{3-}$ to FepDGC to facilitate transfer across the inner membrane; this process is accompanied by ATP hydrolysis, as well as with the TonB/ExbB/ExbD system. Once in the cytoplasm, Fes catalyzes hydrolysis of the Ser ester bonds, forming $Fe^{III}(DHB\text{-}^{L}Ser)_3^{3-}$. At this point the reductase YqiH can reduce Fe(III) in $Fe^{III}(DHB\text{-}^{L}Ser)_3^{3-}$ to Fe(II). OM, outer membrane; IM, inner membrane.

© The AIC 2023. All rights reserved.

Bacteria generally internalize Fe(III)-siderophores in an active energy-dependent manner tied to ATP hydrolysis (Figure 2) [1,2]. The first point of Fe(III)-siderophore recognition and uptake by Gram-negative bacteria occurs via a specific outer membrane receptor (OMR) protein at the cell surface. After crossing the outer membrane, a periplasmic binding protein and inner membrane transport proteins are involved in transporting the Fe(III)-siderophore to the cytoplasm. Once in the cytoplasm, iron must be removed from the Fe(III)-siderophore complex, which may involve subsequent interactions with esterases or amidases depending on the siderophore, as well as reductases to release Fe(II).

The biosynthetic origin, structure and coordination chemistry of siderophores have captured the interests of bioinorganic chemists for decades. Early siderophore investigations demonstrated the staggeringly large proton-independent stability constant of tris catecholate siderophores, such as enterobactin (Ent; 10^{49}) [8] and bacillibactin (BB; $10^{47.6}$) [9] for Fe(III). Experiments addressing how iron is released from Fe(III)-Ent^{3-} led to the discovery of the esterase that hydrolyzes each Ser-ester bond in Fe(III)-Ent^{3-} and the reductase that can then reduce Fe(III) to Fe(II) (Figure 2). Even tris hydroxamate siderophores, such as the desferrioxamines, with proton-independent stability constants for Fe(III) at about $10^{31\pm1}$ are still very high [10,11].

Ester hydrolysis may actually occur in the periplasm in some cases. It is a key component for some bacteria such as *Campylobacter jejuni*, in which the periplasmic binding protein VueE preferentially binds the Fe(III) complex of the enterobactin fragment with two catechol groups and two ^{L}Ser, i,e, (DHB-^{L}Ser)$_2$ [12].

2. Initial Sortie into the Discovery of Marine Bacterial Siderophores

As an inorganic chemist who loves coordination chemistry, I became fascinated by siderophores, which held significance as one of Nature's biological ligands. As a chemist also fascinated by the marine environment, I was intrigued by the unusual transition metal ion composition of the surface ocean water, with the two most abundant transition metal ions being molybdenum and vanadium, yet iron being quite low, and I wondered about the attendant effect on the bioinorganic chemistry of the marine environment. While bacteria are thought to require mM Fe to grow, Fe levels in the ocean are far less than mM over much of the World's surface ocean waters. Intriguingly, over 99% of the Fe(III) in surface ocean waters is complexed by a class or classes of organic ligands called "L" [5,7,13]. Many oceanographers asked, "What is L?" While organic complexation of Fe(III) certainly serves to increase the solubility of Fe(III) in the confines of pH 8 ocean water, the origin and identity of these ligand classes is still a topic of much interest. Independent of the nature of L, we became intrigued with identifying characteristics of siderophores produced by open ocean bacteria.

© The AIC 2023. All rights reserved.

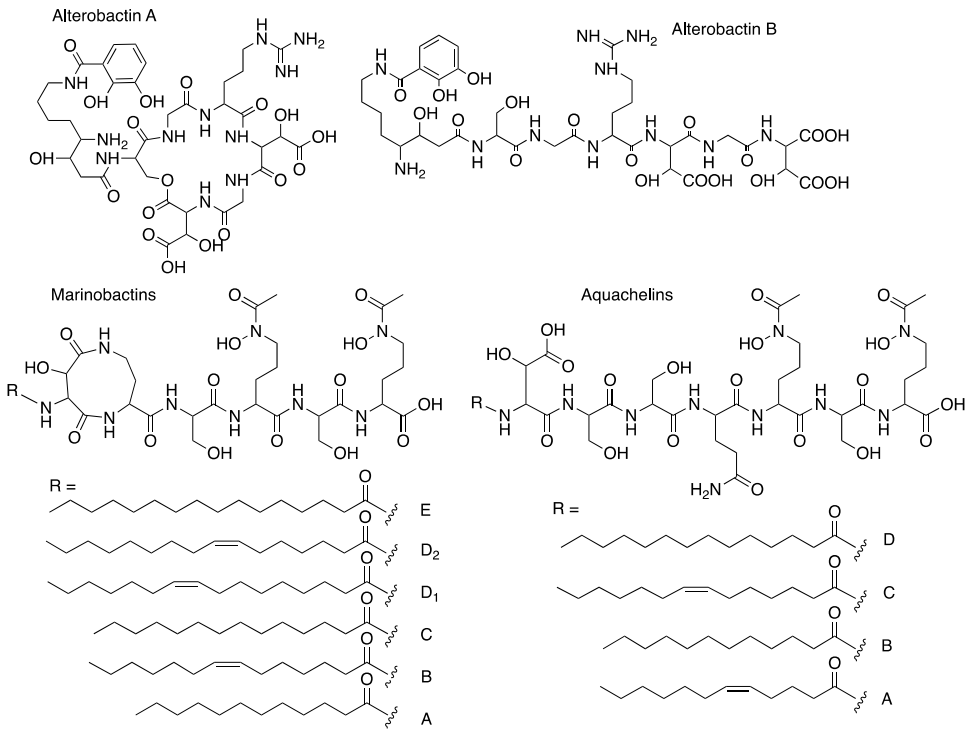

Figure 3. Structures of the alterobactins A and B (*Pseudoalteromona luteoviolea)* [14], marinobactins (*Marinobacter sp.* DS40M6) [15], and aquachelins (from *Halomonas aquamarina* DS40M3) [15].

The alterobactins A and B (Figure 3) [14] were the first siderophores we isolated from a marine bacterium. Alterobactin A has an especially high affinity for Fe(III), with a proton-independent stability constant of 10^{49-53} [14]. The range reflects an estimation of the pK_a of each β-hydroxyl proton because it is too high to measure directly. Square wave voltammetry corroborated the high stability constant of Fe(III)-Alterobactin A giving a value of $10^{51\pm2}$ [16].

After characterizing the alterobactins, the 2nd siderophores we identified from an open ocean bacterial isolate was the well-known terrestrial siderophore, aerobactin (Figure 1) [17]. As a result of the discovery of a common siderophore, we very nearly stopped the project, except that we were also working simultaneously on a series of siderophores from other open ocean isolates that had masses varying by 2 or 28 mass units. The close but distinct retention times on the HPLC of these compounds suggested they were related and possibly indicative of desaturation and variation by $-CH_2-CH_2-$, respectively, such as could occur in fatty acids. This mass variation turned out to be due to a suite of peptidic siderophores with a series of a fatty acid appendages, as shown for the first two suites of peptidic amphiphilic siderophores we isolated, the marinobactins and aquachelins (Figure 3) [15]. Thus, we didn't abandon our investigations into marine microbial siderophores.

© The AIC 2023. All rights reserved.

3. Suites of Amphiphilic Siderophore

Suites of siderophores with fatty acid appendages dominated the next set of siderophores we isolated from marine bacteria, with the discovery of the amphibactins (Figure 4) [18], which are rather hydrophobic with only four amino acids in the head group with a wide range in fatty acid appendages [18].

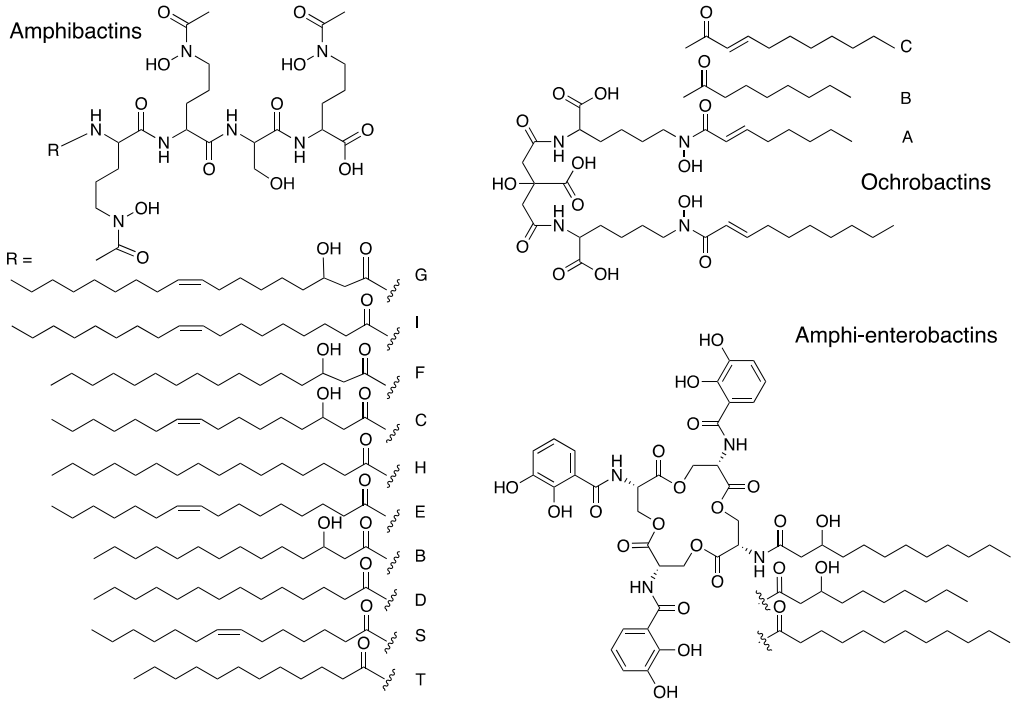

Figure 4. Structures of the amphibactins (*Vibrio* sp. R10) [18], ochrobactins (from *Ochrobactrum* sp. SP18) [24], amphi-enterobactins (from *Vibrio campbellii* BAA1116). This set of amphiphilic siderophores is quite hydrophobic and therefore extraction of the bacterial pellet is required for their isolation.

Subsequent discoveries of families of fatty acyl siderophores with variation in the fatty acid included loihichelins [19], moanachelins [20], and pacifibactins [21]. We also discovered citrate derived siderophores, such as the ochrobactins (Figure 4) in which fatty acids replaced the acetyl group of aerobactin (Figure 1), as well as the amphi-enterobactins (Figure 4) which are expanded version of enterobactin (Figure 1). The tri-Ser macrolactone core of enterobactin is expanded to a tetra-Ser core with a series of fatty acids appended to one of the Ser amines in the amphi-enterobactins [22], but they are also sufficiently hydrophobic that they require extraction from the bacterial pellet.

The fatty acid may serve as a means for the bacterium to retain its siderophore and to limit diffusion. In general investigations on fatty acyl siderophore partitioning into membranes, we found that siderophores with longer fatty acids partitioned to a much greater extent but also that the Fe(III) complexes of the amphiphilic siderophores partitioned less into membranes than the apo

© The AIC 2023. All rights reserved.

siderophore, which suggests a possible functional significance in the recognition and uptake process for Fe(III)-siderophores [23,24].

The amphibactins have been isolated directly from seawater and identified by mass spectral analysis in comparison to our previous mass spectral characterization [25,26]. Other non-amphiphilic hydroxamate siderophores, such as desferrioxamine G and E (Figure 1) are also reported to be widely distributed in the euphotic zone of the Atlantic Ocean [27].

4. Photoreactivity of Fe(III) Siderophores with α-Hydroxy Carboxylate Groups

The photochemistry of ferric complexes of citric acid is well known [28]. Citrate forms the backbone of several siderophores, including aerobactin (Figure 1), in which the central group is an α-hydroxy carboxylate that is one of the coordinating ligands to Fe(III). In peptidic siderophores, β-hydroxyaspartic acid, is also an α-hydroxy carboxylate that coordinates Fe(III). Thus, we reasoned that Fe(III) complexes of β-hydroxyaspartate and citrate in siderophores would likely be photoreactive and undergo ligand oxidation with reduction of Fe(III) to Fe(II).

β-hydroxyaspartate-containing siderophores. The first demonstration of a photoreactive Fe(III) siderophore complex was with the peptidic aquachelin siderophores [29]. Since this time, all investigations of Fe(III) siderophore complexes containing β-hydroxyaspartate have been shown to be photoreactive on UV photolysis into the α-hydroxy-acid-to-Fe(III) charge transfer band. In the case of aquachelin, the photo product retains two hydroxamate ligands (Figure 5) and this binds Fe(III), although with a lower stability constant [29].

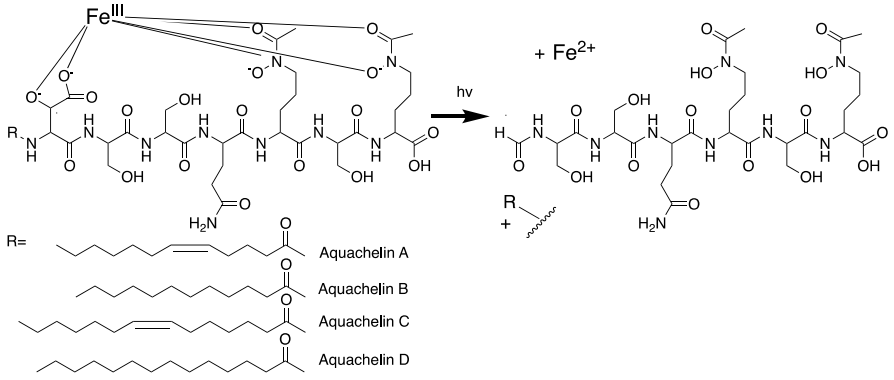

Figure 5. UV Photoreactivity of Fe(III)-aquachelin [29]

© The AIC 2023. All rights reserved.

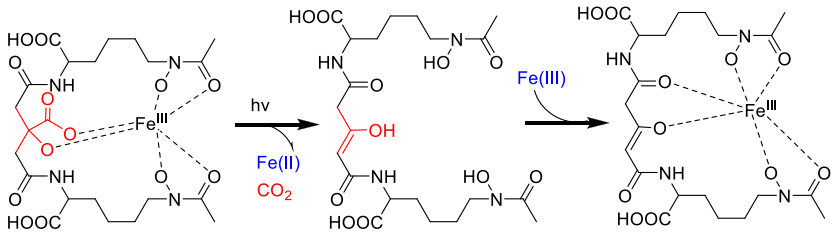

Figure 6. UV Photoreactivity of Fe(III)-aerobactin [31]

Citrate-containing siderophores. Fe(III)-aerobactin with citrate in the siderophore backbone is also photoreactive (Figure 6) [17], as are the Fe(III)-ochrobactins [24], the Fe(III)-synechobactins [30], and the Fe(III)-petrobactins. In these complexes the reaction is quite clean on UV photolysis into the LMCT band with oxidation of the ligand and reduction of Fe(III) to Fe(II) [31]. The decrease of 46 mass units in the apo-photoproduct reflects loss of CO_2 and two H^+. The oxidized citryl group in aerobactin produces the corresponding 3-ketoglutaryl derivative, which is in equilibrium with the enoyl derivative used for Fe(III) coordination [31]. We discovered that the affinity of the aerobactin photoproduct is surprisingly high with nearly the same stability constant as for aerobactin [31,32].

UV photolysis of the ferric complexes of the ochrobactins (Figure 4) [24], the synechobactins [30], and the petrobactins [33] produce the same conversion of the citrate backbone to 3-ketoglutarate and coordination of Fe(III) by the enolate form in the photoproduct.

As shown above, two structural features dominated the types of siderophores we discovered initially in marine bacteria: that is, a) families of amphiphiles, comprising an iron(III)-binding head-group that is appended by a series of fatty acids; and b) the presence of an α-hydroxycarboxylic acid group in the form of β-hydroxyaspartic acid or citric acid, which are photoreactive when coordinated to Fe(III) [29,31]. Many marine siderophores are both amphiphilic and photoreactive when Fe(III) is coordinated.

5. Triscatechol Siderophores Form a New Emerging Class of Marine Siderophores

Triscatechol siderophores may be another emerging class of marine siderophores in which the catechol is 2,3-dihydroxybenzoic acid (DHB). While the triscatechol siderophores enterobactin [Ent; i.e., (DHB-^{L}Ser)$_3$, Figure 1] and bacillibactin [BB, (DHB-Gly-^{L}Thr)$_3$], each coordinate Fe(III) with three 2,3-DHB ligands framed on a macrolactone derived from three ^{L}Ser or ^{L}Thr residues, respectively, they have not been identified in marine bacteria.

© The AIC 2023. All rights reserved.

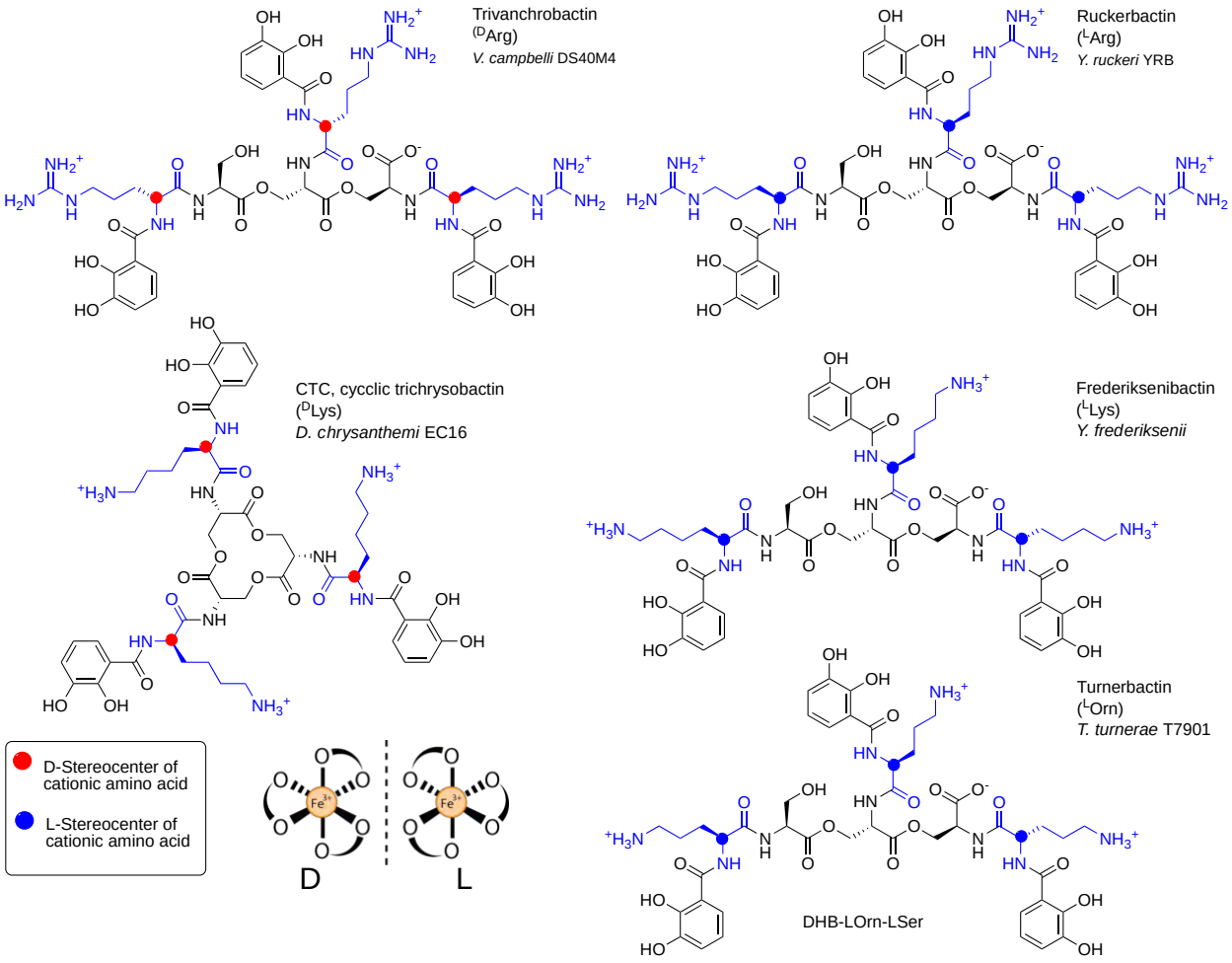

Figure 7. Structures of trivanchrobactin [34], ruckerbactin [35], cyclic tri-chrysobactin, frederiksenibactin [38], and turnerbactin [36]; and a depiction of the D and L stereocenters in the Fe(III)-tris-catecholate complexes. The corresponding siderophore with ^{D}Orn has not yet been reported.

Several related triscatechol siderophores have been isolated from marine bacteria that are distinguished from Ent and BB by the presence of a chiral amino acid inserted between each DHB and the oligo-^{L}Ser ester backbone (Figure 7), including the linear tris-^{L}Ser scaffolds of trivanchrobactin with ^{D}Arg (*Vibrio campbellii* DS40M4) [34], ruckerbactin with ^{L}Arg (*Yersinia ruckerii* YRB) [35], and turnerbactin with ^{L}Orn (*Teredinibacter turnerae* T7901) [36]; these bacteria are all marine isolates. The siderophores with ^{L}Lys and ^{D}Lys are also known and produced by terrestrial isolates. Cyclic trichrysobactin (CTC) with ^{D}Lys is produced by the plant pathogen *Dickeya chrysanthemi* EC16 [37], and frederiksenibactin with ^{L}Lys is produced by the human pathogen, *Y. frederiksenii* ATCC 33641) [38]. Trivanchrobactin and ruckerbactin are true diastereomers with ^{D}Arg and ^{L}Arg, respectively. Frederiksenibactin with ^{L}Lys and CTC with ^{D}Lys are nearly diastereomers, although the former is based on the linear tris-^{L}Ser oligoester and the latter is the cyclic tris-^{L}Ser macrolactone (Figure 7). The biosynthesis of

© The AIC 2023. All rights reserved.

this suite of D/L cationic amine-containing tris catechol siderophores framed on a tri-^{L}Ser oligoester scaffold has been reviewed recently [39], and may well be useful to predicting the full combinatoric suite of this class of siderophores.

The stereochemistry of the amino acid inserted between the DHB and the ^{L}Ser backbone seems to set the stereochemistry of Fe(III) coordination [34,35,37,38]. That is, if an L amino acid is bonded to DHB, the siderophore coordinates Fe(III) in the Δ enantiomeric configuration, and if a D-amino acid is inserted between DHB and ^{L}Ser, the Λ enantiomeric configuration Fe(III)-siderophore confirmation is formed [35,38]. These subtle structural differences suggest the bacteria may have evolved a means to take advantage of the stereochemical differences to promote or control growth.

6. Summary and Future Directions

Our initial foray into marine siderophores started off by screening open ocean water samples for bacteria producing an orange-pink halo when grown on the blue Fe(III)-chromazurol S agar media [40], corresponding to removal of Fe(III) from the blue Fe-CAS complex. We discovered many new siderophores in this manner, although I worried about duplicating our efforts and rediscovering a siderophore we already had previously characterized. The onset of rapid microbial genome sequencing was particularly welcome because it enabled biosynthetic pathways for siderophores to be screened and led to a targeted approach for the discovery of new siderophores.

The question of whether oceanic bacteria make use of metal ions other that iron in their metalloenzymes was posed in the introduction. While that question has not been addressed, it is clear that oceanic bacteria are producing siderophores that coordinate and deliver iron to the source bacterium. However, these siderophores may well be serving to sequester and deliver other metal ions to bacteria also. Preliminary work on the alterobactins shows they can complex molybdate and vanadate, although when Fe(III) is added, the other metals are displaced. Yet the catechol siderophores from *Azotobacter vinlandii*, protochelin and azotochelin have been shown to complex molybdate and vanadate [41], *and* to deliver Mo(VI) and V(V) to the bacterial cell [42,43]. The uptake of Mo(VI) and V(V) is especially important in nitrogen-fixing bacteria due to the demand for Mo, V and Fe in nitrogenases. Other transition metals form complexes with siderophores, including titanium(IV) which binds hydroxamate ligands in siderophores (e.g., desferrioxamine B) and siderophore analogs [44,45]; manganese(III) which binds to pyoverdine [46], and hydroxamate siderophores [47,48]; copper(II) and zinc(II) which bind to yersiniabactin [49,50]; and even zirconium(IV) which binds to hydroxamate siderophores [51,52,53]. In fact, some siderophores may not actually have a preference for Fe(III) but may be part of a growing class of metallophores [54].

© The AIC 2023. All rights reserved.

7. Acknowledgments

I am grateful to all the students and postdocs in my research group who have carried out the investigations on siderophores in my lab. Richard Reid was the first brave student to jump in on this project and his efforts led to the discovery of the alterobactins [14]. Much of our work was in collaboration with Margo Haygood, who has been at SIO-UCSD, Oregon Graduate Institute and the University of Utah – she is an outstanding marine biologist and molecular biologist and an especially a tremendous collaborator and friend. I thank the oceanographers and marine chemists who collaborated with us, including George Luther at University of Delaware, Ken Bruland at UC Santa Cruz, as well as Francois Morel who directed the NSF Center for Environmental Bioinorganic Chemistry (CEBIC) from 1998-2008 (NSF CHE 9810248 & CHE-0221978. I am also grateful to current funding from NSF CHE 2108596.

8. References

1. Crosa JH, Mey AR, Payne SM in Iron Transport in Bacteria, ASM Press, Washington, D.C., 2004.
2. Templeton DM in Molecular and Cellular Iron Transport, Marcel Dekker, Inc., New York, 2002.
3. Martin JH, Gorden RM. *Deep Sea Res.*, 1988, 35, 117-196.
4. Aguilar-Islas AM, Hurst MP, Buck KN, Sohst B, Smith GJ, Lohan MC, Bruland KW. *Prog. Oceanogr.*, 2007, 73, 99-126.
5. Rue EL, Bruland KW. *Mar. Chem.*, 1995, 50, 117-138.
6. Butler A. *Science*, 1998, 281, 207-210.
7. Luther GW, Wu J. *Mar. Chem.*, 1997, 57, 173-179.
8. Loomis LD, Raymond KN. *Inorg. Chem.*, 1991, 30, 906-911.
9. Dertz EA, Xu JD, Stintzi A, Raymond KN. *J. Am. Chem. Soc.*, 2006, 128, 22-23.
10. Spasojević I, Armstrong SK, Brickman TJ, Crumbliss AL. *Inorg. Chem.*, 1999, 38, 449-454.
11. Anderegg G, L'Eplattenier F, Schwarzenbach G. *Helv. Chim. Acta*, 1963, 46, 1400-1408.
12. Raines DJ, Moroz O, Blagova EV, Turkenburg JP, Wilson KS, Duhme-Klair AK. *Proc. Natl. Acad. Sci. U.S.A.*, 2016, 113, 5850-5855.
13. Caprara S, Buck KN, Gerringa LJA, Rijkenberg MJA, Monticelli D. *Front. Mar. Sci.*, 2016, 3.
14. Reid RT, Live DH, Faulkner DJ, Butler A. *Nature*, 1993, 366, 455-458.
15. Martinez JS, Zhang GP, Holt PD, Jung HT, Carrano CJ, Haygood MG, Butler A. *Science*, 2000, 287, 1245-1247.
16. Holt PD, Reid RR, Lewis BL, Luther GW, 3rd, Butler A. *Inorg. Chem.*, 2005, 44, 7671-7676.
17. Haygood MG, Holt PD, Butler A. *Limnol. Oceanogr.*, 1993, 38, 1091-1097.
18. Martinez JS, Carter-Franklin JN, Mann EL, Martin JD, Haygood MG, Butler A. *Proc. Natl. Acad. Sci. U.S.A.*, 2003, 100, 3754-3759.

© The AIC 2023. All rights reserved.

19. Homann VV, Sandy M, Tincu JA, Templeton AS, Tebo BM, Butler A. *J. Nat. Prod.*, 2009, 72, 884-888.
20. Vraspir JM, Holt, PD, Butler, A. *Biometals*, 2011, 24, 85-92.
21. Hardy CD, Butler A. *J. Nat. Prod.*, 2019, 82, 990-997.
22. Zane HK, Naka H, Rosconi F, Sandy M, Haygood MG, Butler A. *J. Am. Chem. Soc.*, 2014, 136, 5615-5618.
23. Xu G, Martinez JS, Groves JT, Butler A. *J. Am. Chem. Soc.*, 2002, 124, 13408-13415.
24. Martin JD, Ito Y, Homann VV, Haygood MG, Butler A. *J. Biol. Inorg. Chem.*, 2006, 11, 633-641.
25. Boiteau RM, Fitzsimmons JN, Repeta DJ, Boyle EA. *Anal. Chem.*, 2013, 85, 4357-4362.
26. Boiteau RM, Mende DR, Hawco NJ, McIlvin MR, Fitzsimmons JN, Saito MA, Sedwick, PN, DeLong EF, Repeta DJ. *Proc. Natl. Acad. Sci. U.S.A.*, 2016, 113, 14237-14242.
27. Mawji E, Gledhill M, Milton JA, Tarran GA, Ussher S, Thompson A, Wolff GA, Worsfold PJ, Achterberg EP. *Environ. Sci. Technol.*, 2008, 42, 8675-8680.
28. Abrahamson HB, Rezvani AB, Brushmiller JG. *Inorg. Chim. Acta*, 1994, 226, 117-127.
29. Barbeau K, Rue EL, Bruland KW, Butler A. *Nature*, 2001, 413, 409-413.
30. Ito Y, Butler A. *Limnol. Oceanogr.*, 2005, 50, 1918-1923.
31. Kupper FC, Carrano CJ, Kuhn JU, Butler A. *Inorg. Chem.*, 2006, 45, 6028-6033.
32. Harris WR, Carrano CJ, Raymond KN. *J. Am. Chem. Soc.*, 1979, 101, 2722-2727.
33. Hickford SJ, Kupper FC, Zhang G, Carrano CJ, Blunt JW, Butler A. *J. Nat. Prod.*, 2004, 67, 1897-1899.
34. Sandy M, Han A, Blunt J, Munro M, Haygood M, Butler A. *J. Nat. Prod.*, 2010, 73, 1038-1043.
35. Thomsen E, Reitz ZL, Stow PR, Dulaney K, Butler A. *J. Nat. Prod.*, 2022, 85, 264-269.
36. Han AW, Sandy M, Fishman B, Trindade-Silva AE, Soares CA, Distel DL, Butler A, Haygood MG. *PLoS One*, 2013, 8, e76151.
37. Sandy M, Butler A. *J. Nat. Prod.*, 2011, 74, 1207-1212.
38. Stow PR, Reitz ZL, Johnstone TC, Butler A. *Chem. Sci.*, 2021, 12, 12485-12493.
39. Reitz ZL, Sandy M, Butler A. *Metallomics*, 2017, 9, 824-839.
40. Schwyn B, Neilands JB. *Anal. Biochem.*, 1987, 160, 47-56.
41. Duhme A.-K, Hider R, Naldrett M, Pau R. *J. Biol. Inorg. Chem.*, 1998, 3, 520-526.
42. Wichard T, Bellenger JP, Morel FMM, Kraepiel AML. *Environ. Sci. Technol.*, 2009, 43, 7218-7224.
43. McRose DL, Baars O, Morel FMM, Kraepiel AML. *Environ. Microbiol.*, 2017, 19, 3595-3605.
44. Uppal R, Israel HP, Incarvito CD, Valentine AM. *Inorg. Chem.*, 2009, 48, 10769-10779.
45. Jones KE, Batchler KL, Zalouk C, Valentine AM. *Inorg. Chem.*, 2017, 56, 1264-1272.
46. Parker DL, Sposito G, Tebo BM. *Geochim. Cosmochim. Acta*, 2004, 68, 4809-4820.
47. Duckworth OW, Sposito G. *Environ. Sci. Technol.*, 2005, 39, 6045-6051.
48. Springer SD, Butler A. *J. Inorg. Biochem.*, 2015, 148, 22-26.

© The AIC 2023. All rights reserved.

49. Koh EI, Henderson JP. *J. Biol. Chem.*, 2015, 290, 18967-18974.
50. Behnsen J, Zhi H, Aron AT, Subramanian V, Santus W, Lee MH, Gerner RR, Petras D, Liu JZ, Green KD, Price SL, Camacho J, Hillman H, Tjokrosurjo J, Montaldo NP, Hoover EM, Treacy-Abarca S, Gilston BA, Skaar EP, Chazin WJ, Garneau-Tsodikova S, Lawrenz MB, Perry RD, Nuccio S-P, Dorrestein PC, Raffatellu M. *Nat. Commun.*, 2021, 12, 7016.
51. Brown CJM, Codd R. *J. Inorg. Biochem.*, 2021, 216, 111337.
52. Richardson-Sanchez T, Tieu W, Gotsbacher MP, Telfer TJ, Codd R. *Org. Biomol. Chem.*, 2017, 15, 5719-5730.
53. Tieu W, Lifa T, Katsifis A, Codd R. *Inorg. Chem.*, 2017, 56, 3719-3728.
54. Reitz ZL, Medema MH, *Curr. Opin. Biotechnol.*, 2022, 77, 102757.

© The AIC 2023. All rights reserved.

The Chemist
Journal of the American Institute of Chemists

Surface Chemistry and Biomolecule Density Impact Adsorbed Cellulase Activity

Danny R. Swofford, Sylvester Guillermo and Thaddeus W. Vasicek†

Department of Chemistry, The Citadel, Charleston, SC 29409
† Corresponding author: tlevasic@citadel.edu

Abstract: Bioethanol produced from inedible biomass has the potential to curtail emissions, maximize usage of agricultural/urban waste and be a renewable energy source. Hydrolyzing cellulose to glucose is a critical step in the production of bioethanol from inedible biomass and can be accomplished through the use of enzymes, cellulases, which hydrolyze cellulose into sugars that are subsequently fermented into ethanol. To diminish the economic impact cellulases impart on the production of bioethanol, cellulases can be immobilized to magnetic nanoparticles enabling their separation and reuse. The functional group and biomolecule density on nanoparticles are intertwining variables that affect the specific activity of immobilized enzymes, a pivotal parameter that need be maximized for an industrial catalyst. This work presents the findings of how functional group and biomolecule density on silica-coated iron oxide nanoparticles relate to the activity of adsorbed cellulases. The adsorption percent correlated to increasing functional group density, while the specific activity was inversely proportional to functional group density. At high functional group densities, the increase in immobilization led to a greater recovery of activity. The results conclude that adsorbing cellulase from dilute solutions to particles with high functional group densities displayed the greatest efficiency for adsorbing cellulases.

Key Words: cellulase, immobilized enzymes, nonspecific absorption, cellulosic ethanol

1. Introduction

There is a critical need to develop sustainable energy sources. Lignocellulose is the most abundant renewable resource and is ~45% cellulose, a polymer of D-glucose linked by β-1,4-glycosidic bonds [1]. Bioethanol derived from cellulose can be a sustainable energy source but requires extensive processing to hydrolyze the cellulose into glucose prior to fermentation into bioethanol.

© The AIC 2023. All rights reserved.

Cellulose hydrolysis can be performed through chemical or enzymatic methods to yield fermentable sugars. Enzymatic hydrolysis of cellulose, using cellulases, has the advantage over non-enzymatic methods as the cellulases operate at gentle temperatures, meaning enzymatic hydrolysis necessitates a lower energy input compared to alternative chemical hydrolysis methods. However, cellulases contribute an appreciable cost to the production of bioethanol which has hindered widespread adoption of enzymatic hydrolysis of cellulose [2,3]. Therefore, lowering the economic cost of cellulases will lead to commercialization of bioethanol from cellulose.

Immobilizing enzymes on solid supports facilitates their separation from product and enables reuse of the enzyme. The chemistry of the support material and method of biomolecule immobilization affect the properties of the immobilized catalyst. There are several types of support being studied for cellulase immobilization such as metal-organic frameworks [4], organic supports [5], and inorganic supports [6]. However, magnetic nanoparticle (MNP) supports facilitate rapid recovery of immobilized catalyst by application of an external magnetic field. The ease with which MNPs can be separated and reused has led to their study as support for cellulase immobilization [7]. The most routine methods of cellulase immobilization are adsorption, covalent attachment, entrapment, and crosslinking [8]. Each method of immobilization offers unique advantages, but adsorption is the simplest method requiring few reagents or steps.

Adsorption relies on nonspecific interactions such as hydrophobic, electrostatic, and/or Van der Waals forces between the enzyme and support. Adsorption, while simple, may lead to deleterious conformational changes of the immobilized biomolecule altering biomolecule activity. Some command over the adsorption process is obtained by controlling the chemistry of the support surface. Amine functional groups are routinely introduced to supports to enhance electrostatic interactions between the support and biomolecule to promote adsorption. A common regent utilized to introduce amine functionality to MNPs is (3-aminopropyl)-triethoxysilane (APTES) [9]. Varying the APTES concentration during modification can be used to introduce varying degrees of amine functional groups [10], which affects immobilized biomolecule densities.

The concentration of the biomolecule solution utilized for immobilization also effects adsorption, with increased adsorption occurring from concentrated biomolecule solutions [11] as the bulk concentration determines the kinetics of the immobilizations process [12]. Concentrated biomolecule solutions will have biomolecules adsorb quickly with close proximity to one another, and lead to a dense protein layer. Slower adsorption kinetics allows initially adsorbed biomolecules time to undergo conformational changes to maximize interactions with the surface. Biomolecules that "spread out" to maximize interactions with the particle surface prevent adsorption by later biomolecules and lower biomolecule density occurs when adsorbed from dilute solutions [12,13].

The surface chemistry and bulk biomolecule concentration jointly determine the adsorption process which determine immobilized quantities and may lead to altered biomolecule activity. Reduced

© The AIC 2023. All rights reserved.

activity is observed at high immobilized biomolecule densities due to steric hindrance imposed by adjacent molecules or by conformational changes at low densities as the biomolecule maximizes contact with the surface [14,15]. It is therefore of great consequence to consider both the bulk biomolecule concentration used for adsorption, and the surface functional group density jointly when optimizing an immobilization method to ensure the support adsorbs an abundance of biomolecules in an active conformation.

Each biomolecule is unique, as will be its interactions with the support [16]. Therefore, the immobilization conditions need be optimized for each biomolecule. In this work MNPs with varying densities of APTES were synthesized and adsorbed with cellulases from two different bulk concentrations. MNPs reacted with high degrees of APTES had increased cellulase adsorption levels, lower specific activities, but higher activity recovery. The cellulase adsorbed to MNPs from dilute bulk solutions had markedly higher immobilization efficiencies, and specific activities, expressing a 4 to 30-fold enhancement in specific activity relative to the free enzyme. These results express the importance in adsorbing cellulases from dilute bulk solutions to MNPs with high APTES densities to ensure efficient immobilization and recovery of cellulase activity.

2. Materials and Methods

Materials

Iron (III) chloride hexahydrate ($FeCl_3 \cdot 6H_2O$) and glutaraldehyde (50%) were purchased from Sigma-Aldrich (St. Louis, MO, USA). Iron (II) chloride tetrahydrate ($FeCl_2 \cdot 4H_2O$), and 3-aminopropyltriethoxysilane (APTES) were purchased from Acros Organics (Geel, Belgium). Cellulase from *T. reesei* was purchased from Abnova (Walnut, CA). Copper (II) sulfate pentahydrate ($CuSO_4 \cdot 5H_2O$), sodium acetate, sodium carbonate, sodium bicarbonate, sodium monohydrogen phosphate, sodium dihydrogen phosphate, ammonium hydroxide (29%) and tetraethyl orthosilicate (TEOS) were purchased from Fisher Scientific (Pittsburgh, PA). Sodium bicinchoninate (BCA), carboxymethyl cellulose sodium salt n ~ 500 (CMC) was purchased from Tokyo Chemical Industry (Portland, USA). The 3,5-dinitrosalicylic acid (DNS) was purchased from Spectrum (New Brunswick, NJ).

Synthesis and Modification of Magnetic Particles

A 47 mL solution containing 60 and 30 mM of Fe^3 and Fe^{2+}, respectively, in 18 MΩ H_2O was heated to 80°C and degassed with N_2. After 30 min of degassing, 2.2 mL of NH_4OH was added dropwise and allowed to react for 1 hr. The black product was washed using degassed 18 MΩ H_2O three times followed by three subsequent washes with ethanol. The volume was brought to 53 mL with ethanol and 2 mL of 200 mM TEOS was added. The hydrolysis of TEOS was initiated by the addition of 5 mL NH_4OH. The solution was placed on

© The AIC 2023. All rights reserved.

a shaker set at 25°C and 350 RPM overnight.

The amine functional groups were introduced to the MNPs by the condensation of APTES. The TEOS modified MNPs were washed with ethanol three times and 30 mg of MNP was added to a scintillation vial containing 10 mL of 3-300 mM APTES in ethanol. The vials were placed on a shaker set at 25°C and 350 RPM for 12 hrs. After amine modification, the MNPs were washed three times with ethanol and dried in a vacuum oven at 60°C overnight.

A ninhydrin assay was performed to determine the surface available amines on the APTES modified particles [17]. In brief, 1.5 mg of MNP was dispersed in 500 µL of 60% ethanol and 100 µl of 20 µM KCN in pyridine, 75 µL of 80% (v/v) phenol in ethanol, and 75 µL of 0.5% ninhydrin in ethanol were added. The solutions were heated to 98°C for 15 min, cooled to room temperature. MNPs were magnetically separated from the supernatant. The absorbance of the supernatants was measured at 570 nm and compared to a hexylamine standard.

Enzyme Immobilization

The MNPs were dispersed in 10 mM acetate buffer pH 5.0 at a concentration of 2 mg/mL. Cellulase in acetate buffer was added to the MNPs at a 1:1 or 0.1:1 mass ratio of cellulase to MNP. The 1:1 and 0.1:1 cellulase:MNP mass ratios are subsequently referred to as either the high or low loadings, respectively. The MNP/cellulase solutions were placed on a shaker set at 25 °C and 350 RPM for 2 hrs, after which the cellulase immobilized MNPs were washed with acetate buffer three times. The supernatant from each wash was collected and analyzed by the BCA assay using BSA as a standard. The amount of cellulase immobilized was determined by mass balance and the immobilization percent was determined according to equation 1. where C_i is the initial concentration of the cellulase solution, V_i is the initial volume of solution, C_s is the concentration of the supernatant and V_s is the volume of the supernatant.

$$Enzyme\ Immobilzed\ \% = \frac{C_i V_i - \Sigma\, C_s V_s}{C_i V_i} \times 100 \quad (1)$$

Activity Assay

The DNS assay was used to determine the activity of the cellulase immobilized MNPs using glucose as a standard. The DNS solution contained 27 mM DNS, 0.5 M NaOH, 0.64 M sodium potassium tartrate, and 25 mM sodium metabisulfite. A total of 200 µL of 0.8% (w/v) CMC in 10 mM acetate pH 5.0 was added to 200 µL of cellulase adsorbed MNPs or free cellulase in 10 mM acetate pH 5.0. The samples were placed on a shaker at 50°C for 30 min, after which 200 µL of supernatant was added to 500 µL of DNS solution and boiled for 5 min. The boiled samples were cooled to room temperature and their absorbance measured at 540 nm.

© The AIC 2023. All rights reserved.

3. Results and Discussion

MNP Modification

MNPs were synthesized and reacted with varying APTES/Fe mole ratios. APTES contains a single primary amine, and the solvent exposed amine density on the MNPs was determined by the ninhydrin assay. The surface amine density correlated to the APTES reactant mole ratio as displayed in Figure 1.

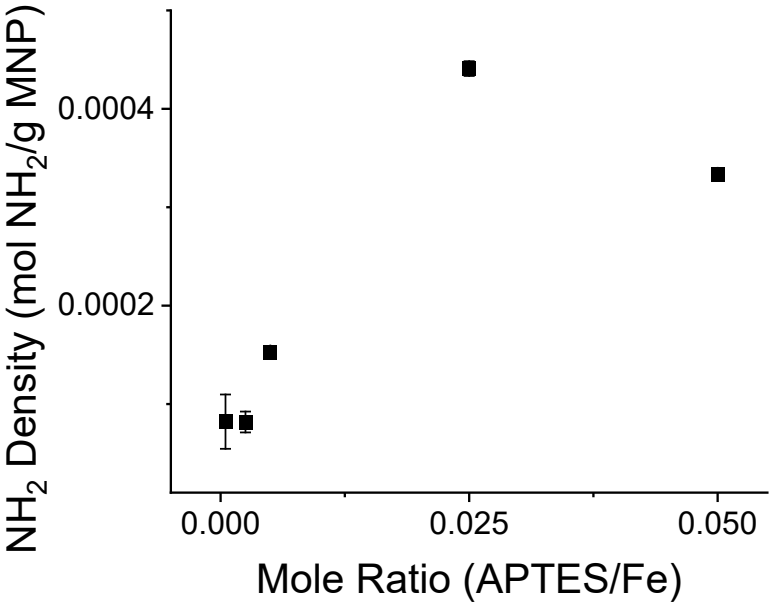

Figure 1. Solvent Exposed Amines Immobilized on MNPs. The APTES/Fe mole ratio refers to the reactant mole ratio. Avg ± 1 S.D., n = 3, measured in triplicate.

However, the greatest surface amine density was not observed at the highest APTES/Fe mole ratio. APTES is capable of forming a multilayer on a surface [18]. The ninhydrin assay quantifies solvent accessible amines [17] and is insensitive to amines buried in a multilayer or amines that are inaccessible to solvent. The decrease in solvent exposed amines on the MNPs at the highest APTES density is therefore interpreted as the development of an APTES structures that have an inaccessible amine group.

Enzyme Immobilization

Cellulase was adsorbed to the modified MNPs in 10 mM acetate pH 5.0 for 2 hrs incubated at 25°C. The amount of cellulase immobilized correlated to the cellulase bulk concentration and APTES density, while the immobilization efficiency was dependent upon the APTES density as shown in Figure 2.

© The AIC 2023. All rights reserved.

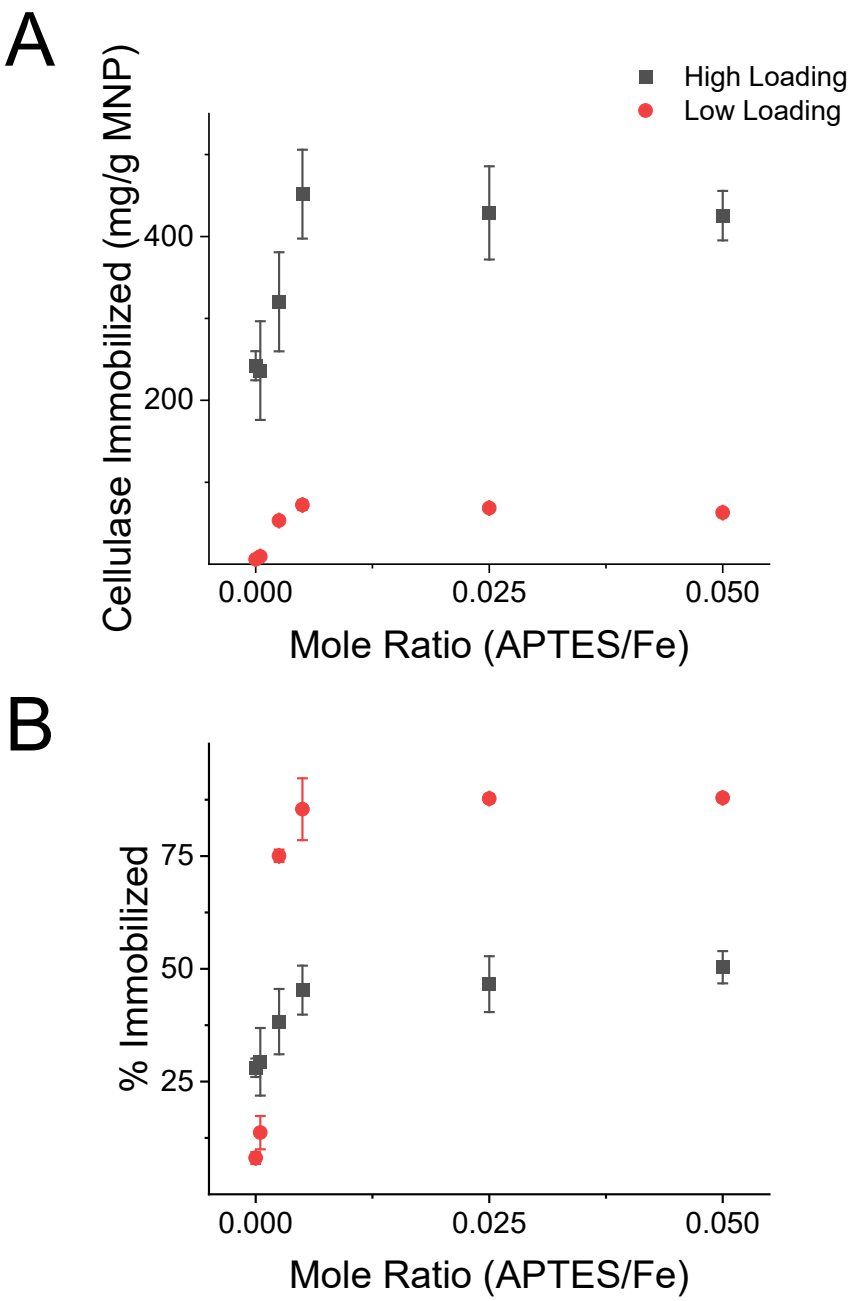

Figure 2. Cellulase Immobilized to MNPs. Immobilization was performed at a 1:1 MNP/cellulase mass ratio (high loading, black square) or a 0.1:1 mass ratio (low loading, red circle) in 10 mM acetate pH 5.0 for 2 hrs at 25°C. The APTES/Fe mole ratio refers to the reactant mole ratio. Avg ± 1 S.D., n = 3, measured in triplicate.

The results were anticipated as increasing the APTES density and bulk protein concentration shift the equilibria to favor adsorption of additional biomolecules. The MNPs appear to approach saturation with cellulase at 70 and 450 mg/g MNP for the low and high loadings, respectively. The difference in saturation values between the two loadings may be caused by different surface structures

© The AIC 2023. All rights reserved.

governed by different adsorption processes between the different loadings. At high biomolecule loadings, a greater saturation value is expected as adsorbed biomolecules form a densely packed structures or form multilayers [11,19]. At low biomolecule loadings, a lower saturation value may be caused by adsorbed biomolecule "spreading out" to maximize favorable interactions with the surface, thereby preventing adjacent biomolecule adsorption on the surface [11]. To elucidate whether adsorbed biomolecules suffered deleterious conformational changes or steric hindrance from adjacent biomolecules, the activity of MNPs were assessed.

Activity Assay

The DNS assay was used to determine the activity of the MNPs in 10 mM acetate pH 5.0 at 50°C for 30 min using CMC as a substrate. The activity was normalized to the dry mass of MNPs and referred to as particle activity. The particle activity correlated to MNPs to the quantity of cellulase adsorbed as displayed in Figure 3A. However, the amount of cellulase adsorbed did not linearly correlate with particle activity, as a sixfold increase in cellulase adsorption at the high loading, relative to the low loading, led to only a twofold increase in particle activity. The nonlinear relationship between adsorbed biomolecule quantity and particle activity implies a change in specific activity.

To examine the changes in specific activity, the particle activity was normalized to the amount of enzyme immobilized. The specific activity was inversely proportional to both the loading density and APTES density as shown in Figure 3B.

© The AIC 2023. All rights reserved.

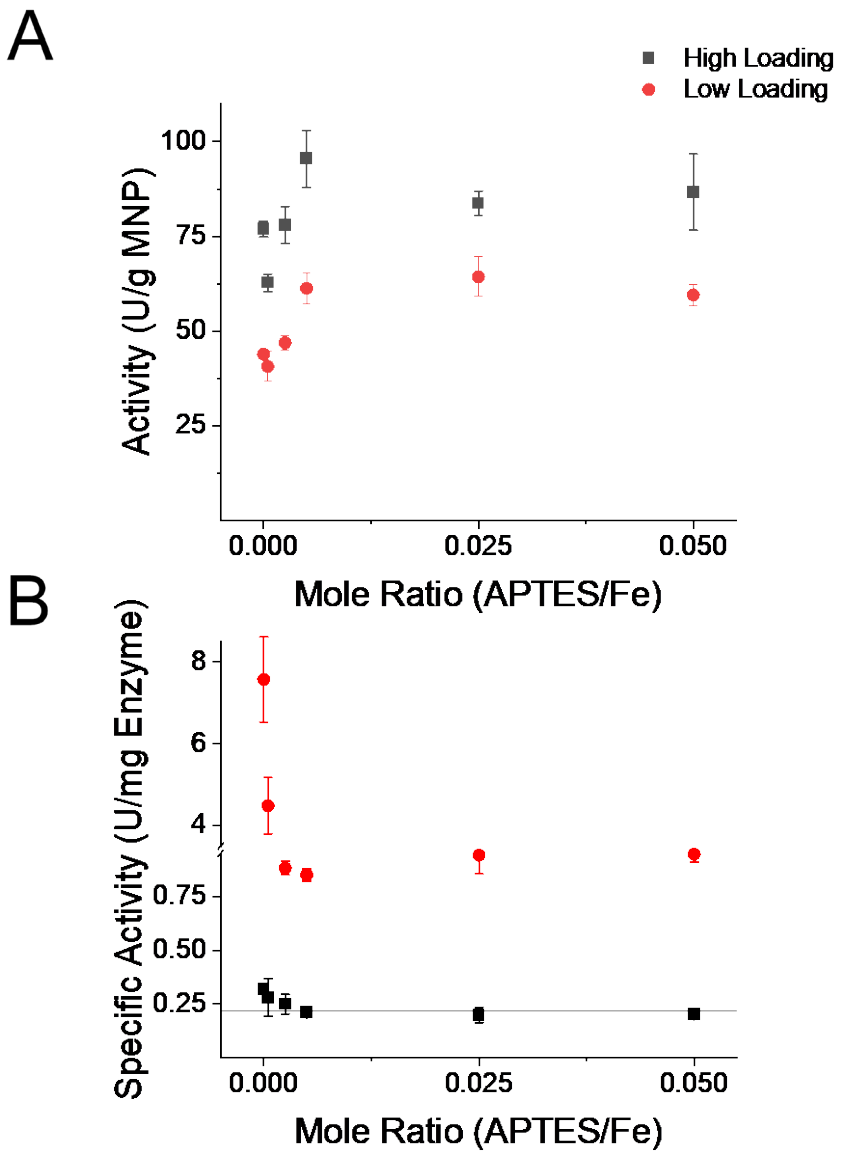

Figure 3. Immobilized Cellulase Specific Activity. Activity was determined using the DNS assay at 50°C in 10 mM acetate pH 5.0. The APTES/Fe mole ratio refers to the reactant mole ratio. Avg ± 1 S.D., n = 3, measured in triplicate. The solid line indicates the specific activity of the control free cellulase.

Interestingly, the immobilized cellulase had up to a thirtyfold enhancement in specific activity relative to the free enzyme. The immobilized cellulase specific activity was inversely related to the APTES density, which ranged from 0.85 to 7.6 U/mg at the low loading and is significantly different from the free enzyme specific activity of 0.218 ± 0.002 U/mg at the 99% confidence interval as determined by a one-way ANOVA with a TUKEY HSD post-hoc test. The enhanced specific activity could be attributed to favorable conformational changes or an immobilized geometry that favors interaction with the substrate. Immobilized lipase exhibits up to a twentyfold hyperactivity as the

© The AIC 2023. All rights reserved.

immobilized form adopts an open conformation with an exposed active site [20]. The surface structure of the adsorbed biomolecules in this work is unknown. However, it is interpreted that the biomolecules are crowded at the high loading and high APTES densities and, as a consequence, have reduced specific activities. Crowding of biomolecules would restrict their ability to interact with substrate and/or restrict biomolecule mobility needed for catalysis causing a reduction in specific activity.

To quantitatively assess how the bulk cellulase concentration and particle APTES density intertwine to determine the efficiency of the adsorption process, the recovered cellulase activity for each sample was calculated. The units of immobilized activity were normalized to the units of activity used during adsorption to calculate the recovered activity as displayed in Figure 4.

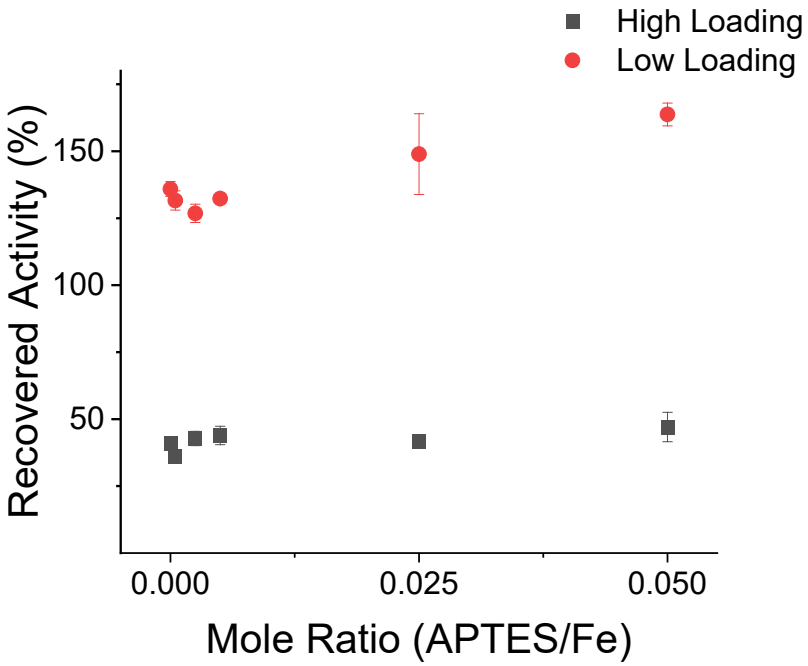

Figure 4. Recovered Cellulase Activity. The activity of immobilized cellulase was normalized to the activity of the cellulase used for immobilization. Avg ± 1 S.D., n = 3, measured in triplicate.

The heightened specific activity and immobilization percentage observed at the low loading led to recovered activities ranging from 127 to 163%, while the high loading had recovered activities ranging from 36 to 47%. The recovered activities illustrate that increasing the APTES functional groups on a surface may be detrimental to the specific activity of immobilized biomolecules, but at high APTES densities a greater recovery of enzymatic activity occurs stemming from the enhanced immobilization percentage. The result from this study indicates increasing the amount of APTES adhered to the surface of the iron nanoparticle will lead to the efficient recovery of catalyst

© The AIC 2023. All rights reserved.

activity, ultimately leading to lower costs of bioethanol produced from cellulose.

4. Conclusion

In the present work, the recovered activity and immobilization efficiency of cellulases adsorbed to magnetic nanoparticles were explored. The APTES functional group density and bulk biomolecule concentration used during immobilization were inversely proportional to the adsorbed biomolecule activity. However, the immobilization efficiency increased with APTES density, which led to a greater recovery of immobilized activity at high APTES densities. These results indicate a promising future for cellulosic ethanol production by immobilizing cellulases from dilute solutions onto MNPs with high functional group densities to ensure an abundance of cellulase is immobilized in an active conformation.

5. Acknowledgment

Funded by The Citadel's Near Center for Climate Studies through a Climatological Research Studies Grant.

6. References

1. Bhaumik P, Dhepe PL in Biomass Sugars for Non-Fuel Applications, The Royal Society of Chemistry, 2016, ch. 1, pp 1-53.
2. Sinitsyn AP, Sinitsyna, OA. Bioconversion of renewable plant biomass. Second-generation biofuels: Raw materials, biomass pretreatment, enzymes, processes, and cost analysis. *Biochemistry (Moscow)*, 2021, *86* (1), S166-S195.
3. Liu G, Zhang J, Bao J. Cost evaluation of cellulase enzyme for industrial-scale cellulosic ethanol production based on rigorous aspen plus modeling. *Bioprocess Biosyst. Eng.*, 2016, 39(1), 133-140.
4. Ahmed IN, Yang X-L, Dubale AA, Li R-F, Ma Y-M, Wang L-M, Hou G-H, Guan R-F, Xie M-H. Hydrolysis of cellulose using cellulase physically immobileized on highly stable zirconium-based metal-organic frameworks. *Bioresour. Technol.*, 2018, 270, 377-382.
5. Ho KM, Mao X, Gu L, Li P. Facile route to enzyme immobilization: Core-shell nanoenzyme particles consisting of well-defined poly(methyl methacrylate) cores and cellulase shells. *Langmuir*, 2008, 24(19), 11036-11042.
6. Khoshnevisan K, Vakhshiteh F, Barkhi M, Baharifar H, Poor-Akbar E, Zari N, Stamatis H,

© The AIC 2023. All rights reserved.

Bordbar A-K. Immobilization of cellulase enzyme onto magnetic nanoparticles: Applications and recent advances. *Mol. Catal.*, 2017, 442, 66-73.
7. Khoshnevisan K, Poorakbar E, Baharifar H, Barkhi M. Recent advances of cellulase immobileization onto magnetic nano-particles: An update review. *Magnetochemistry*, 2019, 5(2).
8. Datta S, Christena LR, Rajaram YRS. Enzyme immobilization: An overview on techniques and support materials. *3 Biotech*, 2013, 3(1), 1-9.
9. Falahati M, Ma'mani L, Saboury AA, Shafiee A, Foroumadi A, Badiei AR. Aminopropyl-functionalized cubic Ia3d mesoporous silica nanoparticle as an efficient support for immobileization of superoxide dismutase. *Biochim. Biophys. Acta, Proteins Proteomics*, 2011, 1814(9), 1195-1202.
10. Jung H-S, Moon D-S, Lee J-K. Quantitative analysis and efficient surface modification of silica nanoparticles. *J. Nanomater.*, 2012, 2012, 593471.
11. Latour RA. The Langmuir isotherm: A commonly applied but misleading approach for the analysis of protein adsorption behavior. *J. Biomed. Mater. Res., Part A*, 2015, 103(3), 949-958.
12. Latour RA. Fundamental principles of the thermodynamics and kinetics of protein adsorption to material surfaces. *Colloids Surf., B*, 2020, 191, 110992.
13. Roach P, Farrar D, Perry CC. Interpretation of protein adsorption: Surface-induced conformational changes. *J. Am. Chem. Soc.*, 2005, 127(22), 8168-8173.
14. Secundo F. Conformational changes of enzymes upon immobilisation. *Chem. Soc. Rev.*, 2013, 42(15), 6250-6261.
15. Saha B, Saikia J, Das G. Correlating enzyme density, conformation and activity on nanoparticle surfaces in highly functional bio-nanocomposites. *Analyst*, 2015, 140(2), 532-542.
16. Rabe M, Verdes D, Seeger S. Understanding protein adsorption phenomena at solid surfaces. *Adv. Colloid Interface Sci.*, 2011, 162(1), 87-106.
17. Sun Y, Kunc F, Balhara V, Coleman B, Kodra O, Raza M, Chen M, Brinkmann A, Lopinski GP, Johnston LJ. Quantification of amine functional groups on silica nanoparticles: A multi-method approach. *Nanoscale Adv.*, 2019, 1(4), 1598-1607.
18. Vandenberg ET, Bertilsson L, Liedberg B, Uvdal K, Erlandsson R, Elwing H, Lundström I. Structure of 3-aminopropyl triethoxy silane on silicon oxide. *J. Colloid Interface Sci.*, 1991, 147(1), 103-118.
19. Vertegel AA, Siegel RW, Dordick JS. Silica nanoparticle size influences the structure and enzymatic activity of adsorbed lysozyme. *Langmuir*, 2004, 20(16), 6800-6807.
20. Bastida A, Sabuquillo P, Armisen P, Fernandez-Lafuente R, Huguet J, Guisan JMA. Single step purification, immobilization, and hyperactiv-

© The AIC 2023. All rights reserved.

ation of lipases via interfacial adsorption on strongly hydrophobic supports. *Biotechnol. Bioeng.*, 1998, 58(5), 486-493.

© The AIC 2023. All rights reserved.

The Chemist
Journal of the American Institute of Chemists

Eco-friendly Method of Synthesis CeO_2 Nanoparticles by Watercress Plant Extract for Removal of Cibacron Red Dye from Aqueous Solutions

Aya Qasim Khanjar[1], Ahlam Mohammed Farhan[1], Ahmed Mahdi Rheima[2*]

[1] Department of Chemistry, College of Sciences for Women, University of Baghdad Baghdad, Iraq

[2] Department of Chemistry, College of Science, Mustansiriyah University Baghdad, Iraq

[*]Corresponding Author: ahmed.rheima@gmail.com

Abstract: Water dye contamination is a serious issue, particularly given that textile mills are the main cause. The development of medicines using nanomaterials has involved a lot of study and testing. This study discusses the environmentally friendly synthesis of CeO_2 nanoparticles using plant extract from watercress and calcination at 400°C for 3 hours. The SEM and TEM were used to examine nanoparticles, which were 36 nm. X-ray diffraction was utilized to determine the crystal structure. The purity of the synthetic material was confirmed by energy-dispersive X-ray spectroscopy (EDX) investigation of the structure of the produced product, which revealed just cerium (Ce) and oxygen (O) elements. The dye Cibacron red was more readily absorbed with the addition of CeO_2 NPs. The Cibacron red dye adhered to the CeO_2 nanoparticles more quickly after 30 minutes of contact. The best models for describing the adsorption process were those of Freundlich and pseudo-second-order with R_2 values greater than 0.9246 and 0.9873, respectively. Thermodynamic analysis was used to determine the parameters of 2.44 kJ/mol, 29.26 kJ/mol K, and 97.68 J/mol ΔG, ΔH, and ΔS. It can be concluded that the CeO_2 NPs function well as a Cibacron red dye adsorbate surface.

Key Words: CeO_2 nanoparticles (NPs)**,** adsorption, Cibacron red dye, green synthesis

© The AIC 2023. All rights reserved.

1. Introduction

Environmental pollution is one of the main issues people nowadays have to deal with, and it becomes more dangerous due to numerous human activities. It has been discovered that environmental pollution is closely related to the global population growth [1]. One of the components that keeps life alive is water. Since millions of chemical compounds are discharged every day, directly or indirectly, to water sources without any treatment [2], freshwater supplies have recently seen a major decline as a result of technological advancement [3]. As a result, the issue of water contamination has attracted a lot of attention in the modern era [1]. Dyes are considered organic pollutants in aqueous systems and can pose a risk to all elements of the environment due to its toxicity, especially when they are present in high concentrations [4]. Dyes include all substances used to color textiles, leather, food, and other materials. Organic compounds are one of the most important components of industrial wastewater. There is a significant risk of long-term consequences since some organic pollutants have the potential to cause malignant diseases [5]. According to WHO reports, the bulk of diseases that spread in undeveloped countries are mostly caused by contaminated drinking water. Researchers have therefore used a variety of techniques to clean industrial water [6,7]. Diverse techniques have been used to cleanse and remove organic pol-lutants from industrial water. They comprise ion exchange, chemical oxidation, photo-oxidation, and the adsorption process, among others [8]. Adsorption is a method that is both efficient and affordable. Data from the WHO show that it is frequently used to clean up contaminated water [9-12]. Nanotechnology is used by many industries and sectors, such as the chemical industry, photoelectrochemical applications, environmental health, medicine, and energy [13,14]. Nanotechnology [15], a crucial advancement in modern science, has made it possible to produce materials with distinctive size, structure, and substance. Production, processsing, and application all involve materials with a diameter less than a nanometer [16,17]. Physical, chemical, as well as biological characteristics at the nanoscale differ from bulk atoms and molecules individually [18-20]. This enables the creation of novel classes of cutting-edge chemicals and materials to satisfy the requirements of high-tech applications [21-24]. Cerium oxide (CeO_2), commonly referred to as nano ceria, is a superior semiconducting substance with a broad band gap energy of 3.19 eV, making it a strong choice for catalytic applications [25]. Due to their potential benefits in a number of applications, including a catalyst, an electrolyte material for solid oxide fuel cells, a diesel fuel additive, a material of high refractive index, an insulating layer on silicon substrates, gas sensors, and more recently biomedicine, significant efforts have been made in recent years to develop new synthetic methods for the preparation of nanostructure cerium oxides [26-30]. The biological impacts of nano ceria have been covered in numerous studies. It is well recognized that cerium oxide nanoparticles, in contrast to other metal oxide nanoparticles, do not have cytotoxic effects and instead offer protection against a variety of cellular damages, such as radiological shocks that encourage the generation of free radicals [31,32]. Cerium oxide nanoparticles have been created using a variety of tech-niques [33]. In this study, the green syn-thesis approach was used to make cerium oxide nanoparticles and used it to remove the Cibacron red dye, which is one of the dyes used in the textile industry in the Wasit

© The AIC 2023. All rights reserved.

Governorate and most of which is disposed of as wastewater. The synthesis of nano-particles using plant extracts is a clean and safe method that does not contain harmful chemicals, but rather uses natural materials from plants.

2. Experimental

Extraction of the Watercress Plant Extract

Watercress plant extract has been collected and washed with deionized water to get rid of any dust. The dry leaves are gently blend-ed in a mixer to obtain homogeneous pow-ders. Then, 10 grams of leaves were ground and combined with 150 ml of deionized water. The mixture was then heated for 30 minutes at 60°C while being stirred. After filtering, the solution was placed in the refrigerator.

Synthesis of CeO_2 Nanoparticles

Cerium oxide nanoparticles were created using the green synthesis method. Accord-ingly, 400 ml of watercress filter had added to 0.01 mole of $Ce(NO_3)_3$ slowly (one drop every second) and stirred for 30 minutes. The yellow powder was repeatedly rinsed with deionized water, separated, and precip-itated. After being dried for an hour at 150°C, the precipitate was calcined for 3 hours at 400°C. The copper oxide nano-particles were produced as a yellowish white powder.

Cibacron Red Dye Adsorption on CeO_2 NPs

The equilibrium isotherm of a particular adsorbent serves as a representation of its adsorbent properties for the purpose of de-signing adsorption operations. A stock sol-ution of the Cibacron red dye (50 ppm) was made in deionized water. 0.01 g of CeO_2 nanoparticles were added to 10 ml of dye solution, and they were then heated to 298 K for 30 minutes. After the solution had been filtered, the dye concentration in the filtrate was measured using a UV-visible absorption spectrophotometer [34-35].

$$Qe = (C_{0\_} Ce)Vsol/M \quad (1)$$

where Qe (mg/g) is the equilibrium adsorption capacity, C_0 and Ce are the beginning as well as equilibrium concen-trations of Cibacron red dye, and M is the mass of the CeO_2 nanoparticles (g). V sol is therefore the volume of Cibacron red (L).

Cerium Oxide Nanoparticles Characterization

X-ray diffraction was used to investigate the sample of CeO_2 nanoparticles (XRD-6000). The morphology of nanoparticles was studied using transmission electron microscopy. The shape of the CeO_2 nano-particles was studied under a scanning electron microscope (SEM). Nanoparticle morph-ology was examined using transmission electron microscopy (TEM).

© The AIC 2023. All rights reserved.

3. Result and Discussion

The X-ray Diffraction of CeO_2 Nanoparticles

X-ray diffraction (XRD) in the 2θ range of 200-700 (Rigaku Miniflex II) utilizing Cu K radiations (λ = 1.54A) operated at a voltage of 30 kV and current of 15 mA was used to analyze the XRD pattern of cerium oxide nanoparticles displayed in Figure 1. The (111), (200), (220), (311), (222), and (400) cubic phase peaks are the diffracted peaks observed at diffraction angles 2θ of 28.270, 32.780, 47.050, 55.940, 59.070, and 69.090.

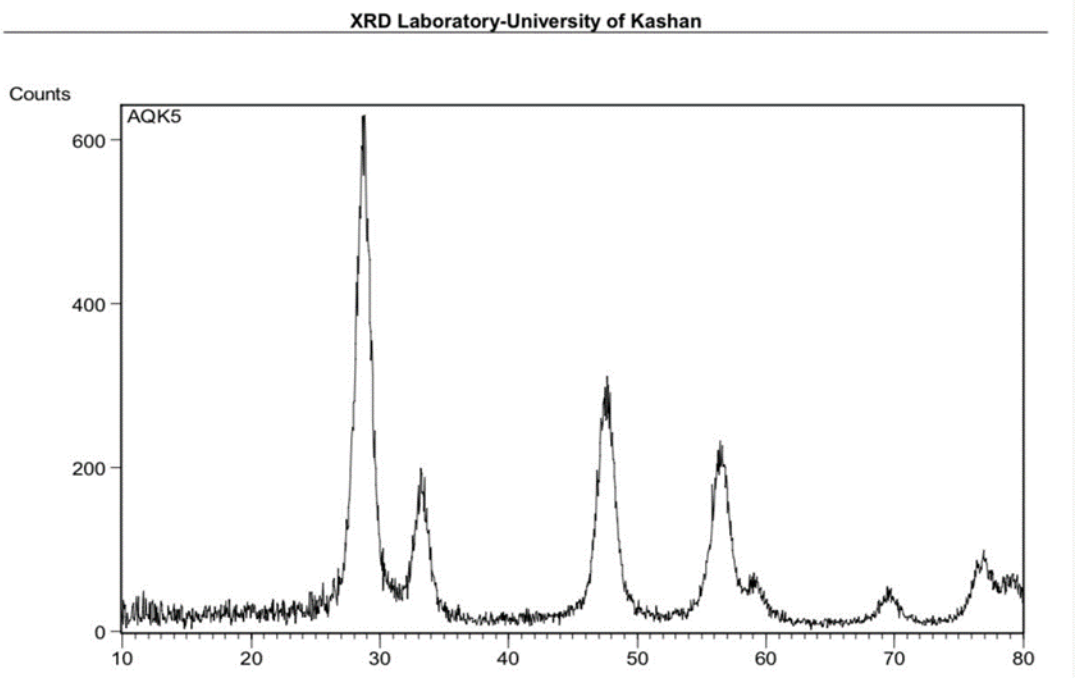

Figure 1. XRD Patterns of Cerium Oxide Nanoparticles

The spectra make it very evident that there are no additional contaminant peaks. Debye-Scherer equation [36] was used to calculate the crystallite size of cerium oxide nanoparticles, which was found to be 22 nm.

Field Emission Scanning Electron Microscope of CeO_2 Nanoparticles

FE-SEM was used to analyze the surface morphology of pure CeO_2 nanoparticles that had been calcined at 400°C. The SEM analysis revealed that the prepared sample was formed as spherical aggregates with a reasonably uniform distribution. Figure 2 displays the crystal nature of the equally-sized manufactured nanoparticles.

© The AIC 2023. All rights reserved.

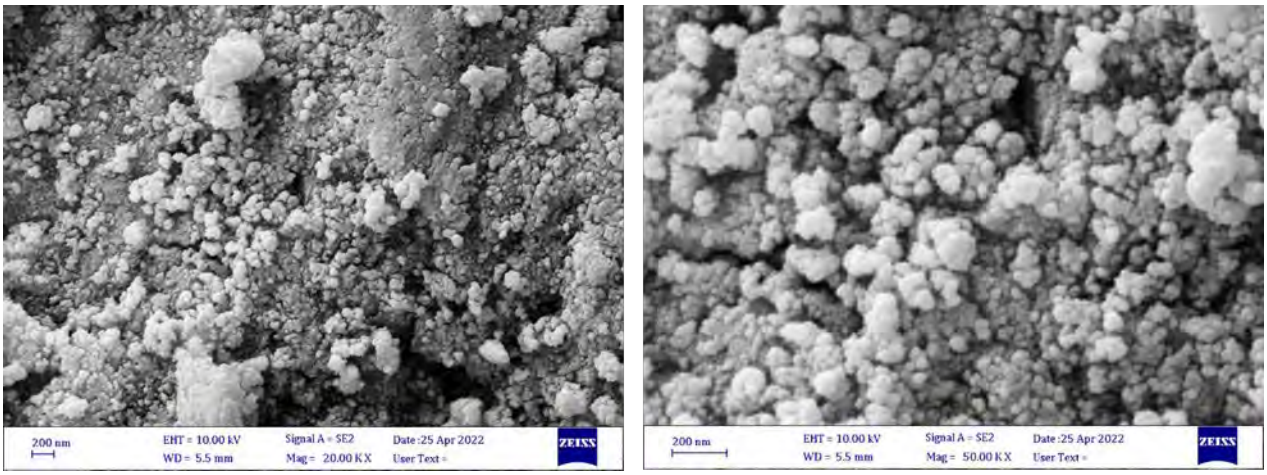

Figure 2. SEM Images of Cerium Oxide Nanoparticles

Transmission Electron Microscopy of CeO_2 Nanoparticles

TEM pictures of the sample were acquired and are displayed in Figure 3 to further the research of the morphology, as well as size, of the product as it was produced. The nanoparticle sizes determined by the XRD diffraction pattern and the TEM picture, which shows average sizes of 36 nm, are closely correlated. Understanding the crystalline characteristics of the nanoparticles is the aim of the TEM study

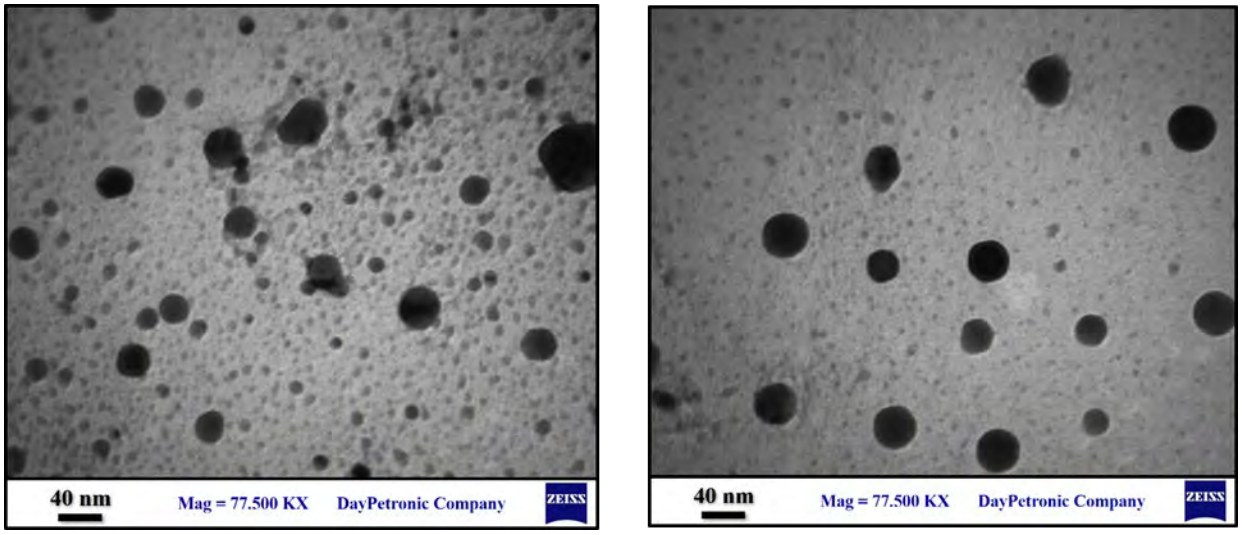

Figure 3. TEM Images of Cerium Oxide Nanoparticles

.

Characterization of Energy-dispersive X-ray Spectroscopes

The chemical composition and purity of the as-produced CeO_2 nanoparticles were examined using EDS analysis as shown in Figure 4.

© The AIC 2023. All rights reserved.

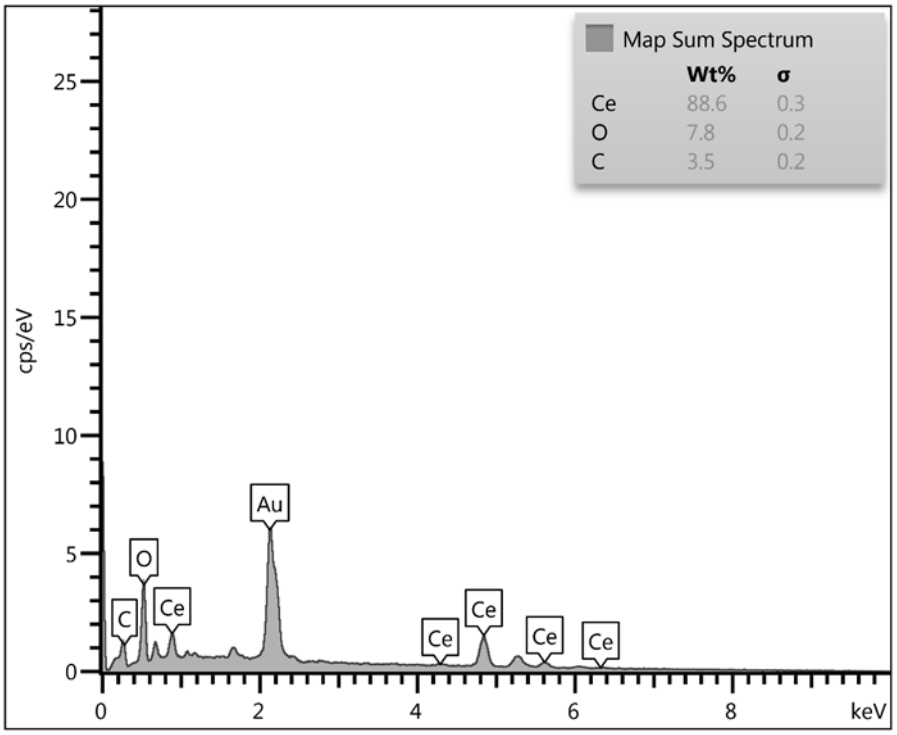

Figure 4. EDX Spectrum of Cerium Oxide Nanoparticles

The presence of Ce, as well as O, in the product is shown by a typical EDX spectrum, as seen in Figure 5. The silicon plates employed in the EDS instrument are what cause the presence of Si peaks in this spectrum.

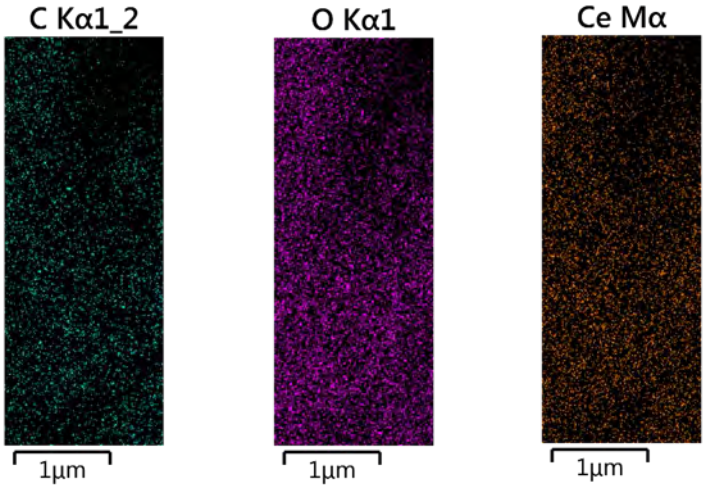

Figure 5. EDAX Mapping of Cerium Oxide Nanoparticles

© The AIC 2023. All rights reserved.

Adsorption Isotherms

The major purpose of the adsorption analysis is to evaluate the correlation bet-ween the dye and adsorption by contrasting the adsorption isotherm with the adsorption data. This study evaluated both the Lang-muir and Freundlich models. The linear Freundlich adsorption process is represented by the following formula [10] [34-36]:

$$\log(Qe) = \log(kf) + (\frac{1}{n}) \log(Ce) \quad (2)$$

The Freundlich constants, kf as well as n, respectively, show the adsorption capacity and intensity. As shown in Figure 6, while n is determined using the slope, kf is deter-mined using the intercept. In the cur-rent study, 1/n was found to be 0.5086 for the Freundlich CeO_2 isotherm. As a result, this research supported the value of physical adsorption. [37].

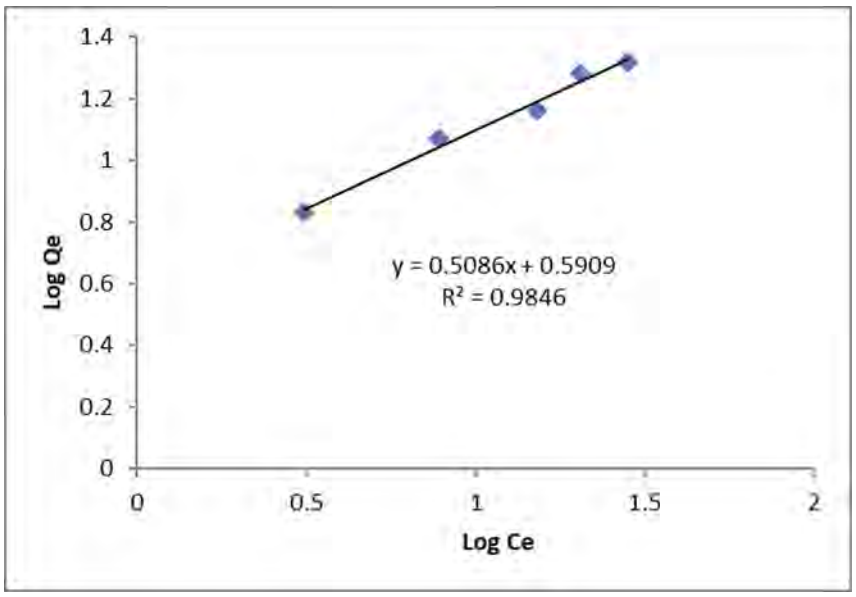

Figure 6. The Freundlich Isotherm Model Plot at 298 K

The Freundlich isotherm (R^2 = 0.9846) provides a better fit for the adsorption. The equation that follows shows how well the data fits the Langmuir adsorption isotherm [36,37]:

$$\frac{Ce}{Qe} = \frac{1}{q\,max} Kl + \frac{Ce}{q\,max} \quad (3)$$

© The AIC 2023. All rights reserved.

The Langmuir constant is Kl (mg/L), but the maximum adsorption of Cibacron red dye is q max (mg/g). The separation factor, often known as the dimensionless constant (Rl) [36], outlines and illustrates the main features of the Langmuir isotherm:

$$Rl = \frac{1}{(1+Kl\ Ci)} \quad (4)$$

According to Figure 7, the dye adheres to CeO_2 the best when the initial dye concentration is Ci (mg/L) and the Rl values are all between (0-1).

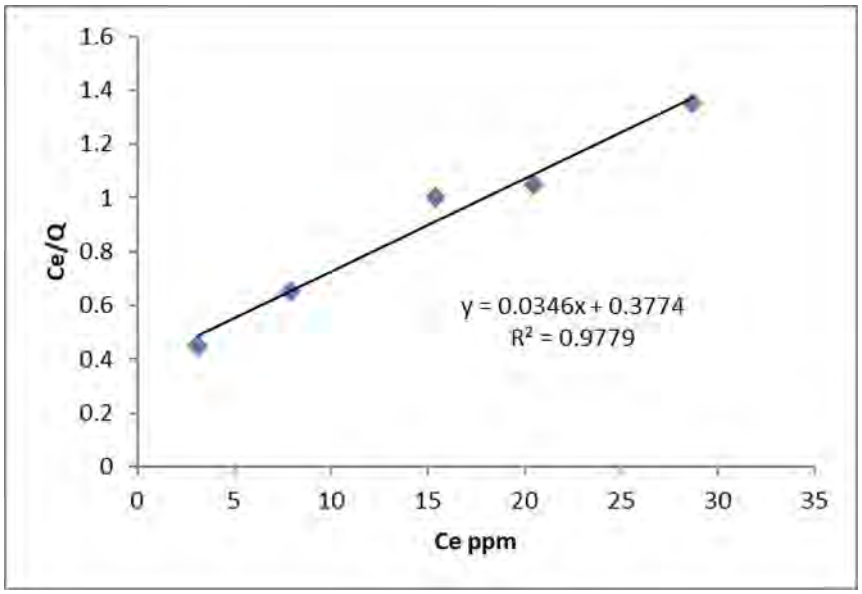

Figure 7. The Langmuir Isotherm Model at 298 K.

The Effect of Contact Time

In series of experiments, 0.01 g CeO_2 nanoparticle and also 10 ml (50 ppm) dye were used to determine both contact time as well as equilibrium time. The liquid was warmed to 298 K with the use of a 200 rpm shaker. Adsorption happens rather quickly in the first 5 to 40 minutes. Due to the active CeO_2 nanoparticles' close association with the dye, quick adsorption is made feasible. After 35 minutes, the dye adsorption rate stabilizes due to the nanoparticles' surface, seen in Figure 8.

© The AIC 2023. All rights reserved.

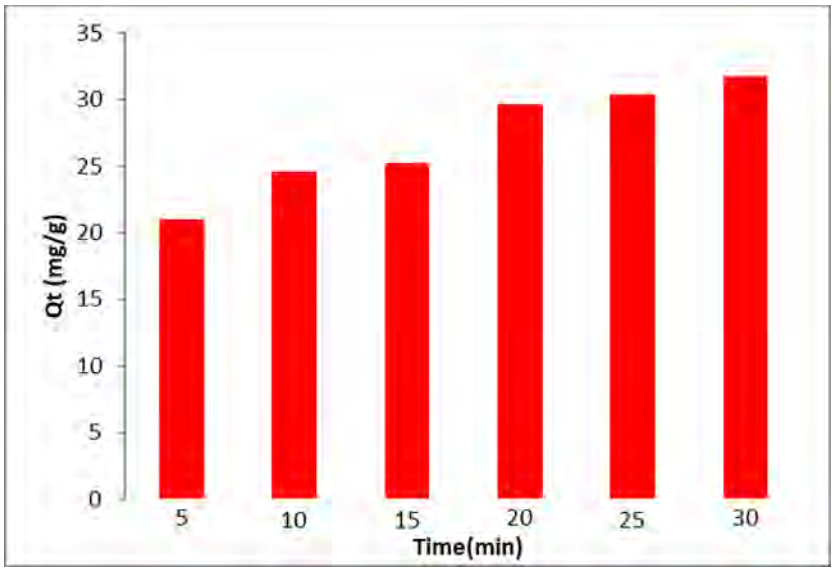

Figure 8. Effect of Time on Dye Adsorption onto the Cerium Oxide Nanoparticles

The Effect of Adsorbent Mass

Different masses of CeO_2 NPs (0.005g, 0.01g, 0.05g, 0.1g, and 0.15g) were added to 50 ppm of dye to evaluate the adsorbent's efficacy. The mixture was shaken at 298 K and 200 rpm. The graph illustrates the link between adsorption volume and mass. First, because nanoparticles have more active sites, adsorption occurs very quickly. Figure 9 shows how increasing the mass of the CeO_2 NPs led to an increase in dye ad-sorption.

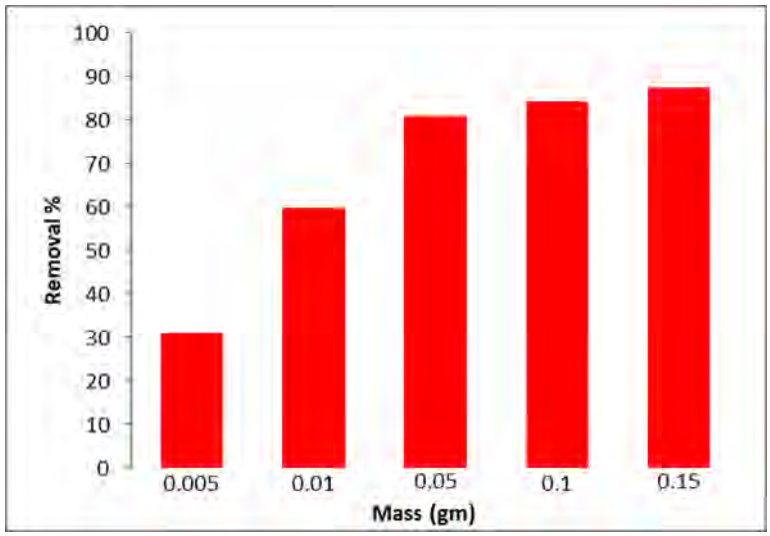

Figure 9. Effect of Adsorbent Mass on Adsorption of Dye onto the Cerium Oxide Nanoparticles

© The AIC 2023. All rights reserved.

The Effect of Temperature

The effect of temperature on dye adsorption on the surface of CeO_2 NPs was investigated at a number of temperatures, including 288 K, 298 K, 308 K, 318 K, and 328 K. With rising temperature, the dye adsorption solution volume increases. As a result, the endothermic process occurs, and the average value of H° increases above zero. This clarifies how the absorption and adsorption processes work. As the temperature, the rate of diffusion accelerates, and a strong bond is established with the adsorbent, the diffusion molecules are absorbed by the holes. Since thermodynamic parameters provide exact information on changes in inherent energy brought on by adsorption, thorough evaluation of these parameters is crucial. The following adjustments were examined to estimate the adsorption process utilizing the free energy of adsorption (. G°), entropy (ΔS°), and also enthalpy (ΔH°) [36-40]:

$$\ln(Ke) = \frac{-\Delta H}{RT} + \frac{\Delta S}{R} \tag{5}$$

$$Ke = \frac{Qe}{Ce} \tag{6}$$

$$\Delta G = \Delta H \_ T\Delta S \tag{7}$$

The equilibrium constant, Ke, the gas constant, and the temperature in Kelvin are all equal to 8.314 J/mol K (K). The interaction was endothermic, as shown by the Van 't Hoff plot in Figure 10 between ln K and 1/T, where the ΔH was 29.26 kJ/mole prevented by slope.

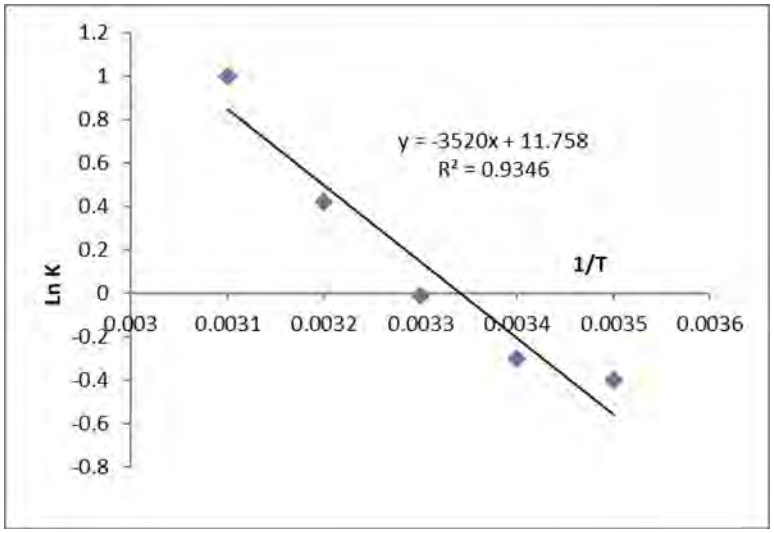

Figure 10. Van 't Hoff Plot Between Ln K and 1/T

The intercept's ΔS, which came out at 97.68 J/mole, showed that the adsorbed particles were still moving very near to the surface. They used the words "absorption" and "adsorption." The positive ΔG value at 293 K, which is 2.44 KJ/mol, points to non-spontaneous adsorption.

© The AIC 2023. All rights reserved.

Dynamics

The kinetics of dye adsorption on the surface adsorbents of CeO_2 NPs determines the uses for adsorbents. The dye analysis revealed that the adsorption equilibrium duration for 0.01 g of the CeO_2 nanoparticle adsorbents was around 30 minutes. Additionally, the following data regarding adsorption was represented in this study using both classical and kinetic models:

Pseudo-first-order mathematical model [36–41]

$$\ln(qe - qt) = \ln(qe) - k1\, t \tag{8}$$

Figure 11 shows the pseudo-first-order rate constant, k1, the equilibrium adsorption capacity, qe (mg g^{-1}), and the amount of dye that has been adsorbed over time, qt (mg g^{-1}) (min^{-1}).

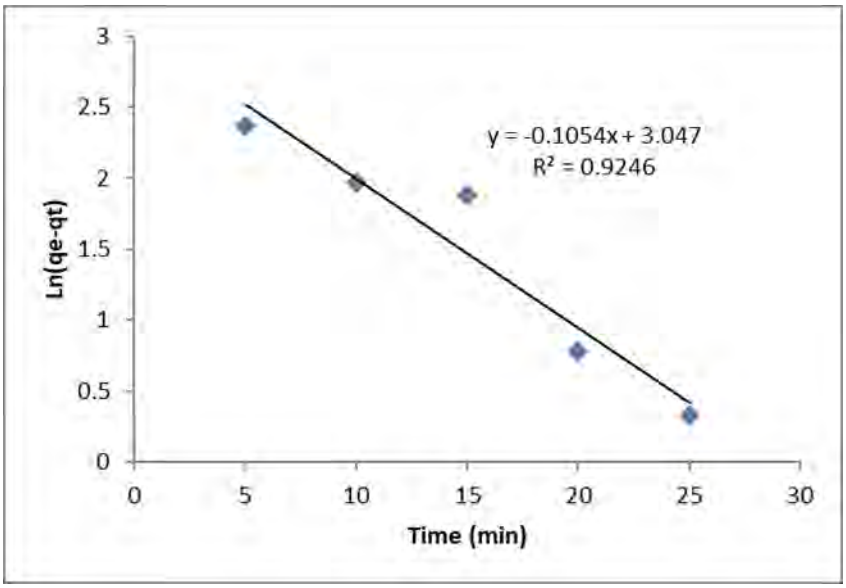

Figure 11. Dynamic of Adsorption of Dye Pseudo-first-order

The pseudo-second-order kinetic model is as follows, as seen in [10-12]:

$$\frac{1}{qt} = \frac{1}{k2\ qe} + \frac{t}{qe} \tag{9}$$

The hypothetical second-order rate constant is denoted by K_2.

© The AIC 2023. All rights reserved.

The pseudo-second-order model with a strong association factor ($R^2 > 0.9873$) may adequately capture the kinetic information, as shown in Figure 12.

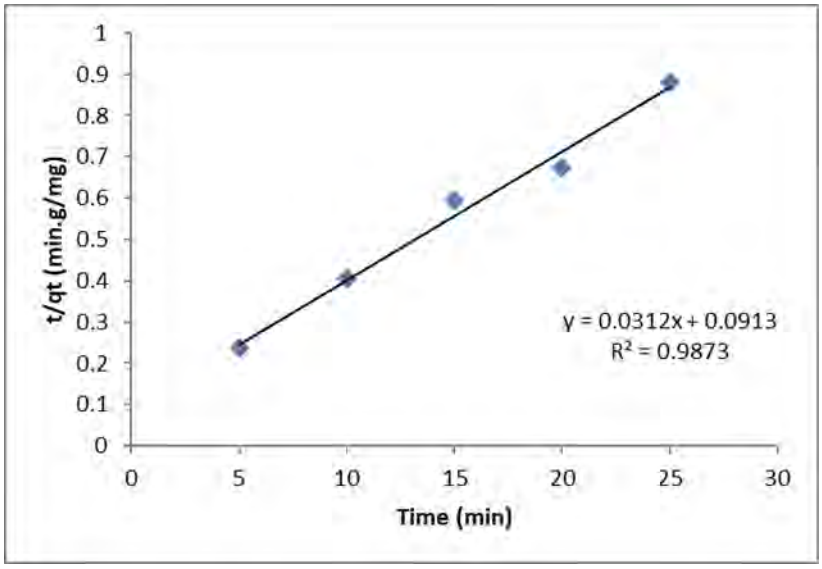

Figure 12. Dynamic of Adsorption of Dye Pseudo-second-order

4. Conclusion

Green synthesis was used to create high-quality CeO_2, and XRD, SEM/EDX, and TEM images were taken. The CeO_2 NPs' particle sizes varied, according to TEM analysis, and ranged from 28-36 nm. The observed adsorption properties are perfect for removing dye from aqueous solutions. In both kinetic and thermodynamic experiments, CeO_2 NPs proved to be effective as adsorbers. The outcomes fit the Langmuir and Freundlich isotherm models rather well. The adsorption is much better captured by the Freundlich isotherm model. The adsorption is endothermic and spontaneous, as per thermodynamics. The slope of the Van 't Hoff plot was used to calculate the enthalpy value, which describes the physical characteristics of the adsorption and is equal to 29.26 kJ/mole. With an R^2 value of 0.9873, this adsorption complies with pseudo-second-order.

5. References

1. Shen F, Zhang L, Jiang L, Tang M, Gai X, Chen M, Ge X. Temporal variations of six ambient criteria air pollutants from 2015 to 2018, their spatial distributions, health risks and relationships with socioeconomic factors during 2018 in China. *Environ. Int.*, 2020, 137, 105556.
2. Kamil AF, Abdullah HI, Mohammed SH. Cibacron red dye removal in aqueous solution using synthesized $CuNiFe_2O_5$ Nanocomposite: thermodynamic

© The AIC 2023. All rights reserved.

and kinetic studies. *Egypt. J. Chem.*, 2021, 64(11), 5-6.
3. Wang X, Chen Y, Li Z, Fang G, Wang Y. Development and utilization of water resources and assessment of water security in Central Asia. *Agric. Water Manage.*, 2020, 240, 106297.
4. Muthukrishnan L. Nanotechnology for cleaner leather production: A review. *Environ. Chem. Lett.*, 2021, 1-23.
5. Chowdhary P, Bharagava RN, Mishra S, Khan N in Environmental Concerns and Sustainable Development, Springer, Singapore, 2020, Role of Industries in Water Scarcity and Its Adverse Effects on Environment and Human Health, pp 235-256.
6. Lesimple A, Jasim SY, Johnson DJ, Hilal N. The role of wastewater treatment plants as tools for SARS-CoV-2 early detection and removal. *J. Water Process Eng.*, 2020, 101544.
7. Saleh IA, Zouari N, Al-Ghouti MA. Removal of pesticides from water and wastewater: Chemical, physical and biological treatment approaches. *Environ. Technol. Innovation*, 2020, 101026.
8. Shah I, Adnan RA. Comprehensive review on the hierarchical performances of eco-friendly and functionally advanced modified and recyclable carbon materials. *J. Iran. Chem. Soc.*, 2020, 17(7), 1521-1537.
9. Heidarinejad Z, Dehghani MH, Heidari M, Javedan G, Ali I, Sillanpää M. Methods for preparation and activation of activated carbon: A review. *Environ. Chem. Lett.*, 2020, 18(2), 393-415.
10. Rheima AM, Mahmood RS, Hussain DH, Abbas ZS. Study the adsorption ability of alizarin red dye from their aqueous solution on synthesized carbon nanotubes. *Dig. J. Nanomater. Biostructures*, 2020, 15(4).
11. Nguyen CH, Tran HN, Fu CC, Lu YT, Juang RS. Roles of adsorption and photocatalysis in removing organic pollutants from water by activated carbon-supported titania composites: Kinetic aspects. *J. Taiwan Inst. Chem. Eng.*, 2020, 109, 51-61.
12. Zhang H, Nengzi LC, Wang Z, Zhang X, Li B, Cheng X. Construction of Bi_2O_3/CuNiFe LDHs composite and its enhanced photocatalytic degradation of lomefloxacin with persulfate under simulated sunlight. *J. Hazard. Mater.*, 2020, 383, 121236.
13. Abdulah HI, Rheima AM, Hussain DH, Abed HJ. Synthesis of Fe_2O_3 nanoparticles by photolysis method for novel dye-sensitized solar cell. *J. Adv. Sci. Nanotechnol*., 2022, 1(1), 1-8.
14. Al-Uqaily RA, Rheima AM, Jaber SH, Mohammed SH, Abbas ZS, Abjel AK, Falih SS in AIP Conference Proceedings, AIP Publishing LLC, 2022, vol. 2450, no. 1, Nano-metal Complex Inhibitor for Mild Steel Corrosion in Acidic Media: A Comparative Study on Inhibitor Concentrations, p 020047.
15. Rheima AM, Anber AA, Abdullah HI, Ismail AH. Synthesis of alpha-gamma aluminum oxide nanocomposite via electrochemical method for antibacterial activity. *Nano Biomed. Eng.*, 2021, 13(1), 1-5.

© The AIC 2023. All rights reserved.

16. Al Marjani M, Aziz SN, Rheima AM, Abbas ZS. Impact of chromium oxide nanoparticles on growth and biofilm formation of persistence Klebsiella pneumoniae isolates. *Nano Biomed. Eng.*, 2021, 13(3), 321-327.
17. Kadhum HA, Salih WM, Rheima AM. Improved PSi/c-Si and Ga/PSi/c-Si nanostructures dependent solar cell efficiency. *Appl. Phys. A*, 2020, 126(10), 1-5.
18. Aboud NAA, Alkayat WM, Hussain DH, Rheima AM in Journal of Physics: Conference Series, IOP Publishing, 2020, vol. 1664, no. 1, A Comparative Study of ZnO, CuO and a Binary Mixture of ZnO 0.5-CuO 0.5 with Nano-dye on the Efficiency of the Dye-sensitized Solar Cell, p 012094.
19. Aziz SN, Al Marjani MF, Rheima AM, Al Kadmy IM. Antibacterial, antibiofilm, and antipersister cells formation of green synthesis silver nanoparticles and graphene nanosheets against Klebsiella pneumoniae. *Rev. Med. Microbiol.*, 2022, 33(1), 56-63.
20. Salman AT, Ismail AH, Rheima AM, Abd AN, Habubi NF, Abbas ZS in Journal of Physics: Conference Series, IOP Publishing, 2021, vol. 1853, no. 1, Nano-synthesis, Characterization and Spectroscopic Studies of Chromium (III) Complex Derived from New Quinoline-2-one for Solar Cell Fabrication, p 012021.
21. Ismail AH, Al-Bairmani HK, Abbas ZS, Rheima AM in IOP Conference Series: Materials Science and Engineering, IOP Publishing, 2020, vol. 928, no. 5, Nano Metal-complexes of Theophylline Derivative: Synthesis, Characterization, Molecular Structure Studies, and Antibacterial Activity, p 052028.
22. Kamil AF, Abdullah H, Rheima AM, Mohammed SH. Photochemical synthesized NiO nanoparticles based dye-sensitized solar cells: a comparative study on the counter electrodes and dye-sensitized concentrations. *J. Ovonic Res.*, 2021, 17(3), 299-305.
23. Mohammed SH, Rheima A, Al-Jaafari F, Al-Marjani, MF. Green-synthesis of platinum nanoparticles using olive leaves extracts and its effect on aspartate aminotransferase activity. *Egypt. J. Chem.*, 202265(4), 1-2.
24. Ismail AH, Al-Bairmani HK, Abbas ZS, Rheima AM. Nanosynthesis, spectroscopic characterisation and antibacterial activity of some metal complexes derived from Theophylline. *Egypt. J. Chem.*, 2020, 63(12), 4951-4962.
25. Trovarelli A, Zamar F, Llorca J, de Leitenburg C, Dolcetti G, Kiss JT. *J. Catal.*, 1997, 169, 490-502.
26. Steele BCH. Mass transport in materials incorporated in electrochemical energy conversion systems. *Solid State Ionics*, 1984, 12, 391-406.
27. Mogensen M, Sammes NM, Tompsett GA. Physical, chemical and electrochemical properties of pure and doped ceria. *Solid State Ionics*, 2000, 129(1-4), 63-94.
28. Zhang F, Chan SW, Spanier JE, Apak E, Jin Q, Robinson RD, Herman IP. Cerium oxide nanoparticles: Size-selective formation and structure analysis. *Appl. Phys. Lett.*, 2002, 80(1), 127-129.

© The AIC 2023. All rights reserved.

29. Tye L, El-Masry NA, Chikyow T, McLarty P, Bedair SM. Electrical characteristics of epitaxial CeO_2 on Si (111). *Appl. Phys. Lett.*, 1994, 65(24), 3081-3083.
30. Ali MM, Mahdi HS, Parveen A, Azam A in AIP Conference Proceedings, AIP Publishing LLC, 2018, vol. 1953, no. 1, Optical Properties of Cerium Oxide (CeO_2) Nanoparticles Synthesized by Hydroxide Mediated Method, p 030044.
31. Xia T, Kovochich M, Liong M, Madler L, Gilbert B, Shi H, Yeh JI, Zink JI, Nel, AE. Comparison of the mechanism of toxicity of zinc oxide and cerium oxide nanoparticles based on dissolution and oxidative stress properties. *ACS Nano*, 2008, 2(10), 2121-2134.
32. Tarnuzzer RW, Colon J, Patil S, Seal S. Vacancy engineered ceria nanostructures for protection from radiation-induced cellular damage. *Nano Lett.*, 2005, 5(12), 2573-2577.
33. Chelliah M, Rayappan JBB, Krishnan UM. Synthesis and characterization of cerium oxide nanoparticles by hydroxide mediated approach. *J. Appl. Sci.*, 2012, 12(16), 1734-1737.
34. Rheima A, Anber AA, Shakir A, Salah Hammed A, Hameed S. Novel method to synthesis nickel oxide nanoparticles for antibacterial activity. *Iran. J. Phys. Res.*, 2020, 20(3), 51-55.
35. Mohammed MA, Rheima AM, Jaber SH, Hameed SA. The removal of zinc ions from their aqueous solutions by Cr_2O_3 nanoparticles synthesized via the UV-irradiation method. *Egypt. J. Chem.*, 2020, 63(2), 425-431.
36. Rheima AM, Mohammed MA, Jaber SH, Hameed SA. Adsorption of selenium (Se^{4+}) ions pollution by pure rutile titanium dioxide nanosheets electrochemically synthesized. *Desalin. Water Treat.*, 2020, 194, 187-193.
37. Aboud NAA, Jasim BE, Rheima AM. Methylene orange dye removal in aqueous solution using synthesized CdO-MnO_2 nanocomposite: Kinetic and thermodynamic studies. *Chalcogenide Lett.*, 2021, 18(5), 237-243.
38. Hussain DH, Rheima AM, Jaber SH. Cadmium ions pollution treatments in aqueous solution using electrochemically synthesized gamma aluminum oxide nanoparticles with DFT study. *Egypt. J. Chem.*, 2020, 63(2), 417-424.
39. Rheima AM, Hussain DH, Almijbilee, MMA. Graphene-silver nanocomposite: synthesis, and adsorption study of cibacron blue dye from their aqueous solution. *J. Southwest Jiaotong Univ.*, 2019, 54(6).
40. Satilmis B. Amidoxime modified polymers of intrinsic microporosity (PIM-1); A versatile adsorbent for efficient removal of charged dyes; Equilibrium, kinetic and thermodynamic studies. *J. Polym. Environ.*, 2020, 28(3), 995-1009.
41. Ezzati R. Derivation of pseudo-first-order, pseudo-second-order and modified pseudo-first-order rate equations from Langmuir and Freundlich isotherms for adsorption. *Chem. Eng. J.*, 2020, 392, 123705.

© The AIC 2023. All rights reserved.

The Chemist
Journal of the American Institute of Chemists

Estimation of Nonlinear Regression Parameters Precision

Prasanth Sambaraju

Independent Researcher
Area of Chemistry: Chemistry Education
(E-mail: prasanth.sambaraju@gmail.com)

Abstract: The aim of this paper is to estimate the parameter precision values in nonlinear regression using Microsoft Excel. In case of simple linear regression, these values can be obtained from regression analysis in Excel. Commercially available programs output these values, but the main limitation is that they force the users to adopt a black box approach. The procedure described here can be adopted to any nonlinear dataset assuming that parameters obtained from solver accurately describe the nonlinear regression model. For one of the nonlinear datasets from NIST Statistical reference datasets, the parameters are initially estimated by using Solver and then by using Finite differences method parameter precision values are calculated. The results obtained were found to be comparable with the reported values.

Key Words: Nonlinear regression, solver, least squares, perturbation

1. Introduction

Regression analysis deals with the relationship between one or more independent variables and a dependent variable. Regression analysis is performed by selecting a suitable function which accurately describes the relationship between the two and estimator to calculate the parameter values. These regression parameters are calculated by least squares method. In linear regression [1], either the parameters are linear or the function describing the model is linear. Nonlinear regression methods are applied when the relationship between dependent and independent variables in is not linear. Nonlinear regression relies on iterative procedure to find the best fit. The process [2] starts with initial values for each parameter, and then by using least squares fitting, the best fit parameter values which minimizes the sum of squared residuals are estimated. Microsoft Excel Solver Add-in estimates parameters for nonlinear regression by least squares method, but it doesn't estimate their precision. The paper aims to use finite difference method to estimate these values.

© The AIC 2023. All rights reserved.

2. Nonlinear Regression

A model is considered to be nonlinear if any of the partial derivatives with respect to any of the model parameters are dependent on any other model parameters, any of the derivatives do not exit or are discontinuous. A nonlinear model can be expressed as (equation 1):

$$y = f(\theta; t) + \epsilon \quad (1)$$

where y is the vector of responses, f is the function used to describe the model, θ is vector of model parameters, t is the predictor variable and ε is the vector of residuals [3].

Rat43 dataset from National Institute of Standards and Technology (NIST) website [4], was selected to estimate the parameter precision by finite difference method. This dataset was selected, as the data can be fitted by using nonlinear regression method and is included in the higher level of difficulty group.

$$y = \frac{\beta_1}{\left(\left(1 + e^{[\beta_2 - + \beta_3 * t]}\right)^{\left(1/\beta_4\right)}\right)} \quad (2)$$

The nonlinear regression model described by equation 2 was used to fit the data, where response variable (y) is the dry weight of onion bulbs, whereas predictor variable (t) is growing time [4]. The model parameters were estimated by using both starting values and the results are given in Table 1.

Table 1. Rat43 Dataset Values

t (growing time)	*y* (onion bulb dry weight)
1	16.08
2	33.83
3	65.80
4	97.20
5	191.55
6	326.20
7	386.87
8	520.53
9	590.03

© The AIC 2023. All rights reserved.

10	651.92
11	724.93
12	699.56
13	689.96
14	637.56
15	717.41

Solver Implementation to Estimate Parameter Values (Table 2)

a) Data is entered in Excel, growing time (*t*) in column A and onion bulb dry weight (*y*) in column B.
b) Initial values for β_1, β_2, β_3 and β_4 given in NIST website were used [4].
c) By substituting different values of *t*, initial values of β_1, β_2, β_3 and β_4 in equation (2) different calculated *y* values were obtained.
d) Sum of squared errors (SSE) was obtained by adding the squared differences between *y* and *y* calculated value. SUMXMY2 function in Microsoft Excel was used to calculate the SSE value. In the parameters worksheet, cells B2 to B16 contains *y* values, cells C2 to C16 contains *y* calculated values which were obtained by using start 1 initial estimates. SSE value was obtained by using the formula "SUMXMY2 (C2:C16, B2:B16)".
e) Best fitted parameter values were obtained by minimizing the SSE value using generalized reduced gradient (GRG) nonlinear method.
f) The process was also repeated by using second set of start values as given in the NIST website [4].
g) Results obtained from both start values were in agreement with the reported values [4].

Table 2. Model Parameter Results Obtained After Least Square Fitting Using Excel Solver

Parameter	Start 1	Values obtained	Start 2	Values obtained	Certified values
β_1	100	699.6415127	700	699.6415126	699.6415127000
β_2	10	5.27712531	5	5.277125383	5.2771253025
β_3	1	0.759629383	0.75	0.759629391	0.75962938329
β_4	1	1.279248389	1.3	1.279248414	1.2792483859

3. Finite Difference Method

For a function with two or more independent variables, the partial derivative of that function with respect to a particular variable is the derivative of that function with respect to that variable, while holding the other variables constant [5]. The partial derivative term of each data point can by calculated by numerical differentiation. The parameter term (β_1) is varied by a small amount from its optimized value while the other parameters terms are held constant. This variation of a parameter by a small amount is called perturbation. The partial derivatives are calculated by using the formula in Equation 7

© The AIC 2023. All rights reserved.

[6] for all data points. Then the process is repeated for all the parameter terms in the model [6]. The Jacobian matrix (J) is constructed from all these partial derivative terms and is given by the following equation (3) [7], where m is the number of nonlinear parameters.

$$J = \begin{bmatrix} \left(\frac{\partial y_1}{\partial \beta_1}\right) & \left(\frac{\partial y_1}{\partial \beta_2}\right) & \cdots & \left(\frac{\partial y_1}{\partial \beta_m}\right) \\ \left(\frac{\partial y_2}{\partial \beta_1}\right) & \left(\frac{\partial y_2}{\partial \beta_2}\right) & \cdots & \left(\frac{\partial y_2}{\partial \beta_m}\right) \\ \vdots & \vdots & \ddots & \vdots \\ \left(\frac{\partial y_n}{\partial \beta_1}\right) & \left(\frac{\partial y_n}{\partial \beta_2}\right) & \cdots & \left(\frac{\partial y_n}{\partial \beta_m}\right) \end{bmatrix} \quad (3)$$

The parameter precision can be estimated from the matrix of partial derivatives (E), which is obtained by multiplying transpose of J with itself ($E = J^T * J$) [7] and is given in equation 4.

$$E = \begin{bmatrix} \Sigma\left(\frac{\partial y_1}{\partial \beta_1}\right)^2 & \Sigma\left(\frac{\partial y_1}{\partial \beta_1} * \frac{\partial y_2}{\partial \beta_2}\right) & \cdots & \Sigma\left(\frac{\partial y_1}{\partial \beta_1} * \frac{\partial y_m}{\partial \beta_m}\right) \\ \Sigma\left(\frac{\partial y_1}{\partial \beta_1} * \frac{\partial y_2}{\partial \beta_2}\right) & \Sigma\left(\frac{\partial y_2}{\partial \beta_2}\right)^2 & \cdots & \Sigma\left(\frac{\partial y_2}{\partial \beta_2} * \frac{\partial y_m}{\partial \beta_m}\right) \\ \vdots & \vdots & \ddots & \vdots \\ \Sigma\left(\frac{\partial y_1}{\partial \beta_1} * \frac{\partial y_m}{\partial \beta_m}\right) & \Sigma\left(\frac{\partial y_2}{\partial \beta_2} * \frac{\partial y_m}{\partial \beta_m}\right) & \cdots & \Sigma\left(\frac{\partial y_m}{\partial \beta_m}\right)^2 \end{bmatrix} \quad (4)$$

The square roots of the diagonal elements of the above E matrix inverse when multiplied by root residual standard deviation (RSD) yields the precision for the respective parameter (equations 5 and 6) [7], where SSE value was obtained from solver implementation and df is the degrees of freedom (difference between number of observation and number of parameters in the model).

$$\beta_{i,\text{precision}} = \text{RSD} * \sqrt{E^{-1}_{ii}}, i = 1, 2, 3, \ldots m \quad (5)$$

$$\text{RSD} = \sqrt{\frac{\text{SSE}}{\text{df}}} \quad (6)$$

© The AIC 2023. All rights reserved.

The individual partial derivatives for the J matrix can be calculated from the following equations (7) [7], where δ (perturbation) can be 10^{-6} or 10^{-7} [7]. The above calculations are performed in Microsoft Excel to obtain the parameter precision values for all the parameters.

$$\left(\frac{\partial y_i}{\partial \beta_1}\right)_{\beta_2,\ldots\beta_4,t_i} \approx \frac{y\left[\beta_1(1+\delta),\beta_2,\beta_3,\beta_4,t_i\right]-y[\beta_1,\beta_2,\beta_3,,\beta_4,t_i]}{\beta_1(1+\delta)-\beta_1}$$

$$\left(\frac{\partial y_i}{\partial \beta_2}\right)_{\beta_1,\beta_3,\beta_4,t_i} \approx \frac{y\left[\beta_1,\beta_2(1+\delta),\beta_3,\beta_4,t_i\right]-y[\beta_1,\beta_2,\beta_3,,\beta_4,t_i]}{\beta_2(1+\delta)-\beta_2}$$

$$\left(\frac{\partial y_i}{\partial \beta_3}\right)_{\beta_1,\beta_2,\beta_4,t_i} \approx \frac{y\left[\beta_1,\beta_2,\beta_3(1+\delta),\beta_4,t_i\right]-y[\beta_1,\beta_2,\beta_3,,\beta_4,t_i]}{\beta_3(1+\delta)-\beta_3} \quad (7)$$

$$\left(\frac{\partial y_i}{\partial \beta_4}\right)_{\beta_1,\beta_2,\beta_3,t_i} \approx \frac{y\left[\beta_1,\beta_2,\beta_3,\beta_4(1+\delta),t_i\right]-y[\beta_1,\beta_2,\beta_3,,\beta_4,t_i]}{\beta_4(1+\delta)-\beta_4}$$

© The AIC 2023. All rights reserved.

4. Results and Discussion

The partial derivative calculations for the first parameter using parameter values obtained from Start 1 values are shown in Figure 1. Values in Column A9 to B23 corresponds to the raw data, values in C9 to C23 correspond to calculated values obtained after solver optimization. For values in D9 to D23, to the first parameter (β_1) δ (10^{-6}) was added and then its corresponding *y* (independent variable) values are calculated. The values in E9 to E23 are calculated as per equation 7. The calculations are repeated for all the parameters to obtain the partial derivative matrix (J), as given in equation 3.

	A	B	C	D	E	F	G	H	I	J
6										
7	1. For paramter β_1									
8	t	y	cal (y) - 1	cal ($y(\beta_1[1+\delta], \beta_2,\beta_3,\beta_4,t_i)$)	$\left(\frac{\partial y_i}{\partial \beta_1}\right)_{\beta_2,\ldots\beta_4,t_i}$					Start 1
9	1	16.08	20.30188	20.3019031	2.9E-02				β_1	699.6415
10	2	33.83	36.41495	36.4149893	5.2E-02				β_2	5.277125
11	3	65.80	64.63606	64.6361257	9.2E-02				β_3	0.759629
12	4	97.20	112.3302	112.330263	1.6E-01				β_4	1.279248
13	5	191.55	187.5353	187.535493	2.7E-01				SSE	8786.405
14	6	326.20	292.3813	292.381567	4.2E-01				δ	1.0E-06
15	7	386.87	413.3579	413.358358	5.9E-01					
16	8	520.53	523.4563	523.456782	7.5E-01					
17	9	590.03	602.693	602.693607	8.6E-01					
18	10	651.92	650.1694	650.170022	9.3E-01					
19	11	724.93	675.4649	675.465532	9.7E-01					
20	12	699.56	688.0892	688.089879	9.8E-01					
21	13	689.96	694.1823	694.182966	9.9E-01					
22	14	637.56	697.0753	697.076022	1.0E+00					
23	15	717.41	698.4383	698.438971	1.0E+00					
24										

Figure 1. Excel Sheet Showing Partial Derivative Calculation One Parameter (β_1)

Click here to view/download complete Excel file

or click here go to Appendix

© The AIC 2023. All rights reserved.

The Jacobian matrix in cells N9 to N23 are obtained by pasting the values of E9 to E23 for first parameter. The values O9 to Q23 in the matrix are obtained similarly from the other three parameters, and the resulting matrix is shown in Figure 2.

	M	N	O	P	Q
7					
8		Jacobian matrix			
9		2.9E-02	-1.6E+01	1.6E+01	-5.6E+01
10		5.2E-02	-2.8E+01	5.6E+01	-8.4E+01
11		9.2E-02	-4.8E+01	1.4E+02	-1.2E+02
12		1.6E-01	-7.9E+01	3.2E+02	-1.6E+02
13		2.7E-01	-1.2E+02	6.0E+02	-1.9E+02
14		4.2E-01	-1.5E+02	9.2E+02	-2.0E+02
15		5.9E-01	-1.6E+02	1.1E+03	-1.7E+02
16		7.5E-01	-1.3E+02	1.0E+03	-1.2E+02
17		8.6E-01	-8.2E+01	7.4E+02	-7.0E+01
18		9.3E-01	-4.6E+01	4.6E+02	-3.7E+01
19		9.7E-01	-2.3E+01	2.6E+02	-1.9E+01
20		9.8E-01	-1.1E+01	1.4E+02	-9.0E+00
21		9.9E-01	-5.4E+00	7.0E+01	-4.3E+00
22		1.0E+00	-2.6E+00	3.6E+01	-2.0E+00
23		1.0E+00	-1.2E+00	1.8E+01	-9.4E-01

Figure 2. Jacobian Matrix

The result in Figure 3 is obtained by taking inverse of matrix E. The first parameter precision is obtained by multiplying the square root of value in N28 and RSD value (equation 8) [7].

	M	N	O	P	Q
26					
27		Inverse of matrix E			
28		0.332721	-0.02439	-0.00254	0.007355
29		-0.02439	0.005432	0.000504	-0.00176
30		-0.00254	0.000504	4.79E-05	-0.00016
31		0.007355	-0.00176	-0.00016	0.000592

Figure 3. Inverse of Matrix E

© The AIC 2023. All rights reserved.

$$\text{RSD} = \sqrt{\frac{8786.404908}{(15-4)}} = 28.26241466$$

$$\begin{aligned} \beta_{1,\text{precision}} &= \text{RSD} * \sqrt{\text{N28 cell value}} \\ \beta_{2,\text{precision}} &= \text{RSD} * \sqrt{\text{O 29 cell value}} \\ \beta_{3,\text{precision}} &= \text{RSD} * \sqrt{\text{P 30 cell value}} \\ \beta_{4,\text{precision}} &= \text{RSD} * \sqrt{\text{Q 31 cell value}} \end{aligned} \quad (8)$$

The results obtained were comparable with the reported values [4] and are given in Table 3.

Table 3. Comparison Standard Deviation of Parameter Estimate Values

Parameter	Values obtained	Reported values
β_1	16.3023271498	16.3022978170
β_2	2.0829153607	2.0828735829
β_3	0.19566584176	0.19566123451
β_4	0.68762926694	0.68761936385

5. Conclusions

The parameter precision results obtained from the finite difference method were comparable to the reported values. Finite difference method offers a convenient approach to estimate nonlinear regression parameter precision values. Even though the method is robust in calculating precision values, limitations due to solver, like lack of convergence during optimization or parameter values inaccurately describing the model, can be encountered. For example, in the case of MGH10 dataset (which is available in the NIST website), the parameter values obtained after solver optimization are incorrect, which in turn leads to inaccurate parameter precision values.

6. References

1. Frank IE. *Chemom. Intell. Lab. Syst.*, 1995, 27, 1-9.
2. Kemmer G, Keller S. *Nat. Protoc.*, 2010, 5, 267-281.
3. Peter LB in Pharmacokinetic-Pharmacodynamic Modeling and Simulation, 2nd ed., Springer, New York, 2011, ch. 3, pp 101-130.
4. NIST StRD Nonlinear regression. Accessed 2022 Jul 14. https://www.itl.nist.gov/div898/strd/nls/nls_main.shtml
5. Billo EJ in Excel® for Scientist and Engineers Numerical Methods, 1st ed., Wiley New Jersey, 2007, ch. 12, pp 263-286.

© The AIC 2023. All rights reserved.

6. Billo EJ in Excel® for Chemists: A Comprehensive Guide, 3rd ed., Wiley, New Jersey, 2011, ch. 15, pp 463-488.

7. Kirkup L in Data Analysis for Physical Scientists: Featuring Excel®, 2nd ed., Cambridge University Press, Cambridge, 2012, ch. 8, pp 335-381.

© The AIC 2023. All rights reserved.

$$\left(\frac{\partial y_i}{\partial \beta_1}\right)_{\beta_2,\ldots,\beta_4,x_i} \approx \frac{y[\beta_1(1+\delta),\beta_2,\beta_3,\beta_4,x_i] - y[\beta_1,\beta_2,\beta_3,,\beta_4,x_i]}{\beta_1(1+\delta)-\beta_1}$$

1. For paramter β_1

x	y	cal (y) - 1	cal ($y(\beta_1[1+\delta], \beta_2,\beta_3,\beta_4,x_i)$)	$\left(\frac{\partial y_i}{\partial \beta_1}\right)_{\beta_2,\beta_3,\beta_4,x_i}$
1	16.08	20.30188	20.301903	2.9E-02
2	33.83	36.41495	36.414989	5.2E-02
3	65.80	64.63606	64.636126	9.2E-02
4	97.20	112.3302	112.33026	1.6E-01
5	191.55	187.5353	187.53549	2.7E-01
6	326.20	292.3813	292.38157	4.2E-01
7	386.87	413.3579	413.35836	5.9E-01
8	520.53	523.4563	523.45678	7.5E-01
9	590.03	602.693	602.69361	8.6E-01
10	651.92	650.1694	650.17002	9.3E-01
11	724.93	675.4649	675.46553	9.7E-01
12	699.56	688.0892	688.08988	9.8E-01
13	689.96	694.1823	694.18297	9.9E-01
14	637.56	697.0753	697.07602	1.0E+00
15	717.41	698.4383	698.43897	1.0E+00

	Start 1
β_1	699.6415
β_2	5.277125
β_3	0.759629
β_4	1.279248
SSE	8786.405
δ	1.0E-06

Parital derivative matrix			
2.9E-02	-1.6E+01	1.6E+01	-5.6E+01
5.2E-02	-2.8E+01	5.6E+01	-8.4E+01
9.2E-02	-4.8E+01	1.4E+02	-1.2E+02
1.6E-01	-7.9E+01	3.2E+02	-1.6E+02
2.7E-01	-1.2E+02	6.0E+02	-1.9E+02
4.2E-01	-1.5E+02	9.2E+02	-2.0E+02
5.9E-01	-1.6E+02	1.1E+03	-1.7E+02
7.5E-01	-1.3E+02	1.0E+03	-1.2E+02
8.6E-01	-8.2E+01	7.4E+02	-7.0E+01
9.3E-01	-4.6E+01	4.6E+02	-3.7E+01
9.7E-01	-2.3E+01	2.6E+02	-1.9E+01
9.8E-01	-1.1E+01	1.4E+02	-9.0E+00
9.9E-01	-5.4E+00	7.0E+01	-4.3E+00
1.0E+00	-2.6E+00	3.6E+01	-2.0E+00
1.0E+00	-1.2E+00	1.8E+01	-9.4E-01

© The AIC 2023. All rights reserved.

2. For paramter β_2

x	y	cal (y) - 1	cal ($y(\beta_1, \beta_2[1+\delta], \beta_3, \beta_4, x_i)$)	$\left(\frac{\partial y_i}{\partial \beta_2}\right)_{\beta_1,\beta_3,\beta_4,x_i}$
1	16.08	20.30188	20.3018	-1.6E+01
2	33.83	36.41495	36.414806	-2.8E+01
3	65.80	64.63606	64.635807	-4.8E+01
4	97.20	112.3302	112.32973	-7.9E+01
5	191.55	187.5353	187.53468	-1.2E+02
6	326.20	292.3813	292.38046	-1.5E+02
7	386.87	413.3579	413.35711	-1.6E+02
8	520.53	523.4563	523.45559	-1.3E+02
9	590.03	602.693	602.69257	-8.2E+01
10	651.92	650.1694	650.16913	-4.6E+01
11	724.93	675.4649	675.46473	-2.3E+01
12	699.56	688.0892	688.08913	-1.1E+01
13	689.96	694.1823	694.18224	-5.4E+00
14	637.56	697.0753	697.07531	-2.6E+00
15	717.41	698.4383	698.43827	-1.2E+00

	Start 1
β_1	699.6415
β_2	5.277125
β_3	0.759629
β_4	1.279248
SSE	8786.405
δ	1.0E-06

Inverse of matrix E			
0.332721	-0.02439	-0.00254	0.007355
-0.02439	0.005432	0.000504	-0.00176
-0.00254	0.000504	4.79E-05	-0.00016
0.007355	-0.00176	-0.00016	0.000592

RSD	28.26241
β_1	16.30233
β_2	2.082915
β_3	0.195666
β_4	0.687629

© The AIC 2023. All rights reserved.

3. For paramter β_3

x	y	cal (y) - 1	cal (y(β_1, β_2,β_3[1+δ],β_4 ,x_i))	$\left(\frac{\partial y_i}{\partial \beta_3}\right)_{\beta_1,\beta_2,\beta_4,x_i}$
1	16.08	20.30188	20.301895	1.6E+01
2	33.83	36.41495	36.414995	5.6E+01
3	65.80	64.63606	64.636171	1.4E+02
4	97.20	112.3302	112.33039	3.2E+02
5	191.55	187.5353	187.53576	6.0E+02
6	326.20	292.3813	292.38198	9.2E+02
7	386.87	413.3579	413.35879	1.1E+03
8	520.53	523.4563	523.45703	1.0E+03
9	590.03	602.693	602.69356	7.4E+02
10	651.92	650.1694	650.16972	4.6E+02
11	724.93	675.4649	675.46505	2.6E+02
12	699.56	688.0892	688.08929	1.4E+02
13	689.96	694.1823	694.18232	7.0E+01
14	637.56	697.0753	697.07535	3.6E+01
15	717.41	698.4383	698.43829	1.8E+01

	Start 1
β_1	699.6415
β_2	5.277125
β_3	0.759629
β_4	1.279248
SSE	8786.405
δ	1.0E-06

© The AIC 2023. All rights reserved.

4. For paramter β_4

	y	cal (y) - 1	cal (y(β_1, β_2,β_3,β_4[1+δ],x_i))	$\left(\frac{\partial y_i}{\partial \beta_4}\right)_{\beta_1,\beta_2,\beta_3,x_i}$
1	16.08	20.30188	20.30181	-5.6E+01
2	33.83	36.41495	36.41485	-8.4E+01
3	65.80	64.63606	64.63591	-1.2E+02
4	97.20	112.3302	112.32995	-1.6E+02
5	191.55	187.5353	187.53506	-1.9E+02
6	326.20	292.3813	292.38102	-2.0E+02
7	386.87	413.3579	413.35773	-1.7E+02
8	520.53	523.4563	523.45611	-1.2E+02
9	590.03	602.693	602.69291	-7.0E+01
10	651.92	650.1694	650.16932	-3.7E+01
11	724.93	675.4649	675.46483	-1.9E+01
12	699.56	688.0892	688.08918	-9.0E+00
13	689.96	694.1823	694.18227	-4.3E+00
14	637.56	697.0753	697.07532	-2.0E+00
15	717.41	698.4383	698.43827	-9.4E-01

	Start 1
β_1	699.6415
β_2	5.277125
β_3	0.759629
β_4	1.279248
SSE	8786.405
δ	1.0E-06

© The AIC 2023. All rights reserved.

The Chemist
Journal of the American Institute of Chemists

Estimation of Serum Tumor Markers and Some Biochemical Parameters of Breast Cancer Patients

Eman Salem Mahmood[1], Mohammed I. Majeed[2], Intisar Ghanim Taha[3]

[1]Department of Basic Dental Sciences, College of Dentistry, University of Mosul, Iraq
[2]Department of Pharmacy, Technical Institute Mosul, Northern Technical University, Iraq
[3]Department of Sciences, College of Basic Education, University of Mosul, Iraq

Abstract: The study's goal was to determine the levels of certain tumor markers (CA15.3, CEA) and some biochemical parameters (calcium, vitamin D_3, alkaline phosphatase, uric acid, creatinine, and urea) in breast cancer women with different stages. Patients in the study were clinically and histologically diagnosed as having early stage One and stage 2 breast cancer, advanced phase 3 breast cancer, or metastatic fourth stage breast cancer. From February 2020 to March 2021, 140 people with tumors visited Mosul's oncology and nuclear medicine facility, were chosen for the current study, and they were separated into three groups: Group 1 had 45 patients (stages I & II); Group 2: 46 patients with (stage III); Group 3: 49 patients with (stage IV); and 45 normal controls. Cancer antigen 15.3 (CA15.3) and carcinoembryonic antigen (CEA) levels were detected.

The current study's findings demonstrate a highly significant increase in CEA and CA15.3 values in women with breast cancer as compared to the control group, and that this increase is associated to advanced stages. Furthermore, there was a significant decline in vitamin D levels in women with breast cancer when compared to the control group, while revealing a significant rise in the levels of alkaline phosphatase, uric acid and creatinine. No significant difference in calcium and urea levels was observed. The study of blood markers and other biochemistry indicators may be a valuable diagnostic technique in tracking the progress of breast cancer illness.

Key Words: Breast cancer, tumor markers, biochemical parameters, cancer antigen 15.3 (CA15.3), carcinoembryonic antigen (CEA)

1. Introduction

Breast cancer is a frequent malignant tumor that kills women, and its prevalence rate in Iraq is growing year after year. The fatality rate from breast cancer is declining, despite

© The AIC 2023. All rights reserved.

the disease's higher incidence rate, due to early detection and improved treatment [1]. Serum tumor indicators are useful in early diagnosis, detecting disease progression, recurrence, tumor metastasis, and evaluating therapy effectiveness [2].

The cancer antigen CA15.3 is a mucin that belongs to a wide family of glycoproteins released by breast cancer cells, and its levels may rise as the disease advances and fall when the tumor reacts to cancer therapy [3]. CA15.3 levels may be greater than normal in cancers of the lung, pancreas, ovary, and prostate, but not as high as in breast cancer. Endometriosis, pelvic inflammatory disease and liver illness are examples of non-cancerous diseases that raise CA15.3. It is also possible to rise during pregnancy [4].

Carcinoembryonic antigen (CEA) is a protein that has a role in cell adhesion. CEA is generally created throughout fetal development; however, it is no longer produced prior to delivery. As a result, it is seldom seen in the blood of healthy people [5]. CEA levels can be found to be elevated in cancers of the colon, lung, liver, breast, prostate, pancreas, ovary, and stomach. It is also elevated in several benign conditions, including inflammatory bowel disease, Crohn's disease, pulmonary infection, and renal failure. Levels are also increased in smokers [6]. Calcium is required for a variety of physiological processes, including gene transcription and cell growth, proliferation, migration, differentiation, and to fight many human illnesses, such as breast cancer and signaling abnormalities [7].

Alkaline phosphatase is a member of the hydrolysis enzyme family. ALP is mostly derived from the bones and liver in healthy persons, with modest contributions from the kidney and leukocytes [8].

In most cases, a high serum ALP content is connected with bile obstruction, cholestasis, liver illness, hepatitis, and malignancy. People with primary and metastatic liver and bone cancers, such as colorectal cancer hepatic malignancies and breast cancer with bone and liver involvement, have higher serum ALP levels [9]. Alkaline phosphatase determination (ALP) isoenzyme activity can aid in the diagnosis and clinical assessment of cancer patients.

2. Materials and Methods

Patients:

Serum samples were collected from 185 women aged 25 to 65 years, 45 of these women were control and 140 women were breast cancer patients attending the oncology and nuclear medicine hospital in Mosul from February 2020 to March 2021.

Group 1: 45 patients with (stages I and II), 46 individuals with (stage III), and 49 patients with (stage IV). All the patients had just been diagnosed with breast cancer and had had no treatment, radiation, chemotherapy, or any other type of hormone therapy

Obtaining Blood Samples:

All patients and controls had 5 mL of blood drawn from them, and the serum was centrifuged for 15 minutes at 4000 rpm before being stored at -20°C until analysis.

© The AIC 2023. All rights reserved.

Methods:

CA15.3, CEA and vitamin D_3 levels in serum were determined by using an Enzyme Immunoassay kit based on the principle of Enzyme-Linked Immunosorbent Assay [ELSA] (Dinabot, Tokyo, Japan). Serum calcium, alkaline phosphatase, uric acid, creatinine, and urea were measured by colorimetric method using a kit of Biolabo's manufacturing. A colorimetric approach was performed for the determination of serum calcium according to procedure in Panteghini et al. (2012) [10], alkaline phosphatase activity was estimated according to procedure in Kind and King (1954) [11], and serum uric acid was determined by an enzymatic method according to procedure in Burtis et al. (2015) [12]. Serum creatinine was estimated using the colorimetric method according to procedure in Mažeikienė and Kaminskas (2012) [13] and urea serum was estimated by the same method according to procedure in Burtis et al. (1999) [14].

Statistical analysis:

SPSS 17 was used to compute the mean and standard deviation for all statistics in the study (SD). The T-Test was used to examine the importance of the distinction in mean values. A p 0.05 number indicates significant, whereas a p >0.05 value indicates non-significant.

3. Results & Discussion

The following are the results of the several biochemical parameters examined in the study for patients and controls:

Table 1. Mean ± SD of Women's Ages and BMI Among Different Disease Stages of Studied Groups

Parameter	Control	Breast Cancer Group		
	n=45	Group 1 n=45	Group 2 n=46	Group 3 n=49
Age (years)	48.9±9.7	49.1±12.4	48.5±9.9	50.2±10.2
BMI (kg/m2)	30.5±6.1	31.4±7.6	30.8±6.6	31.3±6.4

CA15.3 in Breast Serum Cancer:

The data in Table 2 revealed a substantial rise (p 0.001) in serum CA15.3 in the first and second groups, and a significant increase (p 0.0001) in serum CA15.3 in the third group of breast cancer patients vs. control groupings. The results are congruent with

© The AIC 2023. All rights reserved.

those of prior studies which have shown that tumor markers CA15.3 are greater in advanced case breast cancer than in early-stage breast cancer [15]. Additionally, a recent study by Khushk et al. (2021) [16] showed that patients with malignant tumors had considerably higher CEA and CA15.3 values than a person with type I breast cancer [17], underlining the significance of serum CA15.3 as a useful marker for tracking the course of breast cancer and detecting metastasis in patients [18].

Table 2. Levels of CA15.3 and CEA in Patients with Breast Cancer and Control

groups Parameters	Control	First group Mean ± SD	Second group Mean ± SD	Third group Mean ± SD
CA15.3(U/mL)	14.5+1.7	22.6+1.3 **	33.9+2.7**	46.8+2.2***
CEA (ng/mL)	1.42±0.34	3.5±0.2 **	6.3±0.7***	7.5±0.4***

** Significant distinction at p ≤ 0.001

*** Significant distinction at p ≤ 0.0001

Serum CEA in Breast Cancer:

The results in Table 2 demonstrated that there was a considerable rise ($p < 0.001$) in concentrations in the blood serum of CEA in the first group of cancer patients, and a significant rise ($p < 0.0001$) in CEA serum in the second and third groups compared to breast cancer patients within the control groups. A similar finding has been reported by Mohammed et al. (2021) which showed that increased serum levels of CEA were shown in stage III breast cancer [19] and consistent with the study by Yerushalmi et al. (2012) which showed a significant correlation between elevated serum tumor marker levels and tumor stage [20]. Consequently, the usefulness of serum markers for cancer detection is stressed [21].

Serum Calcium in Breast Cancer:

The results in Table 3 show that the serum calcium concentrations of women with breast cancer did not differ significantly ($p > 0.05$). no significant subtle difference at ($p > 0.05$) in serum calcium in the groups of breast cancer women. These findings concur with earlier research [22,23] that found there is no proven connection between the stage of a tumor and calcium levels and subsequent research discovered no link between overall calcium and risk of cancer in postmenopausal individuals [24].

It is generally documented that calcium functions as an intracellular messenger in cell proliferation, death, as well as the transmission of a wide variety of signals [25].

© The AIC 2023. All rights reserved.

Table 3. Serum Level of Some Biochemical Parameters (Calcium, Vitamin D_3, Alkaline Phosphatase, Uric Acid, Creatinine, and Urea) in Patients with Breast Cancer

groups Parameters	Control group Mean ± SD	First group Mean ± SD	Second group Mean ± SD	Third group Mean ± SD
Ca^{+2} (mg/dl)	8.9±0.2	9.1±0.7	9.2±0.52	9.3±0.60
Vitamin D (ng/mL)	21.1±1.12	19.1±1.9 *	18.6±1.8*	18.3±1.3 *
ALP (U/L)	77.8 ±6.5	167±11.38 ***	193.4±4.1 ***	356±5.2 ** *
Uric Acid (mg/dl)	4.22±1.3	6.7±1.3 **	7.4 ±1.1 **	8.4 ±0.9 **
Creatinine (mg/dL	1.04±0.42	1.6±0.37 **	1.8 ±0.55 **	1.8 ±0.5 **
Urea (mg/dl)	35.9 ± 3.8	36.0 ± 1.5	36.3 ± 2.2	36.2 ± 2.7

* Significant distinction at $p \leq 0.005$, ** Significant distinction at $p \leq 0.001$

*** Significant subtle difference at $p \leq 0.0001$

Serum Vitamin D_3 in Breast Cancer:

The results in Table 3 showed a considerable reduction ($p > 0.05$) in serum D_3 vitamin levels in all groups of cancer breast patients. Vitamin D levels and the risk of developing breast cancer have been proven to be inversely related in numerous studies [26,27]. Another study by Park et al. (2015) discovered that blood vitamin D levels of 20 ng/mL were related with a 27% increased risk of breast cancer than someone with appropriate vitamin D levels (25(OH)D > 20 ng/ml) [28]. According to a study by Mawer et al. (1997), blood levels of 25(OH)D3 decrease with increasing tumor stage in breast cancer [29] and that vitamin D_3's active form, 1,25(OH)2D, has an anticancer impact by promoting cellular differentiation, activating apoptosis, blocking angiogenesis, and limiting cancer cell development [30]. Vitamin D has a vital role in inducing apoptosis, neuronal differentiation promotion, has anti-inflammatory and anti-angiogenic effects, and suppresses angiogenesis, invasion and metastasis [31].

Serum Alkaline Phosphatase in Breast Cancer:

Clearly, as seen in Table 3, there was a sharp rise ($p \leq 0.0001$) in alkaline phosphatase serum (ALP) in all groups of breast cancer patients all groups of as compared to the control. These findings support prior research that found a considerable increase in non-metastatic cases, with the number of cases without metastasis going up by a factor of six, while the number of cases with metastasis went up by a factor of four. [32].

Similar to Singh et al. (2013), who discovered a considerable increase in ALP levels at various carcinogenesis development stages [33], Mishra et al. (2004) discovered a continuous increase in ALP levels in metastasis [34]. The increase in ALP indicates that the malignancy has progressed to the bones or liver [35]. The increased serum ALP is caused by the enzyme's quicker de novo synthesis and subsequent regur-gitation into the serum. In breast cancer patients, a gradual rise in serum ALP activity is a sign of metastasis [34].

© The AIC 2023. All rights reserved.

Serum in Uric Acid Breast Cancer:

The outcomes listed in Table 2 revealed a considerable rise ($p \leq 0.001$) in serum uric acid in all groups of breast cancer women as compared to the control. A similar finding has been reported by other investigators [36]. A high amount of serum uric acid is linked to a number of illnesses, the most common of which is renal failure. According to Veni et al. (2011), the dramatically increased uric acid levels in women with breast cancer who have not received any treatment may be connected to oxidative stress [37].

Serum Creatinine Breast Cancer:

Tables 2 and 3 demonstrate that serum creatinine levels in the first, second, and third groups of breast cancer women rise significantly ($p \leq 0.001$) in contrast to healthy controls. Creatinine levels in the blood are regarded as more responsive than BUN in determining renal function. Because renal illness is the sole reason for elevated creatinine levels, Devi et al. observed an increase in creatinine levels in 2015 [38].

Serum Urea in Breast Cancer:

The statistical examination of the data revealed no significant change in serum urea between these groups ($p > 0.05$). All of the groups' results were within the normal range, which is consistent with previous findings [38].

4. Conclusion

Patients with advanced forms of breast cancer reported considerably higher levels of CEA and CA15.3 than those with early-type breast cancer, implying that these tumor markers' serum levels may be more efficient than early detection in maintaining advanced malignancies and may have a vital role in the early detection of metastasis in breast cancer patients.

The examination of serum biochemical characteristics might be a useful diagnostic tool for illness and metastatic surveillance.

5. References

1. Siegel RL, Miller KD, Jemal A. Cancer statistics. *Ca-Cancer J. Clin.*, 2016, 66, 7-30.
2. Bray F, Ferlay J, Soerjomataram I, Siegel RL, Torre LA, Jemal A. Global cancer statistics 2018: GLOBOCAN estimates of incidence and mortality worldwide for 36 cancers in 185 countries. *Ca-Cancer J. Clin.*, 2018, 68(6), 394-424.
3. Lee JS, Park S, Park JM, Cho JH, Kim SI, Park BW. Elevated levels of preoperative CA 15–3 and CEA serum levels have independently poor prognostic significance in breast cancer. *Ann. Oncol.*, 2013, 24, 1225-1231.

© The AIC 2023. All rights reserved.

4. Incoronato M, Mirabelli P, Catalano O, Aiello M, Parente C, Soricelli A. CA15.3 is a useful serum tumor marker for diagnostic integration of hybrid positron emission tomography with integrated computed tomography during follow-up of breast cancer patients. *BMC Cancer*, 2014, 14, 356. 10.1186/1471-2407-14-356
5. Shrivastava V, Ghanghoria A, Mandloi D, Ghanghoria S. A prospective study on analysis of CA15.3 in breast cancer patients as a prognostic marker. *J. Dent. Med. Sci.*, 2015, 14, 5-8.
6. Di Gioia D, Heinemann V, Nagel D, Untch M, Kahlert S, Bauerfeind I. Kinetics of CEA and CA15.3 correlate with treatment response in patients undergoing chemotherapy for metastatic breast cancer (MBC). *Tumor Biol.*, 2011, 32, 777-785.
7. Cross BM, Breitwieser GE, Reinhardt TA, Rao R. Cellular calcium dynamics in lactation and breast cancer: From physiology to pathology. *Am. J. Physiol.: Cell Physiol.*, 2014, 306, C515-C526.
8. Aminian A, Karimian F, Mirsharifi R, Alibakhshi A, Hasani SM, Dashti H. Correlation of serum alkaline phosphatase with clinicopathological characteristics of patients with oesophageal cancer. *East. Mediterr. Health J.*, 2011, 17, 862-866.
9. Ramaswamy G, Rao VR, Krishnamoorthy L, Ramesh G, Gomathy R, Renukadevi D. Serum levels of bone alkaline phosphatase in breast and prostate cancer with bone metastasis. *Indian J. Clin. Biochem*., 2000, 15(2), 110-113.
10. Panteghini M, Bais R in Tietz Textbook of Clinical Chemistry and Molecular Diagnostics, 5th ed., ed. CA Burtis, ER Ashwood, DE Bruns, Elsevier Saunders, Philadelphia, 2012, Serum Enzymes, pp 577-579.
11. Kind PR, King EJ. Estimation of plasma phosphatase by determination of hydrolyzed phenol with amino-antipyrine. *J. Clin. Pathol*., 1954, 7, 322-326.
12. Burtis CA, Ashwood ER, Bruns DE in Tietz Textbook of Clinical Chemistry and Molecular Diagnostics, Saunders (an imprint of Elsevier, Inc., USA), 2015, pp 356, 368.
13. Mažeikienė A, Kaminskas A in Biochemistry Laboratory Manual, Vilnius University, Latvia, 2012, pp 1, 11, 28, 30, 32, 34. ISBN 978-609-459-125-9
14. Burtis CA, Ashwood ER in Tietz Textbook of Clinical Chemistry, 3rd ed., W.B. Saunders, Philadelphia, 1999.
15. Fu Y, Li H. Assessing clinical significance of serum CA15.3 and carcinoembryonic antigen (CEA) levels in breast cancer patients: a meta-analysis. *Med. Sci. Monit.*, 2016, 22, 3154-3162.
16. Singh I, Singh J, Kaur R, Banipal R. Comparative study of CA15.3 levels in pre-treated breast cancer patients and controls. *Int. J. Contemp. Med. Res.,* 2018, 5(3), C1-C4.
17. Khushk M, Khan A, Rehman A, Sheraz S, Tunio YM, Khan ME. The role of tumor markers: Carcinoembryonic antigen and cancer antigen 15-3 in patients with breast cancer. *Cureus*, 2021, 13(7), e16298.

© The AIC 2023. All rights reserved.

18. Daniele A, Divella R, Trerotoli P. Clinical usefulness of cancer antigen 15-3 in breast cancer patients before and after surgery. *Open Breast Cancer J.*, 2013, 5, 1-6, 15.
19. Mohammed F, Gamal L, Mosa M. Assessment of CA15.3 and CEA as potential markers for breast carcinoma prognosis in Egyptian females. *Afr. J. Basic Appl. Sci.*, 2021, 2(1), 44-50.
20. Yerushalmi R, Tyldesley S, Kennecke H, Speers C, Woods R, Knight B. Tumor markers in metastatic breast cancer subtypes: Frequency of elevation and correlation with outcome. *Ann. Oncol*., 2012, 23(2), 338-345.
21. Tang S, Zhou F, Sun Y, Wei L, Zhu S, Yang R, Huang Y and Yang J. CEA in breast ductal secretions as a promising biomarker for the diagnosis of breast cancer: A systematic review and meta-analysis. *Breast Cancer*, 2016, 23, 813-819.
22. Thaw SS, Sahmoun A, Schwartz GG. Serum calcium, tumor size, and hormone receptor status in women with untreated breast cancer. *Cancer Biol. Ther.*, 2012, 13(7), 467-471.
23. Sprague BL, Skinner HG, Trentham-Dietz A, Lee KE, Klein BEK. Serum calcium and breast cancer risk in a prospective cohort study. *Ann. Epidemiol*., 2010, 20, 82-85.
24. Almquist M, Manjer J, Bondeson L, Bondeson A-G. Serum calcium and breast cancer risk: Results from a prospective cohort study of 7,847 women. *Cancer, Causes Control*, 2007, 18(6), 595-602.
25. Ramasamy I. Recent advances in physiological calcium homeostasis. *Clin. Chem. Lab. Med.*, 2006, 44(3), 237-273.
26. Kim Y, Je Y. Vitamin D intake, blood 25(OH)D levels, and breast cancer risk or mortality: Meta-analysis. *Br. J. Cancer*, 2014, 110(11), 2772-2784.
27. Engel P, Fagherazzi G, Boutten A, Dupre T, Mesrine S, Boutron-Ruault M-C, Clavel-Chapelon F. Serum 25(OH) vitamin D and risk of breast cancer: a nested case-control study from the French E3N cohort. *Cancer Epidemiol. Biomarkers Prev.*, 2010, 19(9), 2341-2350.
28. Park S, Lee DH, Jeon JY, Ryu J, Kim S, Kim JY. Serum 25-hydroxyvitamin D deficiency and increased risk of breast cancer among Korean women: A case-control study. *Breast Cancer Res. Treat.*, 2015, 152(1), 147-154.
29. Mawer EB, Walls J, Howell A, Davies M, Ratcliffe WA, Bundred NJ. Serum 1,25-dihydroxyvitamin D may be related inversely to disease activity in breast cancer patients with bone metastases. *J. Clin. Endocrinol. Metab.*, 1997, 82, 118-22.
30. Feldman D, Krishnan AV, Swami S. The role of vitamin D in reducing cancer risk and progression. *Nat. Rev. Cancer*, 2014, 14(5), 342-357.
31. Feldman D, Krishnan AV, Swami S, Giovannucci E, Feldman BJ. The role of vitamin D in reducing cancer risk and progression. *Nat. Rev. Cancer*, 2014, 14 (5), 342-357.
32. Metwallya I, Zuhdya M, Hamdya O. Evaluation of serum alkaline phosphatase as a marker of

© The AIC 2023. All rights reserved.

metastasis in early breast cancer. *Revista de Senologia y Patologia Mamaria*, 2020, 33(2), 45-49.
33. Singh AK, Pandey A, Tewari M, Kumar R, Sharma A, Singh KA. Advanced stage of breast cancer hoist alkaline phosphatase activity: Risk factors for females in India. *3 Biotech*, 2013, 3, 517-520.
34. Mishra S, Sharma DC, Sharma P. Studies of biochemical parameters in breast cancer with and without metastasis. *Indian J. Clin. Biochem*., 2004, 19(1), 71-75.
35. Ritzke C, Stieber P, Untch M, Nagel D., Eiermann W, Fateh-Moghadam A. Alkaline phosphatase isoenzymes in detection and follow up of breast cancer metastases. *Anticancer Res*., 1998, 18(28), 1243-1249
36. Chhabra RJ, Mangukiya K, Sharma N, Sharma R. Estimation of serum uric acid and bilirubin in breast cancer. *Scholars Acad. J. Pharm*., 2015, 4(7), 337-339.
37. Veni GK, Rao DB, Kumar DM, Usha B, Krishna VM, Roa TR. Clinical evaluation of oxidative stress in women with breast cancer. *Recent Res. Sci. Technol*., 2011, 3(1), 55-58.
38. Devi LI, Ralte L, Ali MA. Serum biochemical profile of breast cancer patients. *Eur. J. Pharm. Med. Res.*, 2015, 2, 210-214.

© The AIC 2023. All rights reserved.

The Chemist
Journal of the American Institute of Chemists

Formulation and Sustained-Release of Verapamil Hydrochloride Tablets

Zaid Hamid Mahmoud[1], Ahmed B. Mahdi[2], Yasir S. Alnassar[3], and H. N. K. AL-Salman[4]

[1] College of Sciences, Diyala University, Diyala, Iraq
[2] Anesthesia Techniques Department, Al-Mustaqbel University College, Babylon, Iraq
[3] The University of Mashreq, Baghdad, Iraq
[4] Department of Pharmaceutical Chemistry, College of Pharmacy, University of Basrah, Iraq
***Address for correspondence** (E-mail: Zaidhameed_91@yahoo.com)*

Abstract: Verapamil hydrochloride effervescent tablets are the principal focus of this investigation. Material & Methods: Verapamil hydrochloride floating tablets were made using the direct compression method. HPMC-K15M, karaya gum, sodium bicarbonate, and diluents were homogenized for ten minutes before adding magnesium stearate to each tablet formulation. Each tablet had a total weight of 300 mg. HPMC was utilized in the range of 20-40 mg, and karaya gum was used in the 40-90 mg range. We used a mortar and pestle for kneading the powder combination for another 5 minutes. A Rimek rotating tablet machine was used to compress the mixture into tablet form. The formulations were tested using a variety of criteria following their production. Results & Discussion: The tablet formulation friability range was between 0.3 ± 0.0064 and 0.59 ± 0.0077%. The manufactured tablet formulation's weight fluctuation is within USP guidelines. The range of thickness was discovered to be 4.1 ± 0.48 to 4.2 ± 0.76 mm. The assay for drug content range was between 96.52 ± 0.35 and 102.13 ± 0.53%. For B1, B5, B6, B9, and B10 at 12 hours, more than 75% of the medication was released. B1 showed a maximum of 30% drug release in the first hour and a steady release for up to 12 hours. One possible explanation for B8's low drug release is the creation of a thick gel barrier on top of the tablet.

Key Words: Effervescent, Verapamil, bioequivalence, FDDS, floating tablet

1. Introduction

Floating drug delivery systems "FDDS" or hydrodynamically controlled systems are low-density systems to remain buoyant in the stomach for a long time without affecting the

© The AIC 2023. All rights reserved.

rate at which the stomach empties. While floating on the gastric contents, the drug is gradually taken from the body at the desired rate. Immediately after taking the drug, the stomach's remaining systems are flushed out. A longer period of stomach retention and improved control over plasma medication concentrations are achieved as a result [1]. Additionally, a certain level of floating force (F) is needed to maintain the dose form stable on the surface of the meal so that the buoyancy retention principle can be appropriately applied. Buoyant systems can be made using granules, powders, capsules, tablets, laminated films, and hollow micro-spheres, among other things [2-15].

2. Materials & Methods

Formulation of Effervescent Floating Tablets

Verapamil hydrochloride floating tablets were made using the direct compression method. We blended HPMC-K15M, karaya gum, sodium bicarbonate, and diluents for ten minutes before adding magnesium stearate to each tablet formulation, which included the medicine. Table 1 shows the formulation chart of effervescent floating Verapamil hydrochloride tablets. Each tablet had a total weight of 300 mg. HPMC was utilized in the range of 20-40 mg, and karaya gum was used in the 40-90 mg range. A mortar and pestle were used to knead the powder combination for another 5 minutes [16,17].

Table 1. Formulation Chart of Effervescent Floating Verapamil Hydrochloride Tablets

Ingredients mg	F1	F2	F3	F4	F5	F6	F7	F8	F9	F10	F11	F12	F13
Verapamil Hydrochloride	120	120	120	120	120	120	120	120	120	120	120	120	120
Karaya Gum	40	40	40	40	70	70	70	70	70	90	90	90	90
HPMC K15M	20	40	30	30	20	40	20	40	30	20	40	30	30
Sodium Bicarbonate	20	20	10	30	10	10	30	30	20	20	20	10	40
PVP K30	15	15	15	15	15	15	15	15	15	15	15	15	15
Magnesium Stearate	5	5	5	5	5	5	5	5	5	5	5	5	5
Lactose	70	50	70	50	60	40	40	20	40	30	10	30	00
Total weight	300	300	300	300	300	300	300	300	300	300	300	300	300

© The AIC 2023. All rights reserved.

Technological Characteristics of Floating Tablets

Weight variation test

The average weight of 20 tablets from each formulation is calculated by weighing each tablet individually and averaging the results. The individual weights are compared with the overall average weight. The standard variation for tablets with an average weight of 350 mg is ±5% (equation 1).

$$\% \text{ deviation} = \frac{\text{Average weight of tablet} - \text{individual tablet weight}}{\text{Average weight of tablet}} * 100 \quad (1)$$

Friability

We used a Roche friabilator to grind ten pills into fine powder for four minutes at 25 rpm. They were removed, dedusted, and weighed again. The formula for calculating the percentage of friability in the tablets (equation 2) is [18]:

$$\% F = \{1-(W_t/W)\} \times 100 \quad (2)$$

where % F is percentage friability, W is the initial weight of the tablet, and W_t is the final weight of tablets after revolutions.

Hardness

The average of the three pills taken from each formulation was used in the study. As a result, the Inweka hardness tester is used to determine how hard each tablet is to the touch. It is measured in kilograms.

Thickness and diameter

Mitutoyo micrometer screw gauge is used to measure tablet thickness and diameter. Each formulation has an average of five pills taken. Millimeter (mm) is the unit of meas-urement.

Uniformity of drug content

Five pills were ground to powder at random to determine if the drug content was homogeneous. When the drug is dissolved for 5 hours with intermittent shaking, it dilutes to 100 ml of buffer and stores at room temperature. Filtration removes insol-uble residue by diluting 1 ml of the filtrate to 10 ml with buffer. We decided to measure the absorbance at its highest using a U.V. visible spectrophotometer. The trials were repeated three times for each formulation, and the mean data was recorded for each.

Drug content was calculated using the following equation (3):

$$\% \text{ Drug content} = \text{conc. } (\mu g/ml) \times \text{Dilution factor} \times 100/50 \quad (3)$$

© The AIC 2023. All rights reserved.

Drug-excipient Compatibility Studies

Fourier transforms infrared spectroscopy (FT-IR)

Drug-excipient interaction studies were conducted to assess the drug's integrity and compatibility in the formulation. Fourier transforms infrared FT-IR spectroscopy was used to examine the pure medication and optimized formulations. FT-IR spectra of pure drug and its formulations were obtained by an "FT-IR Shimadzu 8400S" (Japan) spectrophotometer using the KBr pellet method. The samples were scanned from 400 to 4,000 cm^{-1} wave number.

Differential scanning calorimetry (DSC)

DSC was carried out on a pure sample of the medication and its powdered form. Calorimetric measurements were performed using high purity alpha-alumina discs as a reference cell. The dynamic scans were taken in a nitrogen atmosphere at the heat rate ± of 10°C min^{-1}. The energy is measured as Joules per kilocalorie [19].

In vitro floating studies [20]

Floating lag time and total floating time were used to measure *in vitro* buoyancy. A USP dissolving device was used for the test type-II (basket) using 900 ml of 0.1 N HCl buffer solutions at 100 rpm at 37 ± 0.5°C. In this experiment, the floating lag and total time are recorded as the time it took for the formulation to reach the surface of the dissolving medium and the time it took for the formulation to remain there (Figure 1).

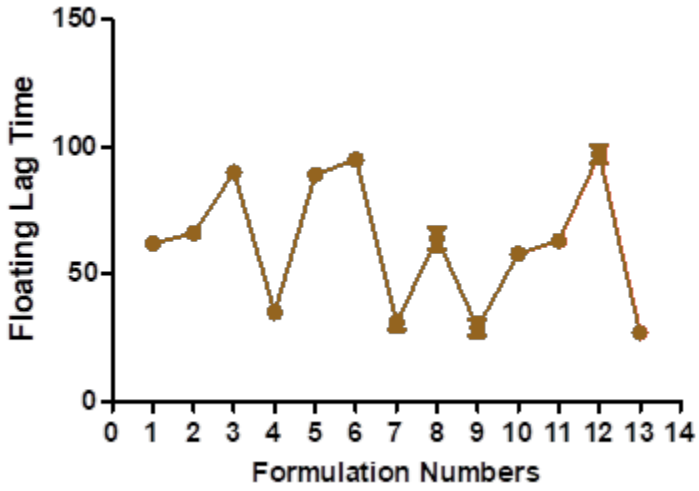

Figure 1. Effect on Floating Lag Time of Different Formulations

© The AIC 2023. All rights reserved.

Water uptake studies [21]

The swelling of the polymers is based on their propensity to absorb water and expand. A USP dissolving apparatus type-II (basket) was used to dissolve the tablet in pH 1.2 hydrochloric acid buffer at 100 revolutions per minute to conduct a water absorption study (RPM). The medium was maintained at 37 ± 0.5°C throughout the study. Regularly, the tablets were taken out, weighed, and blotted to remove any extra water before being put back in. Water uptake (W.U.) (equation 4) is used to describe the swell ability of the tablets.

$$\text{W.U. (\%)} = \frac{\text{Weight of Swollen tablet - Initial weight of tablet}}{\text{Initial weight of tablet}} \times 100 \quad (4)$$

3. Results & Discussion

Technological characteristics of floating tablets

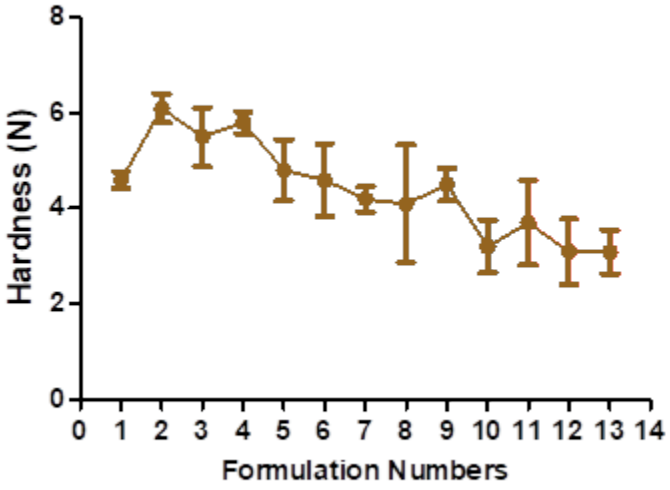

Figure 2. Effect on Hardness of Different Formulations

The hardness of floating tablets ranged from 4.1 ± 1.23 to 6.1 ± 0.306 kg (Figure 2), depending upon the mixture of the polymer used. The tablet formulation's friability ranged from 0.3 ± 0.0063 to 0.59 ± 0.0076%. The manufactured tablet formulation's weight fluctuation is within USP guidelines. The thickness is discovered to be between 4.1 ± 0.48 and 4.2 ± 0.76 mm (Figure 3). The drug content assays ranged from 96.52± 0.37 to 102.03 ± 0.53% (Figure 4).

© The AIC 2023. All rights reserved.

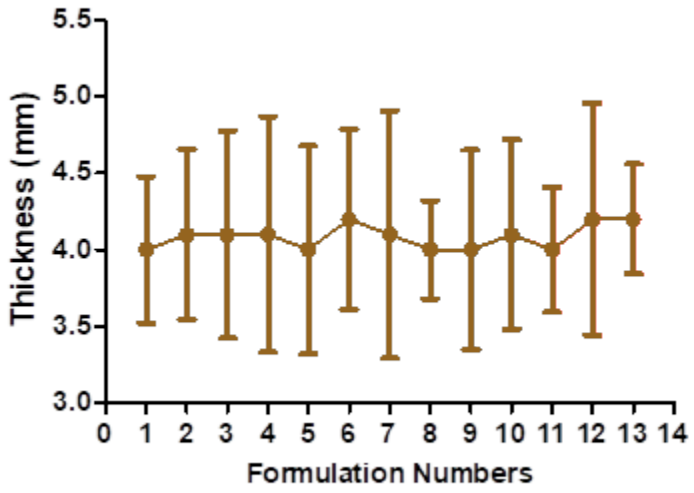

Figure 3. Effect on Thickness of Different Formulations

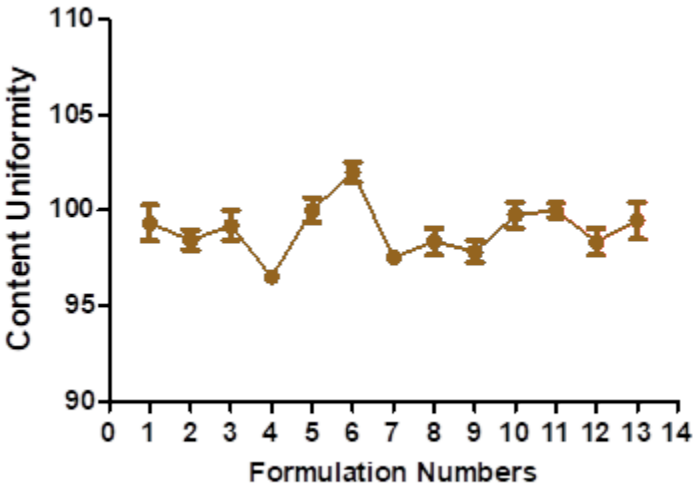

Figure 4. Effect on Content Uniformity of Different Formulations

Fourier transforms infrared spectroscopy (FT-IR)

Potassium bromide dispersion is used to measure the spectra in the solid-state. The FT-IR technology was used to capture the bands. The FT-IR spectral study found that the pure drug and the drug formulation have similar distinctive peaks with slight changes (Table 2). As a result, it was determined that the medication and polymer utilized have no chemical interaction.

© The AIC 2023. All rights reserved.

Table 2. FT-IR Spectral Data of Effervescent Floating Tablet of Verapamil Hydrochloride (B1) and Verapamil Hydrochloride Pure Drug

Functional groups	Frequency of pure drug (cm^{-1})	Frequency of formulation (cm^{-1})
C-H Stretching vibrations of methyl and methylene groups	3030.5-2860	3051.49-2789.16
C-H stretching vibrations of the methoxy group	2840	2843.17
C-O stretching vibrations of the aromatic ethers	1262	1255.70
Sharp weak bond due to C=N stretching vibrations of the alkyl nitrile	2236	2235.57
Skeletal stretching vibrations of the benzene ring	1607, 1518	1599, 1518

Differential scanning calorimetry (DSC)

Screening for compatibility between drugs and excipients is made more accessible with DSC, which provides a wealth of data on potential interactions in a short period (Table 3). Verapamil hydrochloride and formulation B1 underwent a DSC study. An endothermic peak at 138.25°C, the drug's melting point, maybe seen on its therm-ogram. The melting point of the medication is found to be 139.53°C in the matrix tablet formulation B1. The medication and excipients have no interaction, according to the analysis of thermograms obtained using DSC [22,23].

Table 3. DSC Thermogram Data of Effervescent Floating Tablet of Verapamil Hydrochloride (B1) and Verapamil hydrochloride Pure Drug

Drug and formulation	T_o(°C)	T_m(°C)	T_c(°C)	Melting range(°C)
Verapamil Hydrochloride	131.21	139.54	145.74	14.10
Formulation B1	130.98	138.26	144.86	13.86

T_o - Onset of melt, T_m - Melting point, T_c - Completion of melt

© The AIC 2023. All rights reserved.

***In vitro* buoyancy studies**

The tablet turns buoyant when its density drops below 1 g/ml. Tablets made with karaya gum, and HPMC has good gel strength, allowing CO_2 gas to be trapped inside and resulting in a long-lasting buoyancy. The system must float for a few minutes after contact with stomach fluid to prevent the dose form from being pushed into the small intestine with food. Experiments show that as the effervescent agent and karaya gum increases in B13, it takes longer for the system to float in the medium. The more significant concentration of effervescent agents resulted in more CO_2 being produced faster and at a higher rate. A high level of buoyancy necessitated sodium bicarbonate. In general, the gastric emptying time was 4 hours. Because Verapamil hydrochloride is absorbed mainly from the proximal section of the intestine, the longer the medicine is in the stomach, the more it is absorbed (Table 4) [24].

Table 4. Effect of Sodium Bicarbonate on Onset and Duration of Floatation of the Effervescent Floating Tablet of Verapamil Hydrochloride (B1)

Amount of sodium bicarbonate (mg)	Onset of floating (s)	Duration of floating (h)
10	92±3.88	16±0.83
20	62±2.97	21±0.38
30	32±2.52	24±0.67
40	27±0.06	18±0.78

Water uptake studies

At one hour, the B4, B6, and B7 swelled by a large percentage. At the end of 8 hours, B8 exhibited a steady increase in the proportion of swell. The use of karaya gum slows down the water intake in the first hour. During the 8 hours, the levels of B2, B3, and B5 decrease. Sodium bicarbonate concentration does not affect the swelling properties, but lactose concentration in B8 has the most significant effect ($p \geq 0.05$) (Figure 5).

© The AIC 2023. All rights reserved.

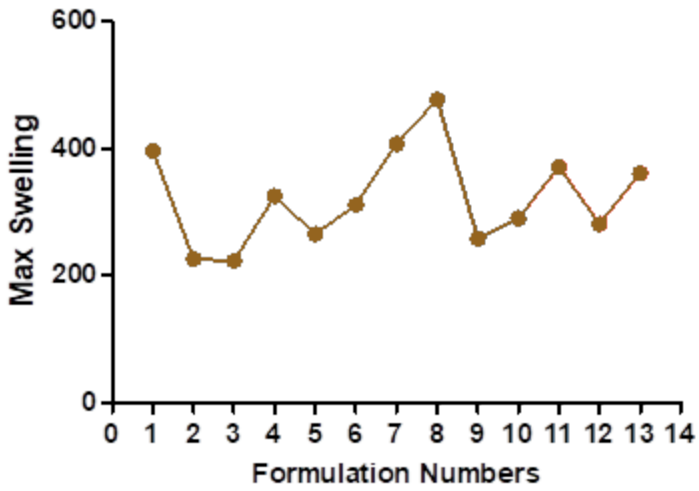

Figure 5. Effect on Max Swelling of Different Formulations

Seipmann and Peppas think that the water content of the tablet has a considerable impact on the diffusion of the medication. To understand why this can be the case, we need to understand how water affects the mobility of polymer chains. Polymer chain relaxation occurs with volume increase, resulting in a significant system swell. Higher water content can also indicate faster stomach fluid entry into the tablet, resulting in faster CO_2 gas generation and reduced floating time. As a result, the tablet swells faster and more rapidly, increasing the tablet's dimensions and decreasing diffusion rates.

***In vitro* drug release studies**

There is more than 75% drug release at 12 hours for each of the following: B1, B5, B6, B9, and B10. At a maximum of 30% in the first hour and for nearly 12 hours, the B1 maintained a steady release of the medication. B8 shows the lowest drug release of all the formulations, which may be due to the substantial gel barrier on the tablet. Other formulations with a more ex-tensive swelling index were shown to have a similar effect on drug diffusion across the gel barrier. B1 had a more excellent lactose content than any of the other samples. An infusion media dispersed into the matrix, leading to drug diffusion and controlled release from tablets (Figures 6 and 7).

© The AIC 2023. All rights reserved.

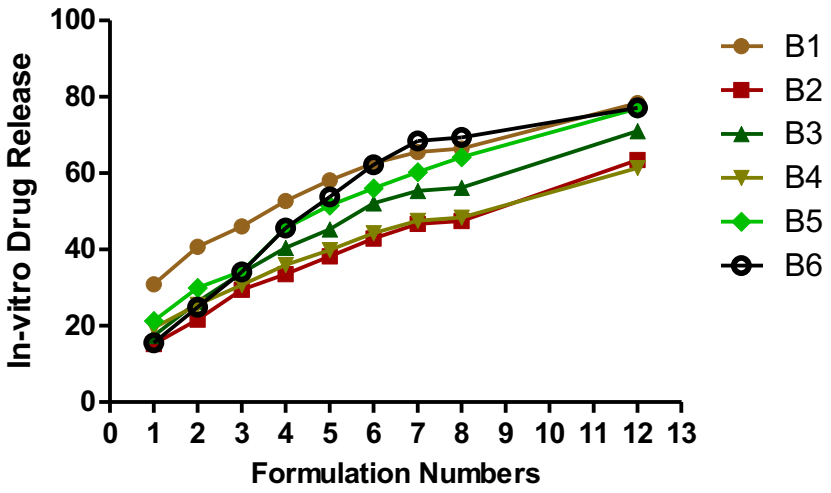

Figure 6. *In-vitro* Drug Release of Different Formulations

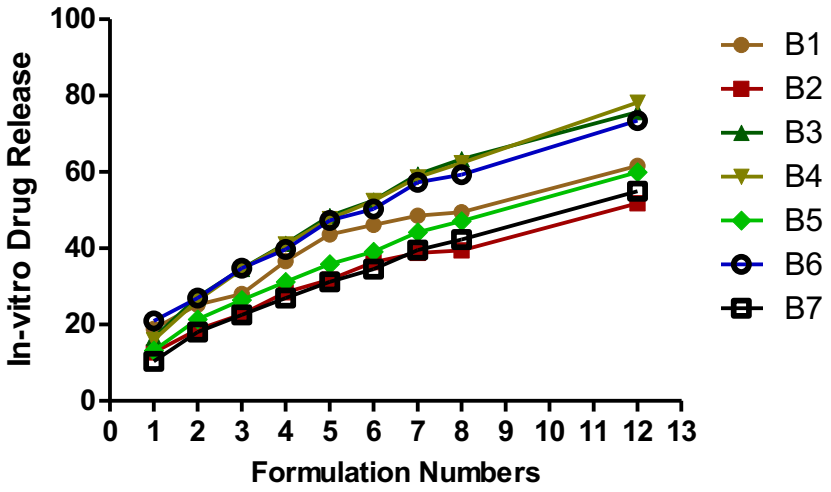

Figure 7. *In-vitro* Drug Release of Different Formulations

Mathematical model fitting of obtained drug release data

To further understand the *in vitro* drug dissolution profiles, we use various mathematical models, including the Korsmeyer-Peppas equation and Higuchi kinetics, to examine the data. The PCP disso v2.08 software was used to determine the release rates k and n for each model. In order to assess the model's accuracy, correlation coefficients (R2) were used. Table 6.08 lists the R2, k, and n values. Korsmeyer-Peppas and Matrix models were compared using R2 values; the Matrix model was found to have the best R2 values, while Korsmeyer-Peppas had the best R2 values for the other models. There is a wide range in the diffusion exponent. Fickian release was observed in B1, B4, and B7, while the non-Fickian or anomalous release was observed in other

© The AIC 2023. All rights reserved.

formulations. With the Fickian release, B4 and B7 are the best-fitting matrix models; with the non-Fickian release, B5 and B12 are the best-fitting matrix models. Fickian diffusion is employed when the value of n in Korsmeyer-Peppas is 0.5 or less, whereas diffusion with n values between 0.5 and 1 is used for anomalous or non-Fickian releases. When the release mechanism is unclear or numerous types of release phenomena are possible, this model is utilized to explore the release of pharmacological polymeric dosage forms. Fick's laws are the foundation of diffusion, which describes the macroscopic transit of molecules along a concentration gradient.

Stability studies

The optimized formulation B1 was subjected to stability testing to determine the effect of formulation additions on both the chemical and biological stability of the medicine. It was tested for 12 months at 25ºC/60 percent R.H., 30ºC/65 percent R.H., and 40ºC/75 percent R.H. During the course of the study, neither the external appearance nor the pharmacological content changed appreciably. Table 5 provides the results of drug content determination during the period when the stability tests were conducted. Long-term and accelerated storage data were analyzed using Sigmaplot 12.0 software, as was the 95 percent confidence interval. According to the findings, the changes in the parameters evaluated were minor and insignificant.

Table 5. Stability Study Data of Effervescent Floating Tablet Formulation (B1) of Verapamil Hydrochloride

Stability condition	Sampling interval (months)	Physical appearance	% Drug content B1 (mean ± S.D*)
25o±2oC/60±5% RH	0	No change	99.36 ± 0.15
	3	No change	99.22 ± 0.13
	6	No change	98.44 ± 0.16
	12	No change	98.36 ± 0.17
30o±2oC/65±5% RH	0	No change	99.35 ± 0.18
	3	No change	99.14 ± 0.14
	6	No change	98.69 ± 0.18
	12	No change	98.15 ± 0.14
40º±2oC/75±5% RH	0	No change	99.36 ± 0.95
	3	No change	98.62 ± 0.78
	6	No change	96.35 ± 0.28

© The AIC 2023. All rights reserved.

4. Conclusion

Direct compression was used to make the tablets. They met pharmacopeial standards for floating tablet technology. More than 8 hours later, the tablets were still floating. After 8 hours, all of the produced formulations have reached complete swelling. Therefore, the percentage of swelling was calculated at that point. More than 75% of the medication was released after 12 hours in F1, F5, F6, F9, and F10. Maximum 30 percent drug release occurred in one hour and continued for over 12 hours with F1. Formulation F1 is deemed the most optimal based on the results of the *in vitro* testing.

5. References

1. Sarawade A, Ratnaparkhi MP, Chaudhari S. Floating drug delivery system: An overview. *Int. J. Res. Dev. Pharm. Life Sci.*, 2014, 3(5), 1106-1115.
2. Bruck SD in Controlled Drug Delivery – Clinical Applications, CRC Press, Boca Raton, 2000, vol. 22, pp 1-15.
3. Janseen GM, Robinson JR in Modern Pharmaceutics, 4th Edition, eds. Banker GS, Rhodes CT, 2002, ch. 15.
4. Gennaro AR, Remington JP in Remington: The Science and Practice of Pharmacy, 20th Edition, Lippinkott Wilkins & Wilkins, Baltimore, 2000, vol. 1, pp 903-930.
5. Chien YW in Novel Drug Delivery Systems, 2nd Edition, CRC Press, pp 1-11.
6. Tahmasebi S, El-Esawi MA, Mahmoud ZH, Timoshin A, Valizadeh H, Roshangar L, Varshoch M, Vaez A, Aslani S, Navashenaq JG, Aghebati-Maleki L, Ahmadi M. Immunomodulatory effects of nanocurcumin on Th17 cell responses in mild and severe COVID-19 patients. *J. Cell. Physiol.*, 2020, 236(7), 5325-5338.
7. Sharaf HK, Salman S, Abdulateef MH, Magizov RR, Troitskii VI, Mahmoud ZH, Mukhutdinov RH, Mohanty H. Role of initial stored energy on hydrogen microalloying of ZrCoAl (Nb) bulk metallic glasses. *Appl. Phys. A*, 2021, 127(1), 1-7.
8. Mahmoud ZH, Barazandeh H, Mostafavi SM, Ershov K, Goncharov A, Kuznetsov AS, Kravchenko OD, Zhu Y. Identification of rejuvenation and relaxation regions in a Zr-based metallic glass induced by laser shock peening. *J. Mater. Res. Technol.*, 2021, 11, 2015-2020.
9. Bahadoran A, Jabarabadi MK, Mahmood ZH, Bokov D, Janani BJ, Fakhri A. Quick and sensitive colorimetric detection of amino acid with functionalized-silver/copper nanoparticles in the presence of cross linker, and bacteria detection by using DNA-template nanoparticles as peroxidase activity. *Spectrochim. Acta, Part A*, 2022, 268, 120636.
10. Mahmoud ZH, Al-Bayati RA, Khadom AA. Synthesis and supercapacitor performance of polyaniline-titanium dioxide-samarium oxide (PANI/TiO_2-Sm_2O_3) nanocomposite. *Chem. Pap.*, 2022, 76(3), 1401-1412.
11. Raya I, Widjaja G, Hachem K, Rodin MN, Ahmed AA, Kadhim MM,

© The AIC 2023. All rights reserved.

Mustafa YF, Mahmood ZH, Aravindhan S. $MnCo_2O_4/Co_3O_4$ nanocomposites: Microwave-assisted synthesis, characterization and photocatalytic performance. *J. Nanostruct.*, 2021, 11(4), 728-735.

12. Suryatna A, Raya I, Thangavelu L, Alhachami FR, Kadhim MM, Altimari US, Mahmoud ZH, Mustafa YF, Kianfar E. A review of high-energy density lithium-air battery technology: Investigating the effect of oxides and nanocatalysts. *J. Chem.*, 2022, 2022.

13. Kaduim D, Mahmoud ZH, Mousa F. Green biosynthesis of iron oxide nanoparticles and testing their inhibitory efficacy against some pathogens. *Asian J. Water, Environ. Pollut.*, 2021, 18(4), 119-123.

14. Mahmoud ZH, Al-Bayati RA, Khadom AA. The efficacy of samarium loaded titanium dioxide (Sm: TiO_2) for enhanced photocatalytic removal of rhodamine B dye in natural sunlight exposure. *J. Mol. Struct.*, 2022, 1253, 132267.

15. Raya I, Widjaja G, Mahmood ZH, Kadhim AJ, Vladimirovich KO, Mustafa YF, Kadhim MM, Mahmudiono T, Husein I, Kafi-Ahmadi L. Kinetic, isotherm, and thermodynamic studies on Cr (VI) adsorption using cellulose acetate/graphene oxide composite nanofibers. *Appl. Phys. A*, 2022, 128(2), 1-9.

16. Brahmankar DM, Jaiswal SB in Biopharmaceutics and Pharmacokinetics, p 348.

17. Oudah KH, Najm MA, Samir N, Serya RA, Abouzid KA. Design, synthesis and molecular docking of novel pyrazolo [1,5-a][1,3,5]triazine derivatives as CDK2 inhibitors. *Bioorg. Chem.*, 2019, 92, 103239.

18. Oudah KH, Najm MA, Roomi AB, Al-saidy HA, Awadallah FM. The recent progress of sulfonamide in medicinal chemistry. *Syst. Rev. Pharm.*, 2020, 11(12), 1473-1477.

19. Najm MA, Abd-Alrassol KS, Qasim QA, Hussein HH, Al-Salman HN. Spectrophotometric determination of folic acid using 1,10-phenanthroline materials with ninhydrin reagent. *Mater. Today: Proc.*, 2021 Nov 12.

20. Al-Salman HNK, Ali ET, Jabir M, Sulaiman GM, Al-Jadaan SAS. 2-Benzhydrylsulfinyl-N-hydroxyacetamide-Na extracted from fig as a novel cytotoxic and apoptosis inducer in SKOV-3 and AMJ-13 cell lines via P53 and caspase-8 pathway. *Eur. Food Res. Technol.*, 2020, 246, 1591-1608.

21. Alassadi EAS, Jasim EQ, AL-Salman HNK, Mosa MN. A comparative study of an *in vitro* release patterns of ceftaroline fosamil from chemically-prepared coated hydroxyapatite nanoparticles. *Syst. Rev. Pharm.*, 2020, 11(3), 797-805.

22. Fayadh RH, AL-Salman HNK, Hussein HH. A quick, simple, and specific stability indicating RP-HPLC technique for determining valsartan in pharmaceuticals was developed and the validated. *Ann. R.S.C.B.*, 2021, 25(4), 16553-16570.

23. Ahmed GS, Abdul Jabbar AS, Jeber MA, Al-Salman HNK, Shari FH, Qasim QA, Hussein HH. Effect of COVID-19 on cancer: With special references to liver cancer. *Int. J. Pharm. Res.*, 2020, 12(4), 3861-3867.

24. Pahwa R, Saini N, Kumar V, Kohli K. Chitosan-based gastro retentive floating drug delivery technology: An updated review. *Expert Opin. Drug Delivery*, 2012, 9(5), 525-539.

© The AIC 2023. All rights reserved.

© The AIC 2023. All rights reserved.

The Chemist
Journal of the American Institute of Chemists

A Conversation with Emma Sagarese

Meyer R. Rosen FAIC,FRSC, CPC,CChE,

President, Interactive Consulting, Inc
Bonita Springs, Florida, United States

Dear Fellow Chemists:

I have been honored by the AIC to write an introduction to this interview I conducted with a chemistry teacher, Emma Sagarese, who teaches the subject at a school for young people having learning difficulties.

As the former Editor-in-Chief of EuroCosmetics, author of numerous books and Chief Scientific Advisor to HBA Global Expo, I am a long- time lover of how chemistry is so valuable to us in the cosmetic and personal care industry.

Introspection- in- depth has led to the evolution of nature's biochemicals and our groups contributions to making "synthetic" chemicals. These have gone to the heart of humanities wishes to look good, feel good and be young in the face of inevitably growing older.

Herein, I share with you the joy of educating and guiding younger people to careers in chemistry. It all began when my grandson told his chemistry teacher, Mrs. Sagarese, that his Grandpa was a chemist. She called me to see if I would be interested in Zoom classes to show her early high school classes a novel approach beyond the Table of the Elements, etc.

I chose the novel approach of having them bring in cosmetic and personal care products and engaged them in looking closely at the "chemicals" in the products they and their families used.

I then conducted an interview with Mrs. Sagarese about the classes we taught and sought an appropriate publication that would benefit our industry and our contribution to it. The AIC has graciously agreed to publish this article/interview, It is the result of that Adventure- one of mentoring young teenagers in their search for what they were going to do when they "grew up."

Finally, as the poet that I am, as well as being a chemist, I also share with you a poem I wrote that goes to the heart of the matter. My wish and invitation to you is that you read it and gain value reflecting upon its deeper conglomerate message.

Meyer R. Rosen FAIC,FRSC, CPC,CChE

© The AIC 2023. All rights reserved.

1. A Conversation with Emma Sagarese

The personal care and cosmetic industry is an ideal area to attract new contributors who will create previously unthought- of- pathways that expand our experience of well- being by making us look good and feel good. This article provides some insight in how to empower the young among us towards achieving that goal.

MR: Hello Emma! I see you are a chemistry high school teacher. How do you look at chemistry?

ES: The way I look at it is grounded in a quote by Walter White:

"Well, technically chemistry is the study of matter. But I prefer to see it as the study of change."

MR: So how did you get started in your career?

EC: Ask anyone about their high school chemistry class and you will get a variety of answers. Some people might say they loved it ("We got to blow things up!") while other might say they hated it ("Oxidation numbers? Stoichiometry? No thanks!"). For me personally, I never felt very strongly about the class one way or the other. However, if you told me when I was a junior in high school that one day I would be up in front of the class TEACHING chemistry, the obnoxious teenage version of myself would have rolled her eyes, continued passing a note to her friend in class, and told you I was going to have a career WAY cooler than being a science teacher. Well, flash forward twenty years and here I am in my fourteenth year of teaching science at Newmark High School in Scotch Plains, New Jersey. Our school is an out of district placement that serves students living with autism spectrum disorders, mood disorders, anxiety disorders, attention issues and other developmental disabilities.

MR: That certainly seems challenging. Please elaborate:

ES: When it comes to my career, I like to think that I did not choose to work in special education as much as it chose me. When I was in high school, I thought I was going to be a physical therapist. I chose to attend a college with a highly ranked physical therapy program and majored in biology. When I was finishing up my bachelors and it actually came time to apply for the Master's program to continue my education and earn my degree in Physical Therapy, I was no longer sure that it was what I wanted to do. I graduated from Stockton College (now University) with a bachelor's degree in Biology and absolutely no idea what to do with it. What followed was a two-year span of odd jobs and a lot of soul searching.

In 2008, I saw an advertisement in the Sunday edition of the Star-Ledger (it's not an urban legend kids…people ACTUALLY can get hired this way.) It was a position as a Classroom Assistant at Newmark High School. I still remember my initial interview like it was yesterday…walking into a hot school building in July (our building didn't have central air until 2013), sitting in a small office, and sweating in a black pinstriped business suit that I have not worn since.

© The AIC 2023. All rights reserved.

As I sat across from the principal responding to her questions and engaging in conversation, I like to think I appeared confident and slayed that interview (spoiler alert…I got the job). However, I also had no true teaching experience at the high school level or in special education, so I did question my own ability to be successful in my new role. I spent one year as a classroom assistant and during that time I passed my Praxis test and applied for my teaching certification. By the next year, I was offered a position as the Newmark High School science teacher and never looked back.

MR: What happened after that?

ES: Earlier this school year, we were in class one day preparing a lab on halogens and a student mentioned that his grandfather was a chemist. He further explained that he had been in the industry for many years and even invented a polymer. In my mind, I thought "Well, that's impressive and interesting" but did not even consider the possibility that something transformative could result from the information I had just been given. Luckily, one of the directors of Newmark Education happened to be in the room as the conversation was happening. She and I had a discussion after class and her immediate response was "How do we get him here?" She had instantly recognized an opportunity that I would have allowed to easily slip away.

MR: Personally, I am so glad your Director asked that question and you followed up on it. What happened then?

ES: After class, my director and I discussed how to proceed with contacting this student's grandfather to see if he would be interested in sharing his knowledge with our Chemistry classes. The student informed me that his grandfather lived in Florida. Since I knew there was little possibility that he could join us in person, I suggested that maybe he would like to connect with the classes via Zoom. Hopeful, but not having super high expectations I gave my contact email to the student to pass along to his grandfather.

Low and behold, I received an email soon after from Meyer Rosen who said he loved chemistry and was the Editor- in- Chief of EURO COSMETIC Magazine. He expressed that he thought connecting with the class via a Zoom call was a great idea and he was happy to participate. We set up a phone conference which allowed us to get to know each other, discuss what topics we were currently covering in Chemistry, and how sharing his knowledge and work experience could make the content we were studying more relatable and relevant to the students.

From our first telephone conversation, I was immediately impressed by Meyer's desire to set goals and accomplish them. Here was a man with a striking resume who had already achieved so much, yet continues to reach for more and seize opportunity as opposed to becoming complacent. It was evident that he genuinely cared about giving today's youth a quality science education and was willing to help me do so by bringing his expertise and experience into my classroom.

MR: I am blushing…what happened after that?

© The AIC 2023. All rights reserved.

ES: Over the next few weeks, Meyer and I ironed out the details and set up a Zoom call with the chemistry classes. **We decided to have the lesson focus on personal care products/cosmetic science.** Each student was asked to bring in a personal care product that we could discuss. Our lesson's focus was on the chemical properties of the care products, exploring the ingredients of each product, breaking down the ingredients to the molecular and atomic level, and discussing the various career opportunities available within the chemical industry. Meyer also explained the safety laws and protocols that must be followed when creating and manufacturing personal care products. It was exciting to see my students engage in the lesson, ask deep questions, and think about the real-world applications of chemistry.

When the lesson was over, I asked the students how they felt about it and the feedback was very positive. Several students stated that they found the information presented to be interesting and relevant. A student from one class said that they "enjoyed bringing in their own (product) to relate to the topic." They also had flattering things to say about Meyer himself and felt that it was exciting to talk to an expert in the chemical industry. One student wrote, "I enjoyed Mr. Rosen's personality. He was an endearing speaker, he had this flair of elderly charm and wisdom which one cannot ignore."

MR: Sounds like the idea of teaching "hard" chemistry by starting with personal care products was a good one. What do you think about it?

ES: I am at a point in my career where I am confident in my teaching ability. I have a wonderful co-teacher and we have created a safe, nurturing, and fun environment for our students. I am no longer just trying to stay afloat and survive. I am SWIMMING in the metaphorical ocean that is the field of education and enjoying the turn of the tide. Working with Meyer was a pleasant and successful experience. I am inspired to seek new ways to make chemistry a positive experience for my students and help them reach their full potential.

MR: Seems this way of approaching high school students is worth much for interesting them in career paths they never thought of before. These days, starting with the next generation of students, as you did, is a great idea. We all need to seek mentors like you and I acknowledge your openness to transforming the quality of chemical education- as well as choosing to do it through the doorway of personal care and cosmetic products.

MR: Thank you so much for our conversation!

…….

Bio of Emma Sagarese

Emma Sagarese is a high school science teacher in Scotch Plains, NJ. She resides in Belleville, NJ with her husband, three children (Scarlett, Joseph, and Mark), and their dog, Duncan. Emma has recently completed her Master's Degree in Special Education through Seton Hall University. In her free time, she enjoys running, traveling, and the month of August.

……..

© The AIC 2023. All rights reserved.

When Youth is Upon Us, Again

In the Beginning
There was
The Glow of Youth-
The Promise of Things to Come

And Then
There was Aging-
The Soft Smoothness
Crinkling to Wrinkling
And the Bloom of the Rose
Turning, Turning
To Life's
Invisible Churning

And Now…
We Stand Tall
Saying, NO!
Not yet

Fall back ye
Demons of the Night!

Banding Together
We Seek
The Scientific
Biochemical Mysteries

© The AIC 2023. All rights reserved.

Skin Deep and Within

We are One in the Fight
Searching to the Farthest
Corners of the Globe

From the Rain Forests
To the Deserts-
To the Oceans and their
Volcanic Fissures

Searching Out the Secrets
Of the Glow's Return-
Soothing the
Wrinkled Brow

Be Gone ye
Feet of Crow!
Give Way to the
Chirping of Spring-
When Youth is
Upon Us Again

When Youth is Upon Us, Again

……,,,

© 2022 by Meyer R. Rosen-Interactive Consulting, Inc.

Click for VIDEO

© The AIC 2023. All rights reserved.

The AIC Code of Ethics

Approved by the AIC Board of Directors, April 29, 1983

The profession of chemistry is increasingly important to the progress and the welfare of the community. The Chemist is frequently responsible for decisions affecting the lives and fortunes of others. To protect the public and maintain the honor of the profession, the American Institute of Chemists has established the following rules of conduct. It is the Duty of the Chemist:

1. To uphold the law; not to engage in illegal work nor cooperate with anyone so engaged;

2. To avoid associating or being identified with any enterprise of questionable character;

3. To be diligent in exposing and opposing such errors and frauds as the Chemist's special knowledge brings to light;

4. To sustain the institute and burdens of the community as a responsible citizen;

5. To work and act in a strict spirit of fairness to employers, clients, contractors, employees, and in a spirit of personal helpfulness and fraternity toward other members of the chemical profession;

6. To use only honorable means of competition for professional employment; to advertise only in a dignified and factual manner; to refrain from unfairly injuring, directly or indirectly, the professional reputation, prospects, or business of a fellow Chemist, or attempting to supplant a fellow chemist already selected for employment; to perform services for a client only at rates that fairly reflect costs of equipment, supplies, and overhead expenses as well as fair personal compensation;

7. To accept employment from more than one employer or client only when there is no conflict of interest; to accept commission or compensation in any form from more than one interested party only with the full knowledge and consent of all parties concerned;

8. To perform all professional work in a manner that merits full confidence and trust; to be conservative in estimates, reports, and testimony, especially if these are related to the promotion of a business enterprise or the protection of the public interest, and to state explicitly any known bias embodied therein; to advise client or employer of the probability of success before undertaking a project;

9. To review the professional work of other chemists, when requested, fairly and in confidence, whether they are:
    a. subordinates or employees
    b. authors of proposals for grants or contracts
    c. authors of technical papers, patents, or other publications
    d. involved in litigation;

10. To advance the profession by exchanging general information and experience with fellow Chemists and by contributing to the work of technical societies and to the technical press when such contribution does

© The AIC 2023. All rights reserved.

not conflict with the interests of a client or employer; to announce inventions and scientific advances first in this way rather than through the public press; to ensure that credit for technical work is given to its actual authors;

11. To work for any client or employer under a clear agreement, preferable in writing, as to the ownership of data, plans, improvements, inventions, designs, or other intellectual property developed or discovered while so employed, understanding that in the absence of a written agreement:
    a. results based on information from the client or employer, not obtainable elsewhere, are the property of the client or employer
    b. results based on knowledge or information belonging to the Chemist, or publicly available, are the property of the Chemist, the client or employer being entitled to their use only in the case or project for which the Chemist was retained
    c. all work and results outside of the field for which the Chemist was retained or employed, and not using time or facilities belonging to a client or employer, are the property of the Chemist;

12. Special data or information provided by a client or employer, or created by the Chemist and belonging to the client or employer, must be treated as confidential, used only in general as a part of the Chemist's professional experience, and published only after release by the client or employer;

13. To report any infractions of these principles of professional conduct to the authorities responsible for enforcement of applicable laws or regulations, or to the Ethics Committee of The American Institute of Chemists, as appropriate.

© The AIC 2023. All rights reserved.

The Chemist
Journal of the American Institute of Chemists

Manuscript Style Guide

The Chemist is the official online refereed journal of The American Institute of Chemists (AIC). We accept submissions from all fields of chemistry defined broadly (e.g., scientific, educational, socio-political). *The Chemist* will not consider any paper or part of a paper that has been published or is under consideration for publication anywhere else. The editorial office of *The Chemist* is located at: The American Institute of Chemists, Inc. 315 Chestnut Street Philadelphia, PA 19106-2702, Email: aicoffice@theaic.org.

Categories of Submissions

RESEARCH PAPERS

Research Papers (up to ~5000 words) that are original will only be accepted. Research Papers are peer-reviewed and include an abstract, an introduction, up to 5 figures or tables, sections with brief subheadings and a maximum of approximately 30 references.

REPORTS

Reports (up to ~3000 words) present new research results of broad interest to the chemistry community. Reports are peer- reviewed and include an abstract, an introductory paragraph, up to 3 figures or tables, and a maximum of approximately 15 references.

BRIEF REPORTS

Brief Reports (up to ~1500 words) are short papers that are peer-reviewed and present novel techniques or results of interest to the chemistry community.

REVIEW ARTICLES

Review Articles (up to ~6000 words) describe new or existing areas of interest to the chemistry community. Review Articles are peer-reviewed and include an abstract, an introduction that outlines the main point, brief subheadings for each section and up to 80 references.

LETTERS

Letters (up to ~500 words) discuss material published in The Chemist in the last 8 months or issues of general interest to the chemistry community.

BOOK REVIEWS

Book Reviews (up to ~ 500 words) will be accepted.

© The AIC 2023. All rights reserved.

Manuscript Preparation

RESEARCH PAPERS, REPORTS, BRIEF REPORTS & REVIEW ARTICLES

- **The first page** should contain the title, authors and their respective institutions/affiliations and the corresponding author. The general area of chemistry the article represents should also be indicated, i.e. General Chemistry, Organic Chemistry, Physical Chemistry, Chemical Education, etc.

- **Titles** should be 55 characters or less for Research Papers, Reports, and Brief Reports. Review articles should have a title of up to 80 characters.

- **Abstracts** explain to the reader why the research was conducted and why it is important to the field. The abstract should be 100-150 words and convey the main point of the paper along with an outline of the results and conclusions.

- **Text** should start with a brief introduction highlighting the paper's significance and should be understood to readers of all chemistry disciplines. All symbols, abbreviations, and acronyms should be defined the first time they are used. All tables and figures should be cited in numerical order.

- **Units** must be used appropriately. Internationally accepted units of measurement should be used in conjunction with their numerical values. Abbreviate the units as shown: cal, kcal, µg, mg, g (or gm), %, ^{o}C, nm, µm (not m), mm, cm, cm^{3}, m, in. (or write out inch), h (or hr), min, s (or sec), ml [write out liter(s)], kg. Wherever commonly used units are used their conversion factors must be shown at their first occurrence. Greek symbols are permitted as long as they show clearly in the soft copy.

- **References and notes** should be numbered in the order in which they are cited, starting with the text and then through the table and figure legends. Each reference should have a unique number and any references to unpublished data should be given a number in the text and referred to in the references. References should follow the standards presented in the AIC Reference Style Guidelines below.

REFERENCE STYLE GUIDELINES

References should be cited as numbers within square brackets [] at the appropriate place in the text. The reference numbers should be cited in the correct order throughout the text (including those in tables and figure captions, numbered according to where the table or figure is designated to appear). The references themselves are listed in numerical order at the end of the final printed text along with any Notes. Journal abbreviations should be consistent with those presented in Chemical Abstracts Service Source Index (CASSI) (http://www.cas.org) guide available at most academic libraries.

© The AIC 2023. All rights reserved.

- **Names** and initials of all authors should always be given in the reference and must not be replaced by the phrase *et al*. This does not preclude one from referring to them by the first author, et al in the text.

- **Tables** should be in numerical order as they appear in the text and they should not duplicate the text. Tables should be completely understandable without reading the text. Every table should have a title. Table titles should be placed above the respective tables.

  Table 1. Bond Lengths (Å) of 2-aminophenol

- **Figure legends** should be in numerical order as they appear in the text. Legends should be limited to 250 words.

  Figure 1. PVC Melt Flow Characterized by Analytical Structural Method

- **Letters and Book Reviews** should be clearly indicated as such when being submitted. They are not peer-reviewed and are published as submitted. Legends should be placed after/under the respective figures.

- **Journals -** The general format for citations should be in the order: **author(s), journal, year, volume, page**. Page number ranges are preferred over single values, but either format is acceptable. Where page numbers are not yet known, articles may be cited by DOI (Digital Object Identifier). For example:

  Booth DE, Isenhour TL. *The Chemist*, 2000, 77(6), 7-14.

- **Books -** For example:

  Turner GK in *Chemiluminescence: Applications*, ed. Knox Van Dyke, CRC Press, Boca Raton, 1985, vol 1, ch. 3, pp 43-78.

- **Patents** should be indicated in the following form:

  McCapra F, Tutt D, Topping RM, UK Patent Number 1 461 877, 1973.

- **Reports and bulletins, etc. -** For example:

  Smith AB, Jones CD, *Environmental Impact Report for the US*, final report to the National Science Foundation on Grant AAA-999999, Any University, Philadelphia, PA, 2006.

- **Material presented at meetings -** For example:

  Smith AB. Presented at the Pittsburgh Conference, Atlantic City, NJ, March 1983, paper 101.

- **Theses -** For example:

  Jones AB, Ph.D. Thesis, Columbia University, 2004.

© The AIC 2023. All rights reserved.

- For material presented at a meeting, congress or before a Society, etc., but not published, the following form should be used:

  Jones AB, presented in part at the 20th American Institute of Chemists National Meeting, Philadelphia, PA, June, 2004.

- For material accepted for publication, but not yet published, the following form should be used:

  Smith AB. *Anal. Chem*., in press

- For material submitted for publication but not yet accepted the following form should be used:

  Jones AB, *Anal. Chem*. submitted for publication.

- For personal communications the following should be used:

  Smith AB, personal communication.

- If material is to be published but has not yet been submitted the following form should be used:

  Smith AB, unpublished work.

Reference to unpublished work should not be made without the permission of those by whom the work was performed.

Manuscript Selection

The submission and review process is completely electronic. Submitted papers are assigned by the Editors, when appropriate, to at least two external reviewers anonymously. Reviewers will have approximately 10 days to submit their comments. In selected situations the review process can be expedited. Selected papers will be edited for clarity, accuracy, or to shorten, if necessary. The Editor-in-Chief will have final say over the acceptance of submissions. Most papers are published in the next issue after acceptance. Proofs will be sent to the corresponding author for review and approval. Authors will be charged for excessive alterations at the discretion of the Editor-in-Chief.

Conditions of Acceptance

When a paper is accepted by *The Chemist* for publication, it is understood that:

- Any reasonable request for materials to verify the conclusions or experiments will be honored.

© The AIC 2023. All rights reserved.

- Authors retain copyright but agree to allow *The Chemist* to exclusive license to publish the submission in print or online.
- Authors agree to disclose all affiliations, funding sources, and financial or management relationships that could be perceived as potential conflicts of interest or biases.
- The submission will remain a privileged document and will not be released to the public or press before publication.
- The authors certify that all information described in their submission is original research reported for the first time within the submission and that the data and conclusions reported are correct and ethically obtained.
- The Chemist, the referees, and the AIC bear no responsibility for accuracy or validity of the submission.

Authorship

By submitting a manuscript, the corresponding author accepts the responsibility that all authors have agreed to be listed and have seen and approved of all aspects of the manuscript including its submission to *The Chemist*.

Submissions

Authors are required to submit their manuscripts, book reviews and letters electronically. They can be submitted via email at aicoffice@theaic.org with "Submission for consideration in *The Chemist*" in the subject line. All submissions should be in Microsoft® Word format.

Copyright Assignment & Warranty Form for The Chemist

It is the policy of *The Chemist* to require all contributors to transfer the copyright for their contributions (hereafter referred to as the manuscript) to The American Institute of Chemists, Inc. (hereafter referred to as The AIC) the official publisher of *The Chemist*. By signing this agreement you assign to The AIC to consider publishing your manuscript the exclusive, royalty-free, irrevocable copyright in any medium internationally for the full term of the copyright. This agreement shall permit The AIC to publish, distribute, create derivative works, and otherwise use any materials accepted for publication in *The Chemist* internationally. A copy of the Copyright and Warranty Form for *The Chemist* will be sent to the author(s) whose manuscript is accepted for publication. The AIC will not publish any accepted manuscript in *The* Chemist without its author(s) fully complying with this requirement.

For further information or if you can any questions please contact the Publisher of *The Chemist* at (215) 873-8224 or via email at publications@theaic.org.

Website: http://www.theaic.org/ Email: aicoffice@theaic.org Phone: 215-873-8224

© The AIC 2023. All rights reserved.

Announcements

INVITATION TO AUTHORS

Authors are invited to submit manuscripts for ***The Chemist,*** the official online refereed journal of The American Institute of Chemists (AIC). We accept submissions from all fields of chemistry defined broadly (e.g., scientific, educational, socio-political). *The Chemist* will not consider any paper or part of a paper that has been published or is under consideration for publication anywhere else.

Research Papers (up to ~5000 words) that are original will only be accepted. Research Papers are peer-reviewed and include an abstract, an introduction, up to 5 figures or tables, sections with brief subheadings and a maximum of approximately 30 references.

Reports (up to ~3000 words) present new research results of broad interest to the chemistry community. Reports are peer- reviewed and include an abstract, an introductory paragraph, up to 3 figures or tables, and a maximum of approximately 15 references.

Brief Reports (up to ~1500 words) are short papers that are peer-reviewed and present novel techniques or results of interest to the chemistry community.

Where to Send Manuscripts?

Please submit your manuscripts by email (aicoffice@theaic.org) to the attention of:

The Editor-in-Chief, The Chemist
The American Institute of Chemists, Inc.
315 Chestnut Street,
Philadelphia, PA 19106-2702
Email: aicoffice@theaic.org

Review Articles (up to ~6000 words) describe new or existing areas of interest to the chemistry community. Review Articles are peer-reviewed and include an abstract, an introduction that outlines the main point, brief subheadings for each section and up to 80 references.

Letters (up to ~500 words) discuss material published in *The Chemist* in the last 8 months or issues of general interest to the chemistry community.

Book Reviews (up to ~ 500 words) will be accepted.

© The AIC 2023. All rights reserved.

American Institute of Chemists

www.TheAIC.org

From its earliest days in 1923 to the present, the American Institute of Chemists has fostered the advancement of the chemical profession in the United States.

The Institute has a corresponding dedication "to promote and protect the public welfare; to establish and maintain standards of practice for these professions; and to promote the professional experience through certification as to encourage competent and efficient service."

The AIC engages in a broad range of programs for professional enhancement through the prestigious Fellow membership category, awards program, certification programs, meetings, publications and public relations activities.

The American Institute of Chemists, Inc.

Officers

David M. Manuta.....*Board Chair*

W. Jeffrey Hurst.....*President*

Edmund Malka.....*Secretary*

J. Stephen Duerr.....*Treasurer*

Board of Directors

Stanley Edinger
Margot Hall
David Devraj Kumar
Dayal Meshri
James Smith
Saligrama Subbarao
Rock Vitale

Advertising: Send insertion orders and advertising materials to AIC.
Visit The AIC Web Site for additional information at www.TheAIC.org

The American Institute of Chemists, Inc.
315 Chestnut Street, Philadelphia, PA 19106-2702.
Phone: (215) 873-8224 | Fax: (215) 629-5224 | E-mail: aicoffice@TheAIC.org

© The AIC 2023. All rights reserved.